DEVELOPMENT OF MICRO-VALVES ACTUATED BY POLYPYRROLE/GOLD

BILAYERS

By

Lance Hyo Oh

Thesis submitted to the Faculty of the Graduate School of the
University of Maryland, College Park in partial fulfillment
of the requirements for the degree of
Master of Science
2003

Advisory Committee

      Professor Elisabeth Smela, Chair
      Professor Amr Baz
      Professor Don DeVoe

ABSTRACT

Title of thesis: DEVELOPMENT OF MICRO-VALVES ACTUATED BY

POLYPYRROLE/GOLD BILAYERS

Degree candidate: Lance Hyo Oh

Degree and year: Master of Science, 2003

Thesis directed by: Elisabeth Smela, Assistant Professor

Department of Mechanical Engineering

and Small Smart Systems Center

Many American women suffer from urinary incontinence that decreases their quality of life. To treat urinary incontinence without surgery, we are developing micro-valves that can be used in the bladder to open and close the flow of urine. A process was developed to microfabricate the valves on a Kapton substrate. The micro-valves are actuated by polypyrrole/gold bilayers, and the open and closed states of the valve are controlled by application of a small voltage (< 1V).

In order to show the feasibility of operating the micro-valves in the human bladder, the valves were tested under various pH (4 – 9), body temperature (30 – 42 $^{\circ}$C), and pressure (10 – 110 cm of water) ranges. The power consumption of the valve was determined; a small silver oxide battery that provides 110 mA-hr of power can be used to power the valve for 30 days. Also, the lifetime of the valves, which was initially tens of

cycles due to delamination of gold and polypyrrole from the substrate, was increased to 1,000 cycles. An adhesion layer of Cr between the Kapton and Au, as well as an electroplated layer of Au between the evaporated Au and electrochemically deposited PPy, were used to prevent early delamination.

Lastly, in order to optimize the performance of the bilayer, we wanted to determine the relationships among PPy thickness and bilayer hinge length, force, and bending angle. A new actuator was designed to collect bending angle and force. Larger bending angles were observed with longer hinges, and smaller bending angles with thicker PPy. Preliminary force measurements were made by stacking weights on the actuators. The thicker the PPy was, the heavier the weight it could lift.

DEDICATION

This thesis is dedicated to my wife, Yoon Nah Cho.

ACKNOWLEGEMENTS

TABLE OF CONTENTS

v

LIST OF FIGURES

x

LIST OF TABLES

1   INTRODUCTION AND BACKGROUND

1.1   MOTIVATION FOR PROJECT

The goal of this project is to develop micro-valves that can be used to treat urinary incontinence without surgery. Urinary incontinence affects 15 - 35% of adult American women [1]. It seriously decreases their quality of life because they are less inclined to work or to participate in social events [2]. The direct health care cost of the problem is estimated in the U.S. to be $26.3 billion per year [2].

Infinite Biomedical Technology (IBT) sponsored and collaborated on this project. With successful design and performance of the valves, IBT will implement the valves in a Foley catheter, which is a tube that continually drains urine from the bladder. Currently, a Foley catheter is used when normal urination is disrupted by an infection, bladder stones, or an injury [3]. Instead, the new Foley catheter will be used to either keep urine in the bladder or drain the urine. Since IBT will commercialize the product, the product had the following requirements:

1. Safe operation in humans

2. Maximum size: 2 x 12 mm^2 to be fit into the Foley catheter

3. Power consumption: watch-battery-operated for 1 month

4. Speed of the valves: 10 sec to open

5. Lifetime (cycles): 360

6. Minimum movement: open and close a hole of size 300 μm

7. Operation environment: urine

In order to choose a material and a mechanism of hinge actuation that meet the requirements above, widely used micro-electro-mechanical systems (MEMS) actuation technologies will be reviewed and evaluated next.

1.2   CURRENT MICRO-ACTUATION USED MEMS TECHNOLOGIES

The bladder environment imposes significant restrictions in terms of size, temperature, pH, power consumption, and biocompatibility. Considering these restrictions, we evaluated the feasibility using 7 different actuators: electrostatic, shape memory alloy (SMA), piezoelectric, thermal, magnetic, polymer gel, and conjugated polymer actuators.

1.2.1   Electrostatic Micro-Actuators

Electrostatic force is most frequently used for MEMS micro-actuators. One example is micro-actuators based on the electrostatic comb-drive mechanism, which use interdigitated finger capacitors to generate forces for their motions [4] (see Figure 1-1). Polysilicon flexible beams have been used as actuation arms, and they balance spring force against the electrostatic force [5].
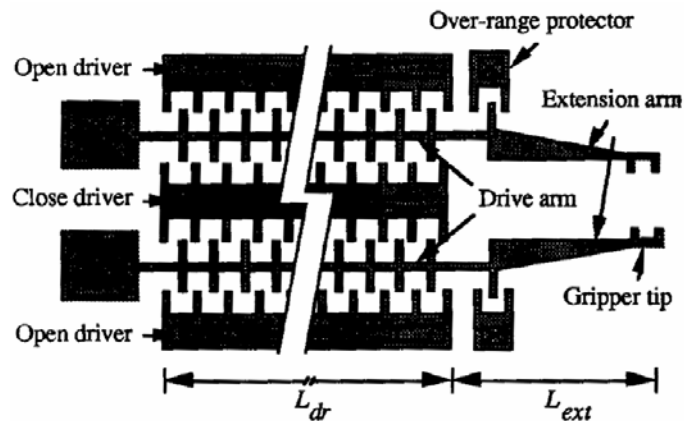
Figure 1-1. Schematic of comb-drive micro-actuator [6].

Actuators based on electrostatic forces, such as comb-drive or capacitive sensing

devices, can operate between 20 and 50 V [7].   Although, comb-drive micro-actuators

typically result in small displacement (10 µm) after voltage is applied [4, 7], Grade et al.

showed a large deflection of micro-mirror (425 µm) that was connected to a comb-drive

actuator [8]. However, electrostatic actuators cannot work in an aqueous environment.

Thus, electrostatic actuators cannot be used for this application unless they were to be

very carefully packaged to keep the capacitors dry.

1.2.2   *Piezoelectric Micro-Actuators*

Another mechanism commonly used for micro-actuators is piezoelectric actuation.

A unimorph based on this mechanism is shown in Figure 1-2. The advantage of

piezoelectric actuation is high accuracy and reliability in producing displacements [9].

However, it requires a large voltage (for example 100 V) to achieve deflection of only 4

µm [10]. Such levels of voltage cannot be obtained from a battery, and so would require

a transformer, but more importantly are too large to be safely used in the human body.
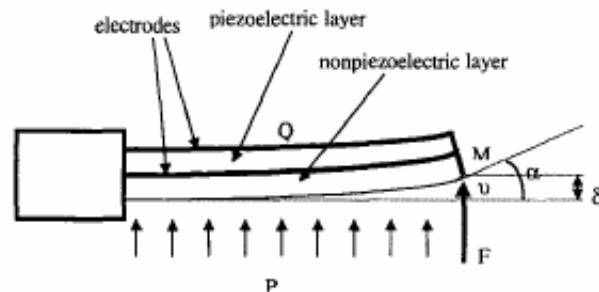
Figure 1-2. Bending unimorph cantilever [9].

1.2.3 Thermal Micro-Actuators

Actuators based on thermal expansion can be used to obtain a large force and deflection. Electrothermal actuators can be categorized into three types: bimorphs, U-beam actuators, and V-beam actuators.

Bimorphs are based on the so-called bimetal structure, which is a sandwich structure of two materials with different coefficients of thermal expansion (CTE) [11]. Under a temperature change, the two materials expand, but the thermal expansions of the two are not the same, which leads to thermal stress and causes the sandwich structure to bend.

Instead of different materials, a U-beam in Figure 1-3 consists of a cold arm and a hot arm, which are made of a single material such as polysilicon. The cross sectional area of the hot arm is less than that of the cold arm. When the same current flows through the two arms, the current density in the hot arm is higher than that in the cold arm. Therefore, more Joule heat is generated in the hot arm, which causes the hot arm to expand more than the cold arm. This difference in thermal expansion causes the tip of the thermal actuator to deflect toward the cold arm [12].
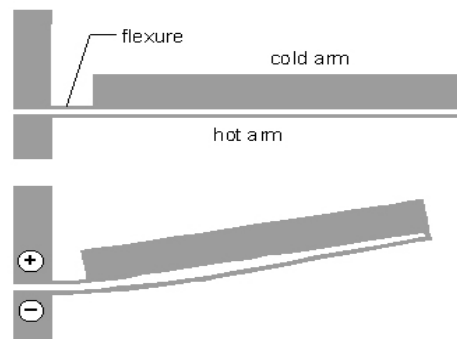
Figure 1-3. A U-beam actuator [12].

Similarly, V-beams are also made of a single material such as polysilicon, but the whole structure is heated uniformly when voltage is applied. The beam is offset slightly in the middle, and the offset controls the deflection direction (see Figure 1-4).
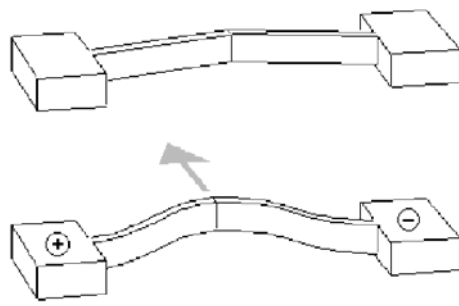
Figure 1-4. A schematic of a V-beam actuator [13].

The advantage of polysilicon U-beams and V-beams is the simplicity of their fabrication. Also, these micro-actuators operate in a voltage and current regime more closely matched to IC circuitry (<10V, <25mA) because the polysilicon has a higher resistivity than that of most metals [13]. However, in an aqueous environment, thermal actuators show only a small actuation displacement due to significant heat loss [14], so these are also not appropriate for the urinary incontinence valve.

1.2.4   SMA Micro-Actuator

Shape memory alloy actuation is based on a crystalline phase transformation. At a low temperature, the martensite phase is easily deformed to a new shape. However, heating the SMA to the austenite phase cause it to recover its original shape with high force.

Lee et al. made SMA micro-actuators from a $Ni_{42}Ti_{50}Cu_8$ alloy because it transforms just above body temperature ($37^{o}C$), which is useful in biomedical application

5

[15]. By changing the temperature from 30°C to 70°C, the SMA film could generate an actuation stress up to 500 MPa. This device had a large actuation force (40 mN) and could be actuated at relatively low temperatures (70°C). However, similar to the thermal actuators, the problem of heating up the actuator in fluid environment is the heat loss.

1.2.5   Electromagnetic Micro-Actuators

Electromagnetic mechanism can be implemented in micro-valves [16]. Wright et al. fabricated an electromagnetic micro-actuator based on a copper magnetic coil and a permalloy cantilever [17]. The cantilever was actuated by applying 25 mA. However, the deflection was only 4 μm was, which does not meet the requirements of our project. The reason for the small deflection is that magnetic force significantly decreases when the cantilever is moved away from the magnetic coil [16] ($F \propto 1/D^2$, where F is magnetic force, and D is distance between magnet and cantilever).

1.2.6   Polymer Gel Micro-Actuator

Polymer gel is also used in bio-fluidic applications such as micro-valves [18] and micro-pump [19]. Hattory et al. reported a micro-pump using a polymer gel [19]. They used polyvinyl methyl ether (PVME), which changes its volume at different temperatures: it swells below 35 ^{o}C, and it contracts over 40 ^{o}C. The pump was heated with a nichrome wire by applying electric current (0.1 A, 20 V). However, there is no watch battery that can apply such high levels of current and voltage. Worst of all, polymer gels are mechanically weak since they have a small Young's modulus [20].

6

1.2.7 *Conjugated Polymer Micro-Actuators*

Conjugated polymers offer the possibility of controlling the mechanical actuation with external electrical stimulus. Electrochemical doping by oxidation/reduction cycling of conjugated polymers such as polypyrrole (PPy) and polyaniline causes volume expansion or contraction, primarily through the migration of ions and solvent from a surrounding electrolyte, which can be the urine itself [21]. These volume changes are reversible.

Unlike other actuators, PPy actuators satisfy all the requirements below.

	Valve requirement list	PPy actuators
Maximum size:	2 x 12 mm^2	✓ Micro-processable
Power consumption:	watch-battery-operated for 1 month	✓ Small power consumption occurs when changing from one state to another (see Section 2.10 for the calculation)
Speed:	10 sec to open	✓ For 1 μm thick PPy, 2 sec to actuate
Minimum movement:	Open and close a hole size of 300 μm	✓ Out-of-plane rotation angle: $0 \sim 180^O$
Lifetime:	300 cycles	✓ Above 1000 cycles
Operation environment:	urine	✓ Work well in urine
Safety	Low voltage	✓ Operating voltage: below 1 V

A possible concept of a micro-valve utilizing conjugated polymers is shown in Figure 1-5. This valve consists of a cap and a bottom plate, which are fabricated separately by using microfabricated processes such as photolithography, wet etching, dry

etching, and metallization. The cap is aligned and glued to the bottom plate. When

voltage is applied to an electroactive hinge, a flap attached to the hinge rotates and drains

urine. The advantage of this design is that a hinge deflection translates into a large

actuation motion of the flap.
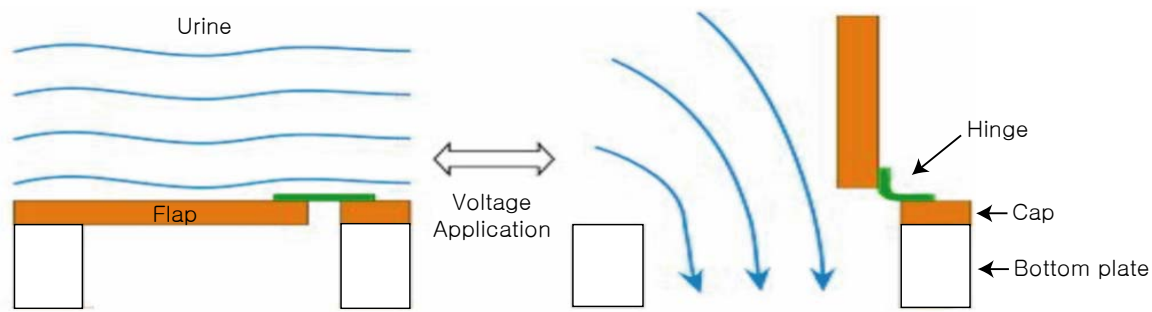
Figure 1-5. Concept of micro-valves for urinary incontinence. When the valve is closed, urine is accumulated in the bladder. When the valve is opened, urine flows through a hole in the bottom plate. The open and closed state of the valve can be controlled by application of a small voltage.

1.3   CONJUGATED POLYMERS

Conjugated polymers are characterized by alternating single and double bonds

along the polymer backbone (Figure 1-6 (A)). In this structure, a delocalized positive

charge appears when an electron is removed from the polymer. The removal of electrons

(oxidation) can be done electrochemically by applying a positive voltage, which leaves

the material electrically conducting. To maintain charge neutrality, the positive charges

on the polymer backbone are compensated by the incorporation of negatively charged

anions into the polymer (Figure 1-6 (B)). The backbone returns to the neutral state with

addition of electrons (reduction) by applying negative voltage, and anions respond by

exiting the polymer (Figure 1-7). This is the case when the polymer is prepared with a

small, mobile anion.
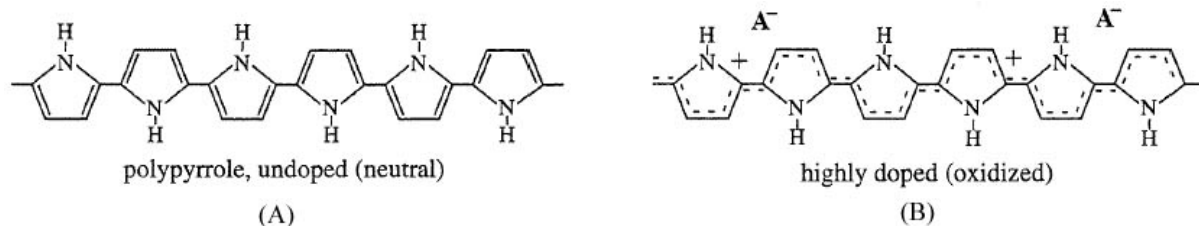
Figure 1-6. Chemical structure of polypyrrole in (A) neutral and (B) oxidized forms.
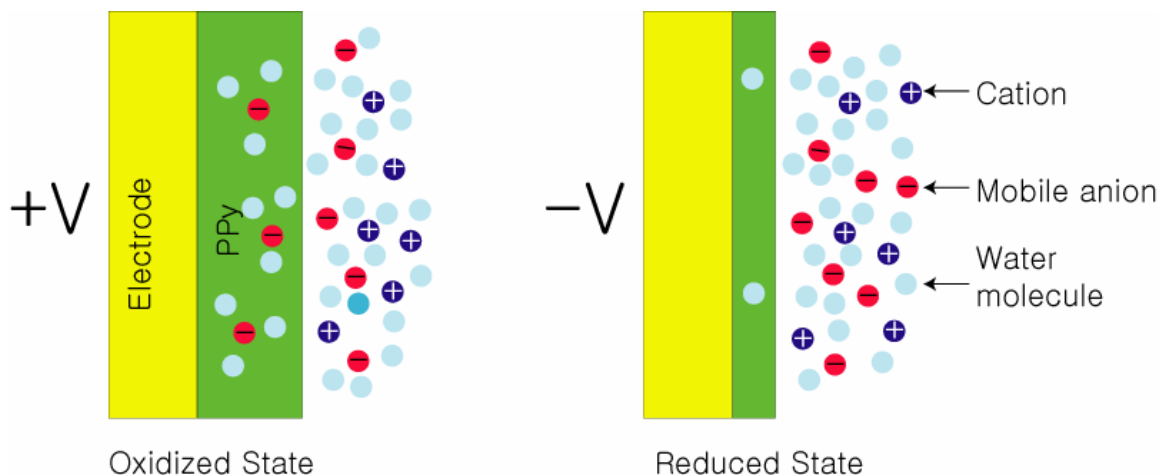
Figure 1-7. Schematic of the oxidation and reduction of PPy prepared with a mobile anion. When negative voltage is applied to the electrode, the PPy contracts because anions leave the PPy. When the polarity of the voltage is reversed, the ions and water migrate into the PPy causing it to expand. The anion transport is to maintain charge neutrality.

On the contrary, when the polymer is prepared with a large, immobile anion, it expands upon electrochemical reduction due to the influx of cations to compensate the immobile anion (Figure 1-8). The polymer contracts upon electrochemical oxidation because cations leave the polymer. In order for expansion and contraction of volume to occur, the polymer needs to be surrounded by a liquid electrolyte as a source of ions. Since these ions are surrounded with water molecules [22, 23], water transport with ions accounts for most of volume change [24]. Also, water transport can occur independently due to osmotic pressure. [25].

9
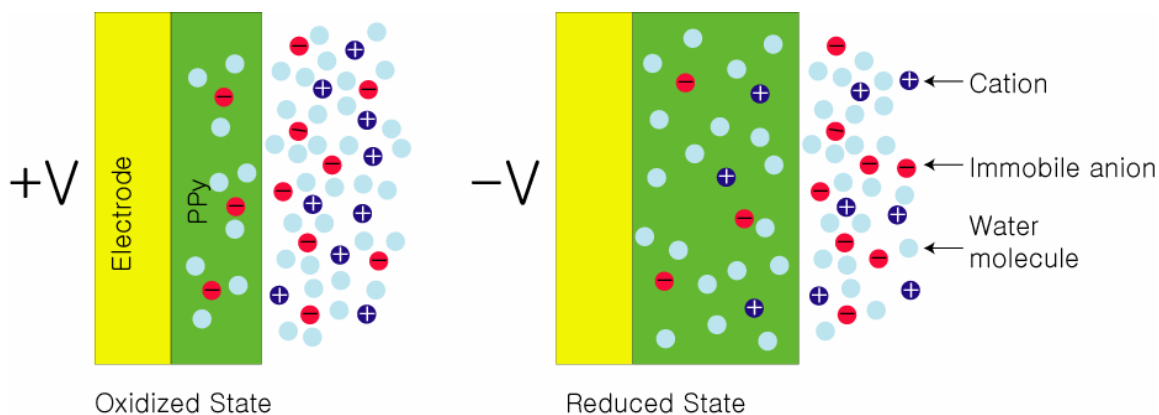
Figure 1-8. **Schematic of the oxidation and reduction of PPy prepared with an immobile anion. When negative voltage is applied to the electrode, the PPy expands because cations and water molecules enter the PPy. When the polarity of the voltage is reversed, the ions and water migrate out of the PPy causing it to contract.**

PPy prepared with dodecylbenzenesulfonate (DBS⁻) (Figure 1-9) is one of the best conjugated polymers for actuation [21, 26]. The DBS anion is immobile in the polymer, so there are negligible long-term behavior changes due to effects such as salt draining [27]. In addition, PPy(DBS) actuators respond smoothly to a change in potential, and immobile anions have been shown to generate higher swelling [28] and to have higher energy density [29] and greater electrochemical stability [30]. For PPy(DBS) films with a thickness of 1 μm, most of the volume change occurs within approximately 2 sec of the application of a step voltage from 0 V to −1 V. Thus, the actuation time with PPy actuators is sufficiently rapid at low voltage, making them suitable for use in biomedical applications.
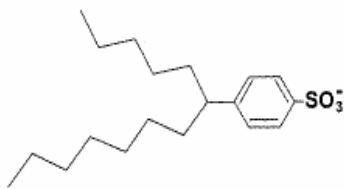
Figure 1-9. Structure of dodecylbenzenesulfonate (DBS⁻).

1.4   ELECTRODEPOSITION OF PPY(DBS)

For the valves described in this thesis, PPy is electrochemically deposited onto an inert metal electrode by using an aqueous solution of 0.1 moles/liter (M) NaDBS and 0.1 moles/liter (M) pyrrole. To electroplate the PPy, a voltage is applied using a potentiostat that has three electrodes: a working electrode (WE), a reference electrode (RE), and a counter electrode (CE). The WE is connected to the electrode on which the PPy film is deposited. The RE provides a reference potential against which the potentiometric measurement can be made; Ag/AgCl is used as the RE. In the RE, a chemical reaction (Equation 1) is at equilibrium. Thus, no current flows through the RE. The CE provides the current for the reaction; a piece of platinum foil, a gold-covered wafer, or graphite can be used. Typically, CE should be ten times bigger than WE.

A typical electrochemical cell setup is shown in Figure 1-10.   In this setup, copper clamps were used to hold the electrodes and to apply voltage at the same time. Copper clamps should never be immersed in an aqueous solution because they get corroded and contaminate the solution when voltage is applied.

Equation 1. Reference electrode chemical reaction

$$AgCl(s) + e^- \leftrightarrow Ag(s) + Cl^-(aq)$$
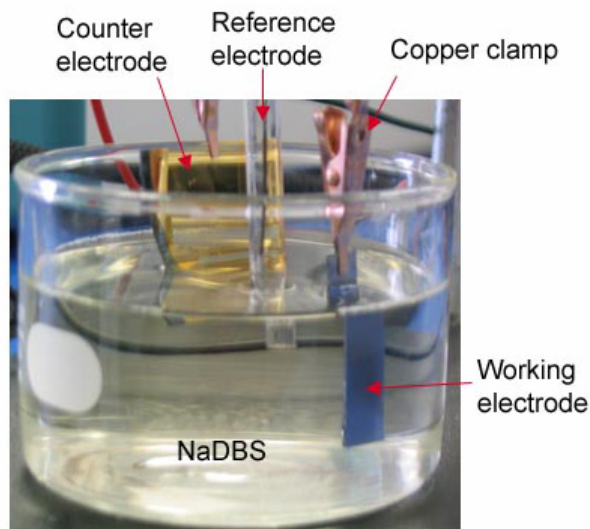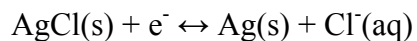
Figure 1-10. A typical electrochemical cell setup.

By applying a constant voltage or current, the PPy film grows at a near constant rate (Figure 1-11). At higher potentials, the film grows faster, but it becomes more non-uniform (the edge of the film gets thicker than the center). The deposition rate depends exponentially on the applied potential above 0.5 V vs. Ag/AgCl [31].
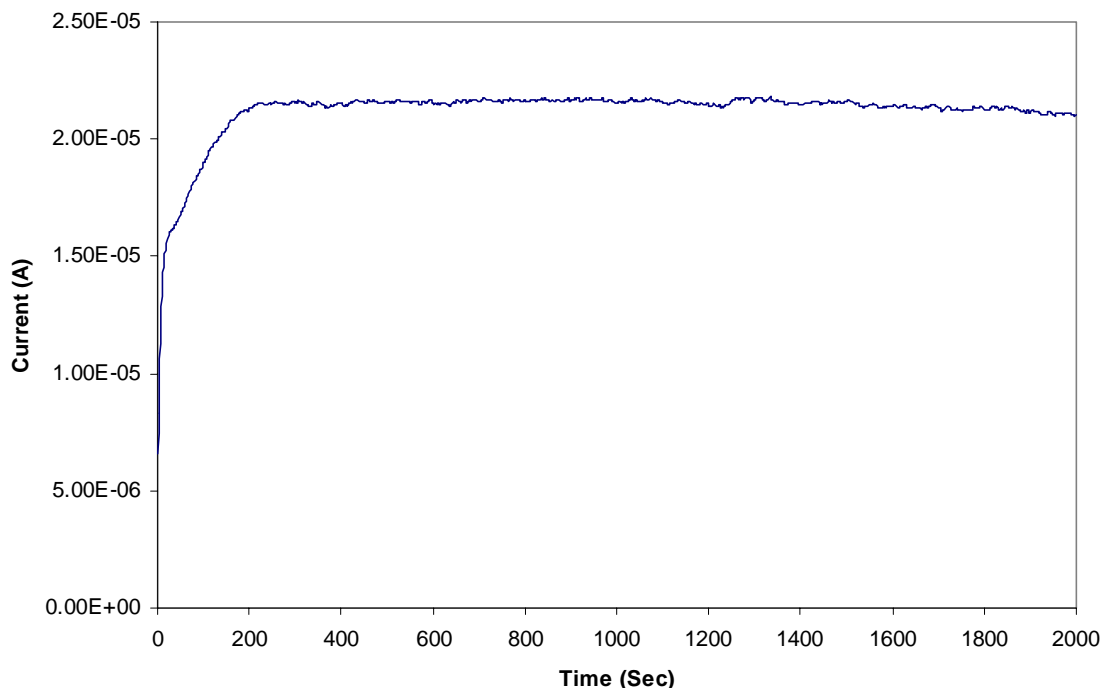
Figure 1-11. Chronoamperogram showing a typical PPy deposition in 0.1 M aqueous pyrrole and 0.1 NaDBS. The potential is held at 0.5 V vs. Ag/AgCl.

During the deposition of PPy, the removal of an electron from pyrrole creates a radical cation that reacts with a second radical and forms a dimer. This grows by more addition of these units. The growing PPy chains reach a certain length and become insoluble, which make them precipitate onto the working electrode. The chains interconnect to each other by crosslinking (Figure 1-12) at the β-positions of the pyrrole molecule (Figure 1-13). During the polymerization, DBS anions move inside the material to maintain charge neutrality; one DBS anion for every approximately four PPy monomer units is incorporated. Since DBS anions are large, they are trapped in the PPy film (Figure 1-14). Thus, the DBS anions never leave the film at any state.

13
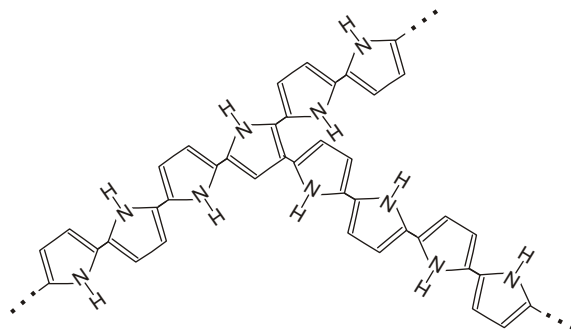
Figure 1-12. Crosslinked PPy.
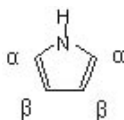
Figure 1-13. Chemical structure of pyrrole.
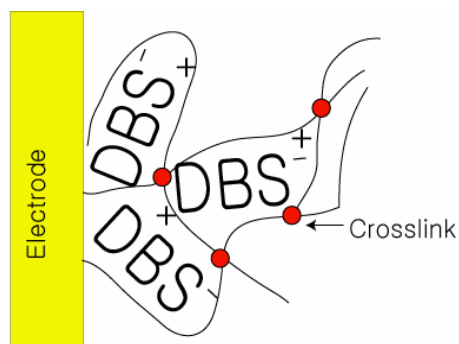
Figure 1-14. Enclosed bulky DBS anions in the PPy film after deposition.

1.5   PPY(DBS) BILAYER ACTUATORS AND ACTUATION

Previously, PPy bilayer actuators have been utilized in the development of blood vessel connectors (Micromuscle AB), microrobot arms [32, 33], and "cell clinics" [34]. The fabrication process of this bilayer involves the use of micromachining technologies including photolithography, thin film deposition, and etching [21, 31, 32].

A new MEMS process was developed to fabricate the first generation of PPy micro-valves made from a Kapton substrate, which is presented in the next chapter. A

14

thin film of gold serves as the electrode and as the non-volume-changing component of the bilayer. When the PPy contracts, the gold layer (with fixed dimensions) transforms the linear displacement of PPy into a curling movement in the out-of-plane direction (Figure 1-15) [35]. If a rigid plate is attached to the bilayer, the plate will be rotated by the applied voltage (Figure 1-16). The micro-valve design incorporates this curling movement. Since this valve can be actuated at low voltages (less than 1 V), the design is compatible with in-vivo application.
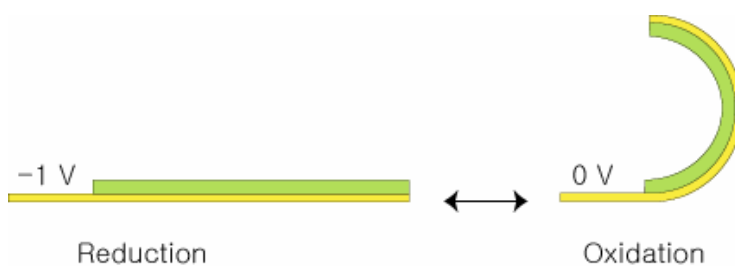
Figure 1-15. Contraction of the PPy layer (green) in x-y causes a PPy/Au layer to bend out of the plane.
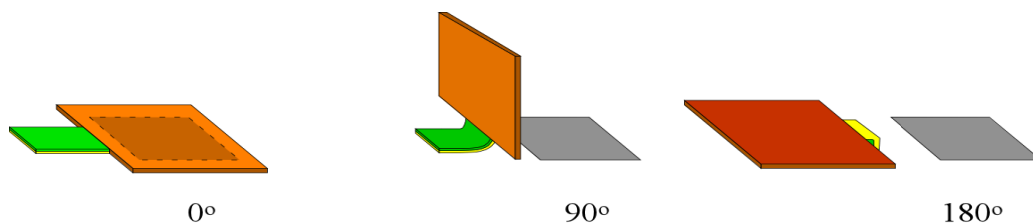
Figure 1-16. A rigid plate attached to the bilayer will be rotated when the bilayer bends. If the flap is covering a hole, the hole will be blocked; when the plate lifts, the hole is opened [36].

The actuators are stimulated by applying either a triangular or square wave voltage signal. The triangular signal entails cycling between 0 V and -1 V vs. Ag/AgCl at different scan rates. This signal is used to plot a cyclic voltammogram (CV) shown in Figure 1-17 that helped us to analyze electrochemical phenomena in the actuator. The anodic and reduction peaks are due to the current flowing in and out of the PPy during

15

the oxidation and reduction reactions. The square wave signal involved stepping between

0 V and −1 V vs. Ag/AgCl, which was used to test the lifetimes of the actuators.
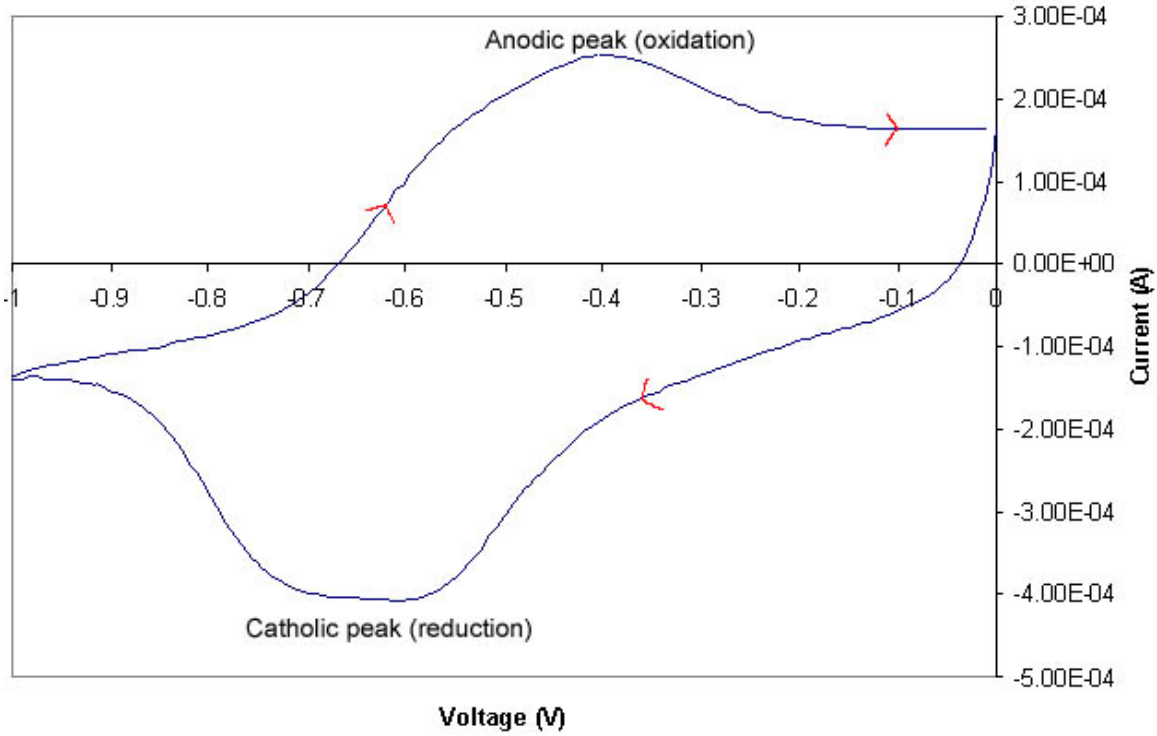
Figure 1-17. An example of a cyclic voltammogram. At the anodic peak, PPy is oxidized and contracts, while PPy is reduced and expands at the catholic peak.

2 FABRICATION AND CHARACTERIZATION OF 1ST GENERATION MICRO-VALVES

2.1 OVERVIEW

PPy actuators were previously reported to work in a wide variety of electrolytes including human urine [21]. In our lab, however, PPy actuation in human urine had to be verified since this project was critically dependent on it.

In order to verify the actuation, the first generation of micro-valves had to be developed and fabricated. We developed a new MEMS process to fabricate PPy micro-valves made from a Kapton substrate (transparent flexible plastic sheet). We used Kapton instead of silicon because we did not have a double-side mask aligner, which is necessary to perform back-to-front alignment of silicon. Thus, we tried transparent substrates: glass cover slips (100 μm), Dupont Mylar film, and Dupont Kapton film.

In order to make the flap in Figure 1-5, we had to etch all the way though the substrate. The problem with the glass slides was etching deeper than 20 μm using positive photoresists such as Shipley 1813: they delaminate from the glass in an aqueous hydrofluoric acid (HF) at any dilution ratio. The glass could be etched with a negative resist, MicroChem SU-8 50, in aqueous HF, but I did not find a proper method to strip the resist. The problem with Mylar film was that it is as flexible as a food film stretch sheet, which is hard to handle during the fabrication processes; it gets easily wrinkled and folded. We chose Dupont's Kapton HN because we could obtain films with 50 μm thickness, which was rigid enough for handling during the fabrication process but thin enough to etch through. In addition, it has stable properties over a wide temperature range (−269 to 400°C) and excellent chemical resistance [37].

17

The micro-valves were tested under pH (4 - 9), body temperature (30 – 42 ^{o}C), and various pressure ranges (10 – 110 cm of water). These are the range of conditions IBT anticipated in the lower part of the human bladder. We expected the valves to work in this pH range since Shimoda et al. successfully tested PPy actuators in this range [26]. However, we had to confirm this in our lab. For the temperature and pressure studies, we did not find any prior publications, so we were not sure how PPy actuators would behave in these ranges. Two kinds of pressure tests were performed: static and dynamic pressure tests. For the static pressure test, the PPy actuator was operated at different pressure levels from 10 to 110 cm of aqueous electrolyte. In the dynamic pressure test, the valves were placed over open holes to see if they would open and drain the electrolyte and prove the feasibility of using PPy bilayers for micro-valves.

Piyush Seth of IBT and I performed all the experiments together in this chapter except for the development of the fabrication sequence, which was completed with Yingkai Liu. The same process was used to fabricate micro-origami (See Appendix 0).

2.2 FABRICATION OF THE PPY ACTUATORS

The process that used to fabricate all the samples for the characterization tests is shown in detail in Figure 2-1. The Kapton film was cut into pieces ~5×5 cm^2 with scissors to fit it into a 3-in mask aligner. To remove grease and dirt, it was rinsed with acetone, methanol, isopropanol, and deionized (DI) water and dried with N$_2$ (step 1 of Figure 2-1). A 0.4-micron layer of Au metal was thermally evaporated onto the Kapton

film (step 2)[1]. Photoresist (Shipley 1813) was spin-coated at 4000 rpm on top of the gold

(step 3), and subsequently patterned with a mask. This process was accomplished by

exposing the photoresist to 350 nm UV light at 9 mW/cm^2 for 15 sec and then immersing

in Shipley CD-30 developer for 30 sec to selectively remove the light-exposed

photoresist (step 4). The substrate was then immersed in a commercial Au etchant

(Transene) to remove the exposed gold (step 5). Using the same process as above, the

photoresist was patterned again on the gold to pattern PPy (step 6). The substrate was

immersed in an aqueous solution of 0.1 M pyrrole and 0.1 M NaDBS to deposit PPy on

the gold by electrochemical polymerization (step 7). The photoresist was exposed to UV

and stripped off in CD-30 developer (step 8). Neither commercial photoresist stripper

nor acetone and methanol can be used to strip the photoresist because the photoresist

stripper attacks the PPy, and acetone dehydrates the PPy [31]. In our lab, we observed

that the PPy film shrunk after it was immersed in methanol and dried.

To make the PPy/Au hinge of the actuator, the first step is to deposit Al (by

thermal evaporation), which is used as a mask to pattern the Kapton in step 11, on the

back side of the Kapton. Photoresist is patterned using the same processes described

above. A 20 μm line is etched in the Al using a commercial Al etchant (Transene, Type

A) (step 9). In order to protect the PPy on the other side of the substrate during the next

step, a layer of Al is deposited on the front side (step 10). A March Jupiter III reactive

ion etching (RIE) system was used to etch the Kapton (step 11) in an oxygen plasma

under 0.3 mTorr at 200 Watts. A RIE-etched 35-micron hinge is created beneath the Al-

---

[1] This step was a major problem during the actuation of the device due to the delamination of Au from the

Kapton film.

patterned 20 μm line due to anisotropic etching and undercutting of the Al. The Al is

then removed using Al etchant, which leaves a completed flap (step 12).

1. Start with Kapton.

2. Evaporate Au.

3. Spin-coat photoresist (PR).

4. Pattern the PR.

5. Pattern the Au.

6. Pattern the PR again and electrochemically deposit PPy.

7. Remove the PR.

8. Evaporate Al on the back side.

9. Pattern Al.

10. Evaporate Al on the front side.

11. RIE-etch Kapton with oxygen plasma.

12. Remove Al on both sides with Al etchant.

Legend:
- Kapton
- Cr
- Au
- PPy
- Al
- Photoresist (PR)
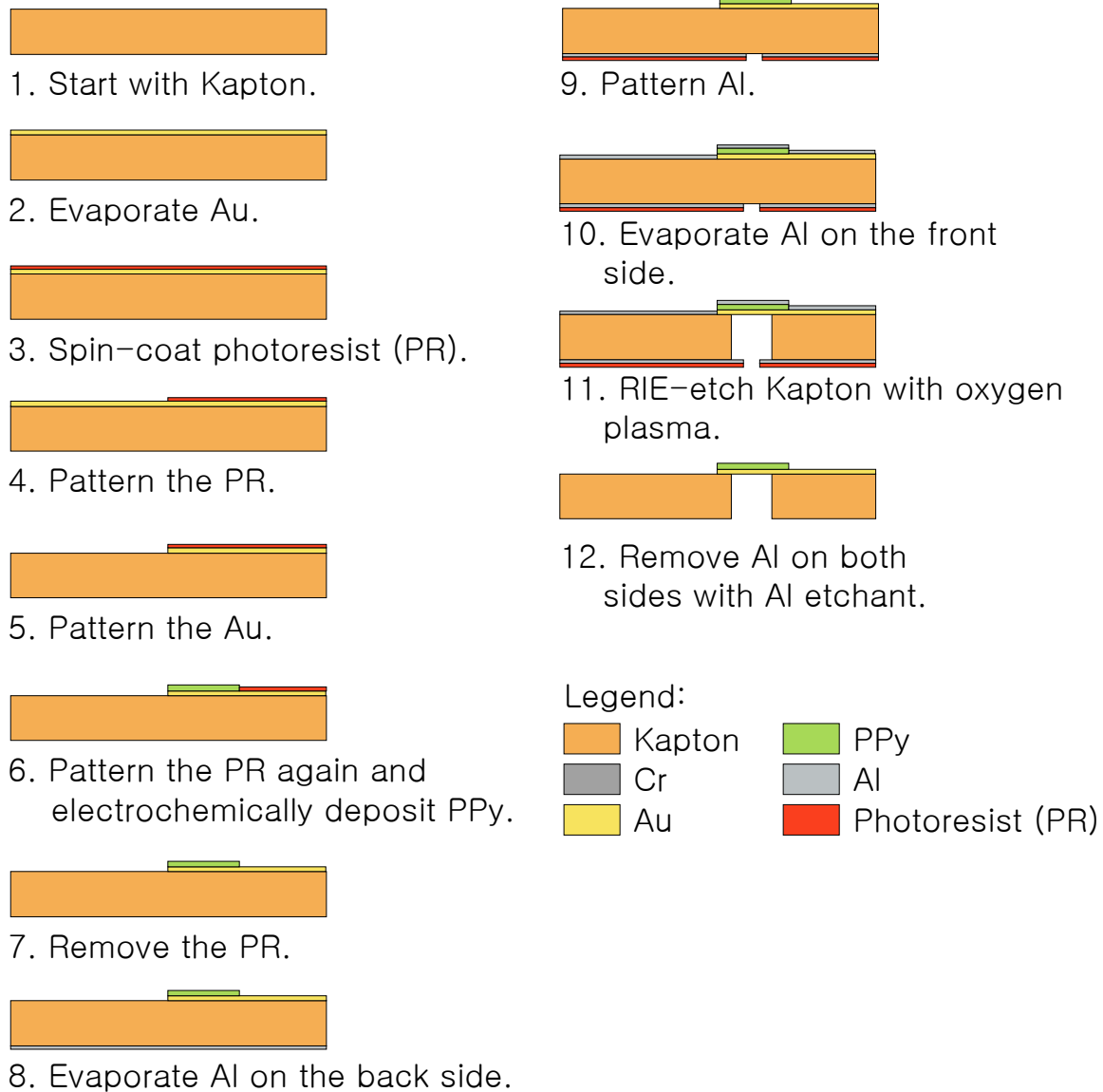
Figure 2-1. Fabrication sequence of PPy actuator.

2.3   ACTUATION OF THE PPY FLAP

A three-dimensional schematic view and photos of a flap are shown in Figure 2-2.

In order to actuate the PPy/Au hinges, the flap was immersed in 0.1 M aqueous NaDBS,

and voltage was applied. Electrochemical oxidation causes the bilayer to bend

20

(corresponding to a valve open state). Reduction returns the bilayer to the flat state (corresponding to a valve closed state). Also, different angles of the PPy actuator from 0 to 180° can be held by applying fixed potentials between 0 and -1 V as shown in Figure 2-2 and Figure 2-3. These prototype devices were characterized and tested as described in the following sections.
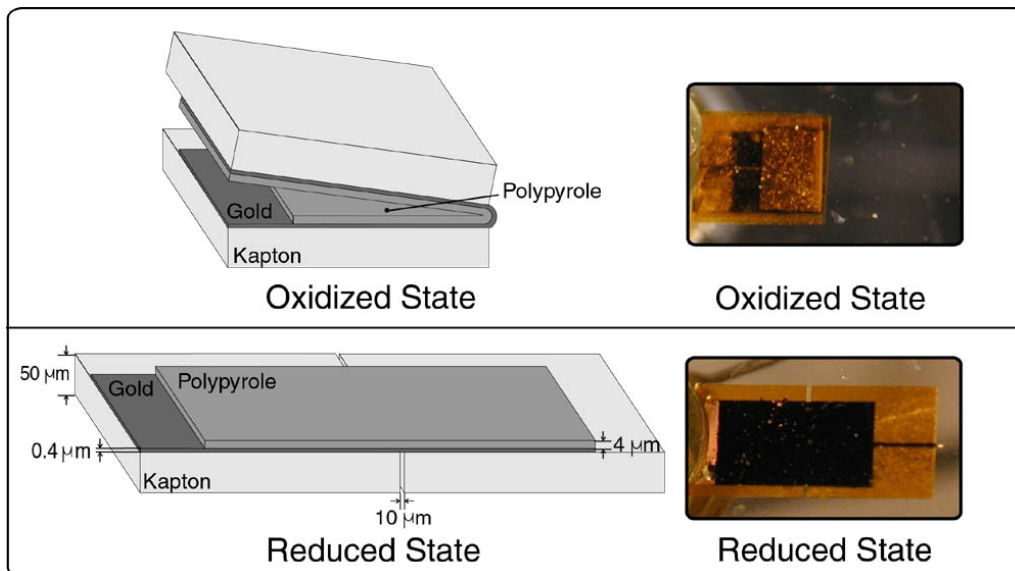
Figure 2-2. Schematics and overhead photographs of the PPy actuator, shown in the oxidized (open) and reduced (closed) states in an electrolyte solution. The overall dimensions are 4 x 8 mm^2. Schematics courtesy of IBT.
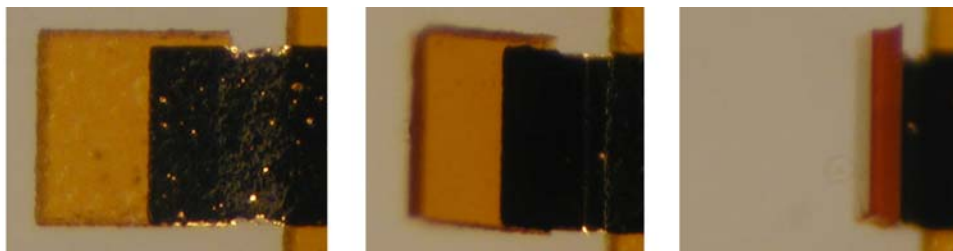
Figure 2-3. Kapton plate 430×430 μm^2 at 0°, 45°, and 90°.

2.4 OPERATION IN URINE

Motivation:

Three actuators were tested to determine the feasibility of operation in urine. Since Jager et al. reported that the PPy actuators work well in urine, the actuators were expected to bend at least 10° in less than 10 sec to be used as valves. As long as we could see a small bending angle, we could always increase it with a different hinge design (presented in Chapter 5).

Experiment:

The actuation of the PPy bilayer was carried out in a simulated human urine (Human Urine Control, Quantimetrix). The simulated urine was purchased because it has a consistent amount of ions and constant pH level (7, measured with pH paper) and does not have a smell, while the properties of human urine vary each time it is collected.

The bilayer device was clamped to hang in a bath as shown in Figure 2-4. The electrochemical setup included an Ag/AgCl reference electrode (RE) and a platinum counter electrode (CE) connected to the potentiostat. The gold CE reacted and turned black in the urine during operation. Thus, platinum was used for the counter electrode.

A digital camera was fixed in a place to be parallel to the actuator. Square wave potential steps from 0 to -1 V were applied to actuate the bilayer. One picture was taken when the bilayer was fully reduced, and another one was taken after it was fully oxidized. These images were transferred to a computer, and the "Measure Tool" function in Adobe Photoshop was used to measure the angle difference between the two positions.

22
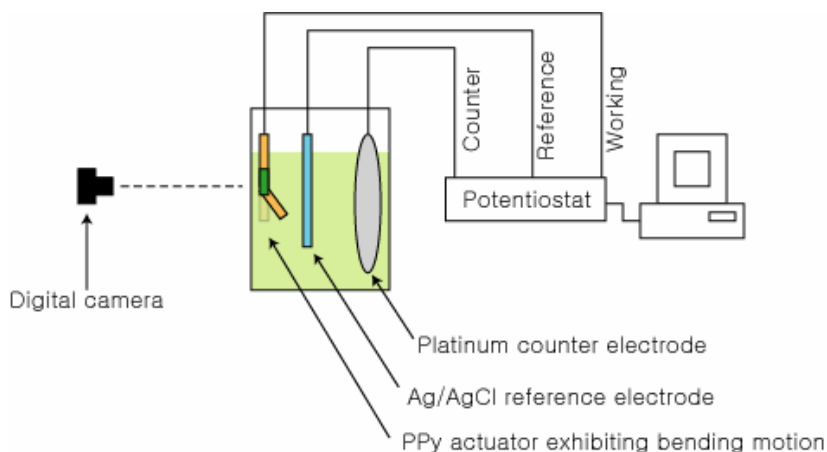
Figure 2-4. Electrochemical setup sketch showing the system used to test the operation of micro-valves in urine.

Results:

From the four samples, a mean angular displacement of 49° with a standard deviation of 22° was obtained (see Figure 2-5). This confirmed that they work in urine as expected from Jager's article [21] and proved that the actuators can be used as valves. However, the standard deviation was unacceptably large, which might have been due to delamination of Au from the Kapton substrate. After 20 voltage steps, the Au layer started to delaminate from the Kapton, which led us to study delamination in Chapter 3.

Prior to the actuation in the urine, the same four samples were actuated in 0.1 M aqueous NaDBS whose pH level was also approximately 7. A mean angular displacement of 84° with a standard deviation of 44° was obtained (See Figure 2-5). Two samples (#1 and 3 in Figure 2-5) showed small difference while the other two (#2 and 4) showed significant difference in the bending angles in different electrolytes; even though the cause of this was not understood, we learned that the actuation bending angle was different in electrolytes containing different types of ions (the simulated urine contains mainly Na^+, K^+, and Cl^-, (see Appendix 6.2)). However, no significant difference in

23

speed was observed; the PPy bilayer actuated in less than 10 sec in both urine and

NaDBS solution.
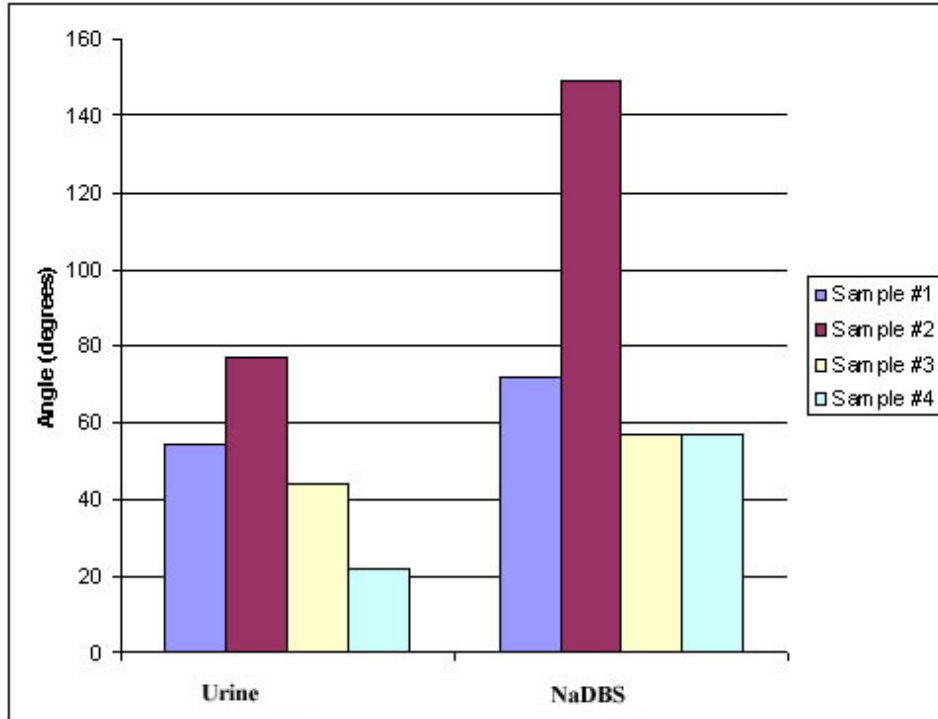
Figure 2-5. Angle measurements in urine and NaDBS solution.

2.5 TESTING AT BODY TEMPERATURE

Motivation:

The ability of the actuator to operate consistently throughout the human body

temperature range is important. For this experiment, the beaker containing urine in

Figure 2-4 was heated on a hotplate. Two samples were tested in the temperature range of

30 to 42 °C. While this range was a little extreme for normal temperature (30 and 42 $^{\circ}$C

would cause hypothermia and brain damage, respectively), we wanted to make sure that

our testing range was well outside the limits of what would be expected.

Results:

Figure 2-6 shows the actuator angular displacements plotted against temperature. The results show a small increase in angular displacement with increase in temperature. As long as the valves can actuate in this range of temperature, which was proven in this experiment, the small increase in angular displacement is not a concern.
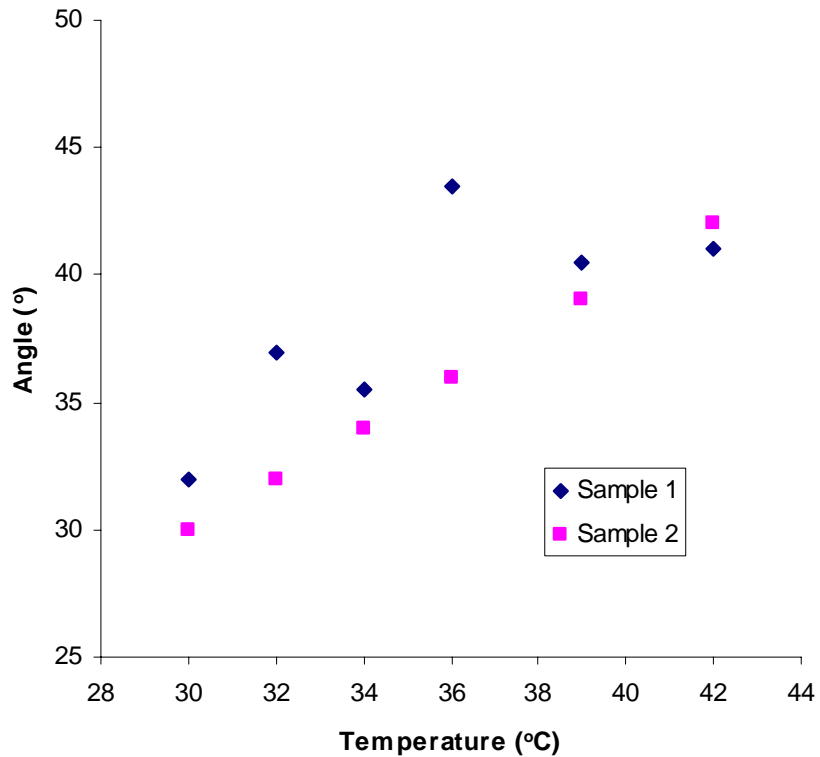
Figure 2-6: Angular displacements observed in urine at varying body temperatures (range 30-42 °C).

2.6   PH TESTING

Motivation:

The pH level of urine varies from 4 to 9. Regardless of pH level in urine, the actuator must work consistently without much difference in bending angle. The previously described electrochemical setup was used to test actuators at various pH levels.

25

Aqueous solutions of 0.1 M NaDBS with different pH levels (9.0, 8.2, 7.0, 6.0, 5.1, and 4.0, monitored using a pH meter) were prepared by adding sodium hydroxide (NaOH) or hydrochloric acid (HCl) to the neutral NaDBS. However, introducing mobile anions, Cl⁻ to the NaDBS solution can interfere with the actuation of the bilayer [38]. Each device was actuated by applying potential steps from 0 to −1 V. Due to delamination of Au from the Kapton substrate, 4 new samples were used for each pH level.

Results:

Figure 2-7 shows the normalized actuation angles plotted against pH. The data were normalized against neutral pH, 7, because of large standard deviation in the data, which might be due to the delamination. As observed in the plot, the actuation angle is independent of pH. The average standard deviation was about 8°. These results confirm the prior literature indicating that the material will function at the relevant pH levels [26].
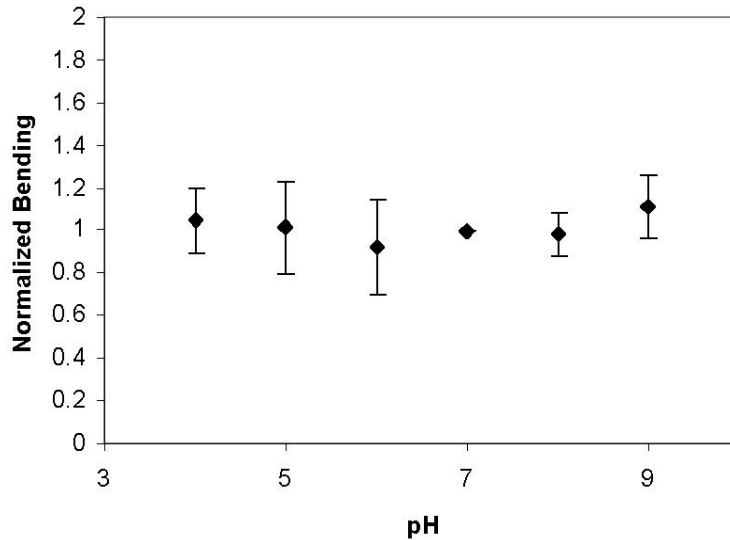
Figure 2-7. **Normalized bending angle of actuator in different pH levels from 4 to 9. For this experiment, 4 samples were used, and each sample was actuated at each pH level. Then, the bending angle data point at each pH level was divided by the bending angle at pH 7 (the control value) to obtain the normalized bending angle values. Finally, the normalized bending angle values from the 4 samples were averaged.**

2.7   STATIC PRESSURE TESTING IN BLADDER-URETHRA SETUP

Motivation:

When urine accumulates in a human bladder, the pressure on the bottom of the bladder increases. A normal full bladder creates approximately 20 cm of water pressure. However, the actuator has to work under extreme conditions that may arise from patient activities that increase the pressure on the bladder (such as sneezing). In the pressure range of 10 to 110 cm of water, two new actuators were evaluated. Regardless of this level of pressure, the actuators should be able to rotate the flaps.

Experiment:

A plastic column setup (Figure 2-8) was developed to observe the performance of the actuator under the typical pressures encountered in the human bladder. The plastic

column setup was made by gluing a transparent acrylic pipe to a plate; transparent acrylic was used to allow us to see the actuation of the valve through the pipe or plate. Prior to gluing the two pieces, two holes were drilled into the plate; one is to insert an Ag/AgCl reference electrode, and the other one is to insert a gold screw. The purpose of the gold screw is to hold the actuator on the plate and to apply step voltages to the PPy bilayer at the same time. For the counter electrode, a sheet of flexible Kapton evaporated with gold was used. During the gluing of the pipe and plate, the sheet of Kapton was sandwiched between them with one end of the Kapton sheet outside the container. This is so that a potentiostat can be clamped on the Kapton counter electrode in order to apply voltage.

Static pressure tests were performed by varying the pressure heads from 10 to 110 cm of 0.1 M aqueous NaDBS on the actuator.
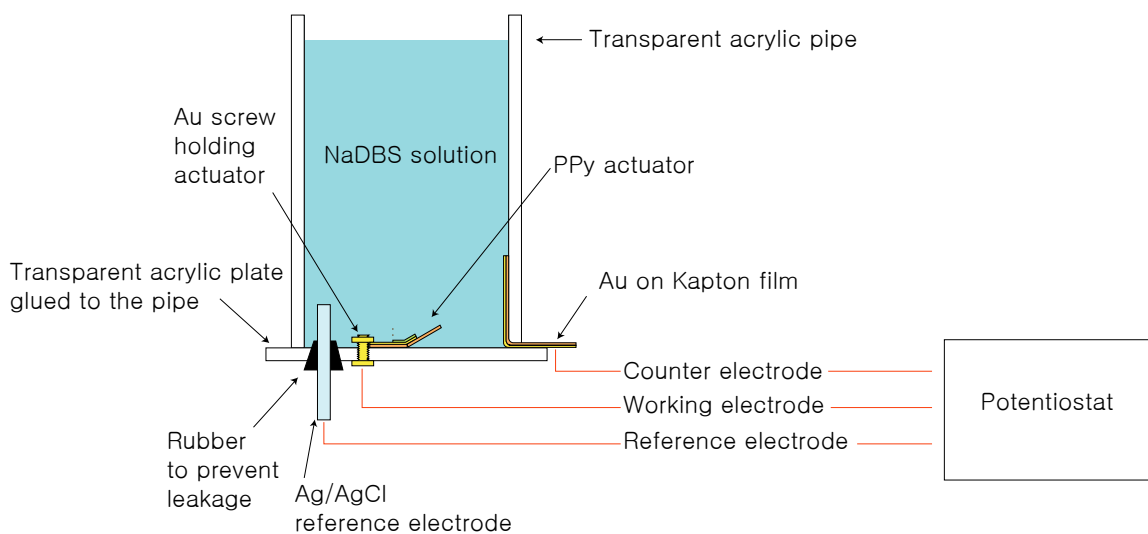
Figure 2-8: Micro-valve pressure test, in which the bilayer was able to bend (corresponding to valve open state) and straighten (valve closed state) under pressures ranging from 10 to 110 cm of water.

Results:

The actuators bent 180° in all the cases, showing that they work in the pressure range of 10 to 110 cm of water.

2.8   DYNAMIC PRESSURE TESTING IN BLADDER-URETHRA SETUP

Urine gets accumulated and stored in the bladder, and then it must be drained when the micro-valves open. Thus, it was important to confirm that the valve could open under some pressure and to drain an aqueous solution. During this test, design flaws of the design were learned through trial and error. There were 4 attempts, which led to a successful design.

2.8.1   1st Attempt

First, a hole (3 mm in diameter) on the bottom of the plastic column (see Figure 2-8) was drilled. Then, the actuator was placed over the hole. Figure 2-9 shows the setup.

We noticed that there was significant leakage between the actuator and the hole. However, the actuation was attempted anyway. Even with a small amount of leakage, the PPy actuator did not move at all in this setup. Apparently, the PPy/Au bilayer did not have enough strength to work against pressure and leakage flow of aqueous NaDBS.
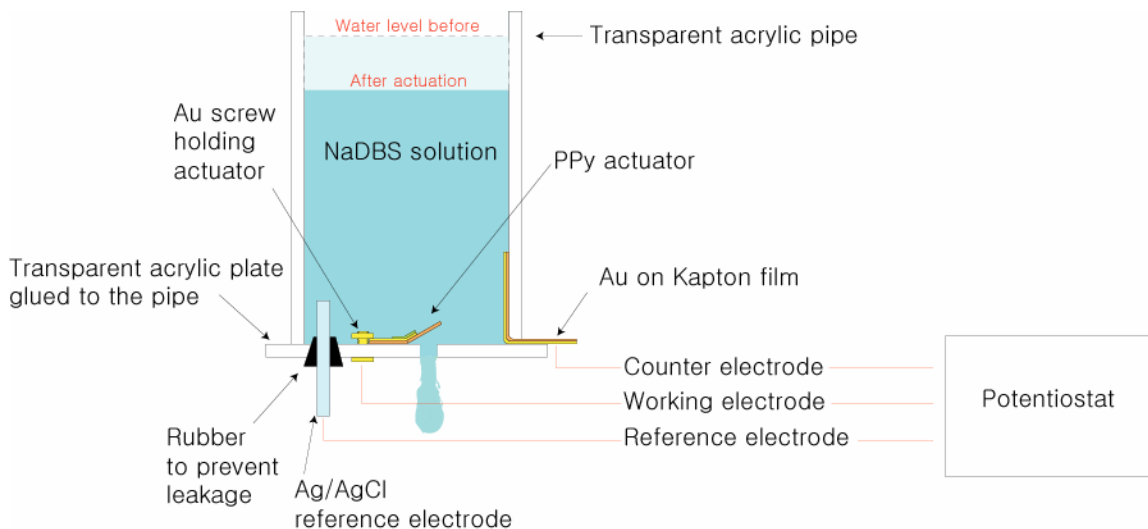
Figure 2-9. A setup sketch of micro-valve pressure test. Voltage was applied to the valve while water was flowing through a hole (3 mm in diameter).

2.8.2   *2nd Attempt*

In order to give more power to the hinge to work against the flow, the actuator design was modified to have 22 PPy/Au hinges in series as shown in Figure 2-10. This actuator was used in the setup of Figure 2-9. Thus, instead of pushing a flat plate against the water pressure, the actuator would curl. However, this design was also unable to overcome the force generated by fluid leaking through the hole; only a few front hinges that were not covering the hole could bend.
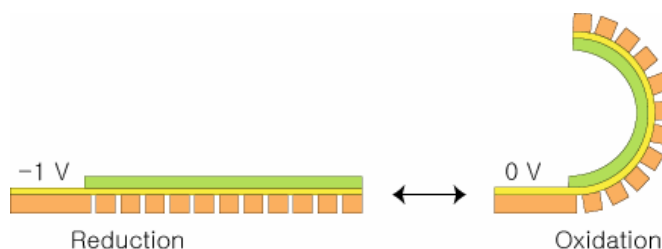
Figure 2-10. Curling actuator with multiple PPy/Au hinges.

2.8.3   3rd Attempt

IN the two setups above, there was only one hole the fluid was gushing through, which might created too large a force for the actuator to overcome. To prevent this, PPy micro-valves, a top piece with an array of 72 PPy actuators (Figure 2-11 (A)) and a bottom piece with a corresponding 72 holes (Figure 2-11 (B)), were designed. Due to surface tension, water did not flow through holes smaller than 300 μm in diameter at a pressure of 10 cm. Holes 300 μm in diameter were etched with an oxygen plasma in the RIE system by using a patterned Al layer as a mask. Under a stereomicroscope, the two pieces were aligned and pressed together after gluing at the extra space on the actuator (see Figure 2-11) with commercial Superglue (cyanoacrylate). Finally, these micro-valves were placed over a hole and glued to the acrylic bottom as shown in Figure 2-12.
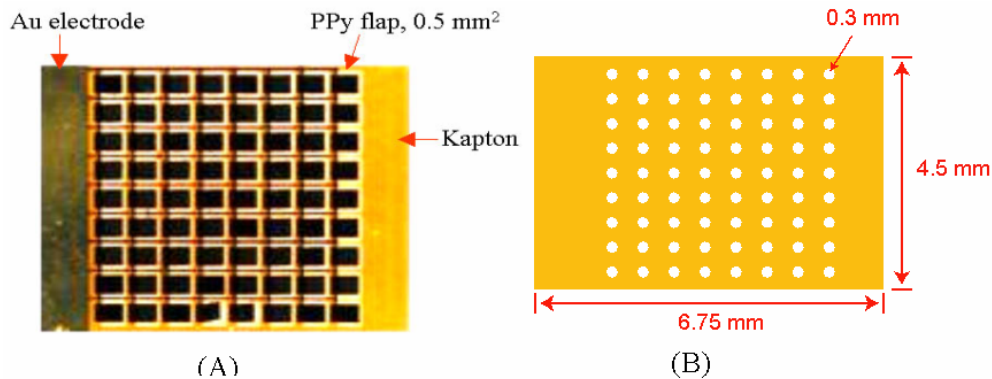
Figure 2-11. (A) is an actual microfabricated PPy flap (top piece), and (B) is a sketch of Kapton bottom piece with multiple holes (300 μm in diameter). Note that extra spaces on left and right edges were used to glue two pieces together and to glue it to the setup apparatus in Figure 2-12.
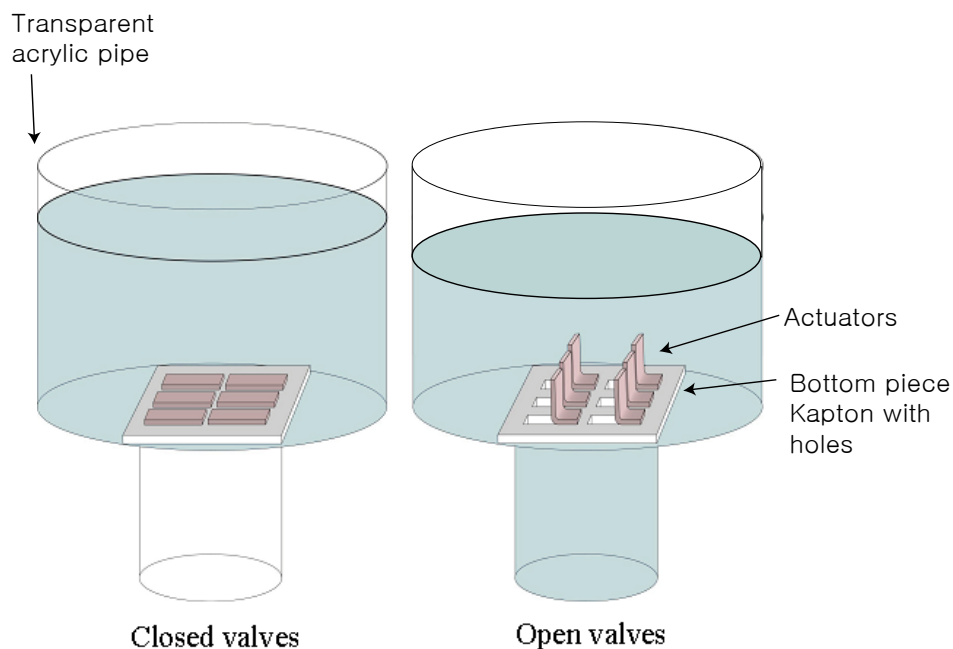
Figure 2-12. Dynamic flow test. Micro-valves were placed over a hole and glued to a plastic bottom plate. Sketches courtesy of IBT.

In this setup, there was a gap between the Kapton sandwich and the bottom plate since only the two edges were glued to the plate, and the Kapton sandwich was bowed. Through this gap, there was a significant amount of leakage. Even though the PPy flaps could open and close, we could not determined if there was a change in water flow due to the leakage, which means that the function of these micro-valves could not be verified.

During the assembly of the two pieces, we observed that glues were likely to spread to the flaps when the two pieces were pressed together. The other problem was aligning the two pieces together, which was carried out under a stereomicroscope after the glue was applied to one of the pieces. This was time-consuming and difficult. Also, the samples were easily wasted if they were misaligned: the glue spread to flaps and could not be removed.

Due to the poor adhesion between the two pieces with the superglue and difficulty in applying the glue on a small area, glue that has better adhesive property and is micro-processable was required. First, two readily available photoresists, Shipley 1830 and Micro Chem SU-8 were tried, but the adhesion to Kapton was very poor; two Kapton sheets came apart easily with a small pulling force. Also, UV curable glues (Norland NOA 68, 72, and 77) were tried by Piyush Seth, but the adhesion was also poor. Even though Kapton film does not chemically react with commercial glues, relatively good adhesion was shown with epoxy and superglue gel. Because the Superglue gel (CVS) was viscous, it did not spread as much as the Superglue. The strongest adhesion was observed when the gluing area on the Kapton was roughened with oxygen plasma in the RIE system (pressure: 0.3 mTorr, power: 200 Watts, and etching time: 40 min), and then superglue gel was applied. The combination of roughened Kapton and UV curable glue was never tried and should be tried in the future.

2.8.4 Successful Setup and Design

For the previous design, there were 3 layers to test micro-valves: a plastic plate with a big hole, a Kapton sheet with multiple holes, and micro-valves. We believed that there was leakage between each layers. Thus, in order to reduce the leakage, a sheet of Kapton with 0.4 mm holes was directly glued to the end of the acrylic pipe (eliminating the plastic plate) after the top piece shown in Figure 2-13 was aligned and glued to the bottom piece. Also, there were gluing areas on the left and right edges and between the columns of PPy flaps. A viscous superglue gel was applied to those gluing areas to attach the top and bottom pieces. For easier alignment, the PPy flap size was increased to 0.7 mm^2. Figure 2-14 shows the modified setup sketch.
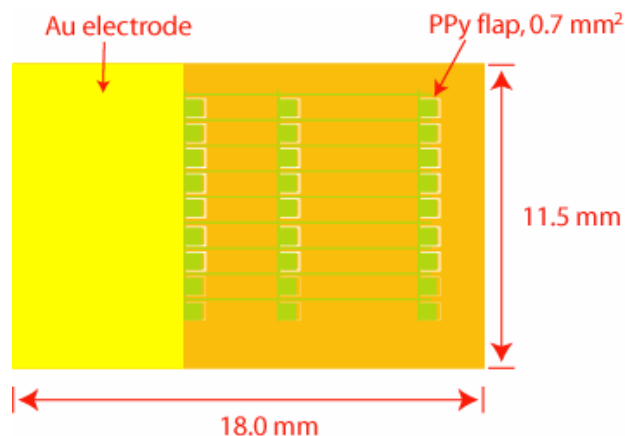
Figure 2-13. Modified design of top piece of micro-valves. The size of PPy flap was increased to 0.7 mm² for easier alignment to a bottom piece with 0.4 mm holes. There are extra gluing spaces on left and right edges and between the columns of PPy flaps.
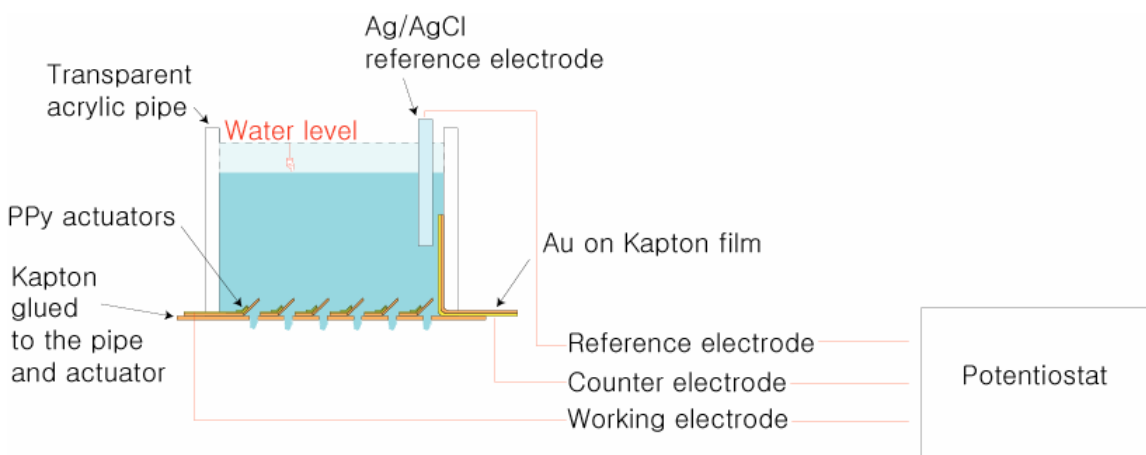
Figure 2-14. Sketch of Successful modified dynamic pressure setup. The bottom plastic plate in Figure 2-12 was replaced with a sheet of Kapton with holes on which PPy actuators were glued.

These micro-vales could successfully open against a flowing aqueous NaDBS under about 1 cm depth of the solution. The change in flow rate was observed and measured; a beaker was placed beneath the setup, and the fluid flow was measured before and after actuation. When the flaps opened and closed, the average flow rate changed from 13.2 ml/min to 8.9 ml/min respectively. Even though there was still a leakage

34

between the two pieces, the feasibility of using PPy micro-valves for application in urinary incontinence was finally established.

2.9   LIFE CYCLE TESTS

Motivation:

The PPy micro-valves have to work for at least 30 days (360 cycles). Step voltages alternating between 0 V and –1 V were used to determine the maximum number of cycles that the actuator could complete without failure. In initial tests, the actuator withstood only 230 cycles of operation because delamination occurred at the interface of the gold layer and the Kapton. Thus, the lifetime of the actuator had to be increased.

Oxygen plasma treatment was reported to improve the adhesion between Al and Kapton [39]. Therefore, we tried this to improve the adhesion between gold and Kapton.

Experiment:

The Kapton film was etched for 40 min under 0.3 mTorr at 200 Watts, which etched about 14 μm of Kapton. Then, the fabrication process sequence in Figure 2-1 was followed. The peak-to-peak roughened surface is about 2.0 μm. After the etching, the Kapton surface changed from hydrophobic to hydrophilic. The lifetime was tested with 5 new actuators by applying step voltages.

Results:

The actuators performed 5000 cycles in the urine without failing. This is an order of magnitude (13 times) longer than desired for our application. However, even though

the bilayer of PPy and Au adhered well to the roughened Kapton, the Au electrode where the voltage was applied delaminated with a slight touch.

2.10 POWER CONSUMPTION

Motivation:

In a human bladder, only tiny batteries can be inserted and used to actuate the micro-valves. To see whether the PPy actuators could be powered for 1 month with a tiny battery, the power consumption of the actuators was determined.

Results:

Using a potentiostat, the actuators were electrochemically actuated. The charge and discharge energy (i.e. the energy to actuate and relax) of the device was measured 10 times as shown in Figure 2-15. By integrating the current in Figure 2-15, the power required for the actuator to open and close 8 times (i.e. the average number of female urinations per day, which IBT gave us) is 0.067 mA-hr. Additionally, the power required to maintain the closed state of the actuator for 24 hours was determined to be 1.14 mA-hr. The power was consumed in order to maintain the closed valve because the PPy has to be kept reduced by applying -1 V (when the application of voltage is stopped, the PPy inherently gets oxidized instantly). The total power consumption per day is therefore 1.21 mA-hr, and a total power consumption of 36.3 mA-hr will be required for 30 days. To give a sense of perspective, typical AA batteries deliver 1200 mA-hr, and a small silver oxide battery provides 110 mA-hr of power (Energizer No. 301, 11.6 mm in

diameter and 4.2 mm in thickness). Thus, the silver oxide battery can be used to operate the micro-valves for at least 30 days.
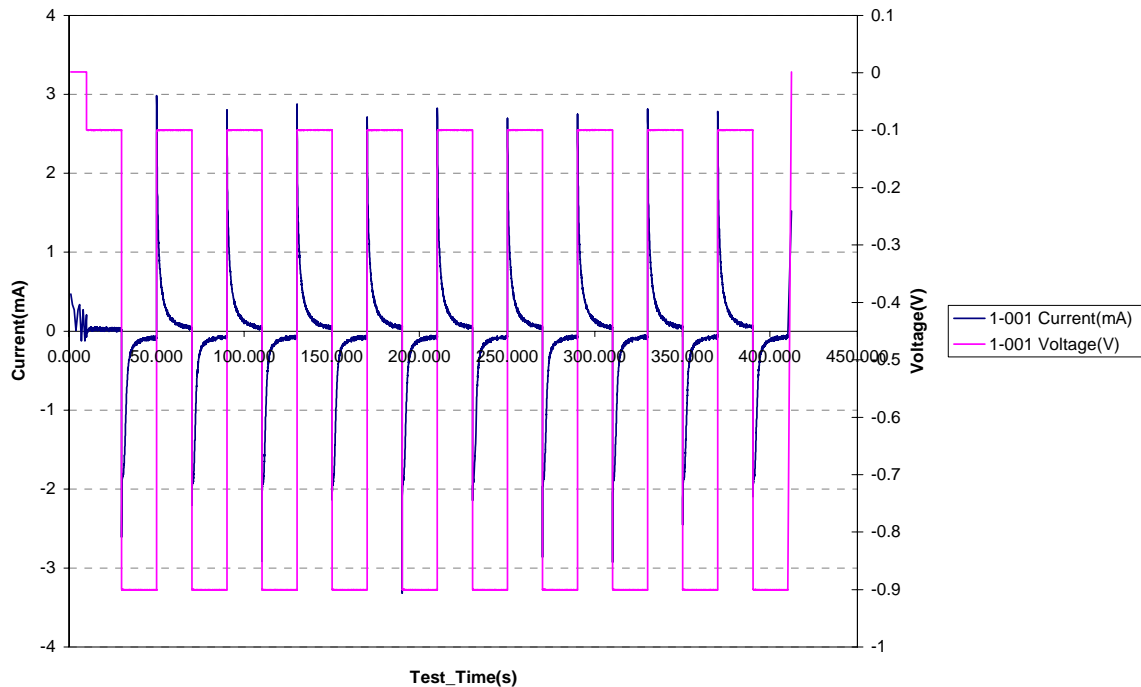
Figure 2-15. Current and voltage vs. time. Voltage switched between -0.1 to -0.9 V since PPy is fully oxidized and reduced at these values.

2.11 FAIL-SAFE

Motivation:

In case there is a loss of electrical signal or batter power, the valve should automatically open. Our fail-safe design takes advantage of the inherent properties of PPy. Without an applied potential, it spontaneously reverts to its oxidized (valve open) state in the presence of oxygen. If the battery runs out, the PPy(DBS) micro-valves thus automatically open due to a loss of reducing potential.

Experiment:

In order to validate this fail-safe mechanism, the PPy actuator was tested in the static pressure setup shown in Figure 2-8 . The sample was initially powered with a constant voltage of −1 V vs. Ag/AgCl, which maintained the actuator in the reduced or closed state. The potentiostat was then unplugged, disconnecting the power.

Results:

In open circuit, with no applied potential, the actuator returned to its oxidized or open state. In other words, the micro-valve will open to allow the bladder to empty in case of electronic or power failure.

2.12 CONCLUSIONS

The PPy actuators were tested, and they met the specifications in Table 2-1, showing that PPy bilayer can potentially be used in micro-valves for urinary incontinence. However, during actuation, delamination of Au from Kapton was observed. Thus, the delamination problems at different interfaces were thoroughly studied to increase the lifetime, which is described in Chapter 3. Another problem was that the micro-valves were able to actuate under only 1 cm of the NaDBS solution during the dynamic pressure test. In order for PPy actuators to have enough force to work against the flow of urine in human bladder, the hinge design had to be studied, and this work is presented in Chapter 5.

Table 2-1. Specification of PPy actuator.

	Specification	Prototype micro-valve
Operation environment	Urine	✓ Operates in urine
Operating temperature	$30 – 42^{\circ}C$	✓ $30 – 42^{\circ}C$
Operating pH	$4 – 9$	✓ $4 – 9$
Operating pressure	10-110 cm of water	✓ 10-110 cm of water
Dynamic operation	Opens flow of fluid	✓ But only 1 cm
Lifetime	360 cycles	✓ 5000 cycles
Power consumption	110 mA-hr/30 days	✓ 36.2 mA-hr/30 days
Fail safe	Opens under power failure	✓ Opens when power is cut off

2.13 RECOMMENDED FUTURE WORK

There was a major problem of leakage when the dynamic pressure test was performed. The PPy micro-valves could not completely close and seal holes to prevent the leakage. Thus, better sealing the top and bottom pieces will be necessary.

3 DELAMINATION STUDIES

3.1 OVERVIEW

During the fabrication and actuation processes in Chapter 2, we encountered several delamination problems. While operating the actuators, Au delaminated from the Kapton substrate, and PPy delaminated from Au. In addition, Al delaminated from PPy during the fabrication. Because of these delaminations, a lot of samples had to be made for the experiments in Chapter 2 because one sample could withstand only a few cycles of actuations. Another problem with delaminations was irreproducible results; there were large standard deviations in the experimental results in Chapter 2. Therefore, in this chapter, I present methods to improve adhesion at these interfaces (Figure 3-1). The delamination studies were done in collaboration with Yingkai Liu and Abraham Daiub, who are students of Dr. Smela; Abraham Daiub and I worked together on the 1st interface, and Yingkai Liu and I worked together on the 3rd interface.
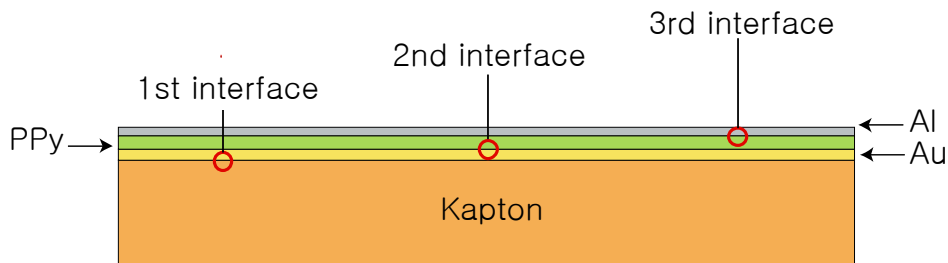
Figure 3-1. Three interfaces where delamination occurs: 1. Kapton/Au, 2. Au/PPy, 3. PPy/Al.

In order to test the adhesions at the 1st and 2nd interfaces, we used a tape test, as illustrated in Figure 3-2. The tape test is the most commonly used way to test adhesion between evaporated metal and substrate since it is cheap and fast. It is a threshold test to verify if evaporated metal sticks better to the tape than the substrate. In our lab, tape tests

were used to test the adhesion between Kapton and Au, and the adhesion between the

PPy and Au. We used Scotch Tape (3M). The tape was placed on both the top and

bottom of the sample. The bottom tape held the sample in place while the top tape was

used to test the adhesion. After the top tape was pressed gently with a finger tip to

remove the air gap between the tap and surface, it was slowly peeled from the edge of the

sample.
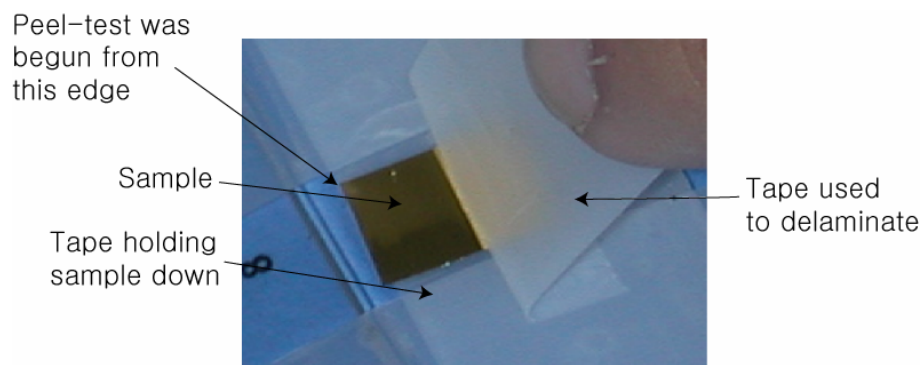
Figure 3-2. Illustration of tape-test. The tape completely covers the sample.

3.2   1ST INTERFACE, KAPTON/AU LAYER

One of the problems we encountered with PPy actuators was that Au adhered

poorly to Kapton during electrochemical cycling. When we applied a square wave signal

between 0 and −1 V vs. Ag/AgCl to the PPy actuators, Au started to delaminate after as

few as 20 cycles. (We cycled from 0 to −1 V vs. Ag/AgCl because we obtain the greatest

strain from PPy by switching the polymer from a completely oxidized state at 0 V to a

completely reduced state at −1V.)

We started by testing whether Au would delaminate from Kapton HN without

electrochemical cycling. We cut four 1 cm x 1.5 cm pieces of Kapton that had been

coated with 2000 Å of Au by e-beam evaporation. We did the tape-test, and Au did not

come off with the tape from the sample. The remaining two samples were submerged in 0.1 M aqueous NaDBS and subjected to a triangular signal from 0 V to -1V vs. Ag/AgCl with a ramp rate of 0.01 V/s for one cycle. The samples were then rinsed and dried and tape-tested. Au delaminated from Kapton HN as it was pulled out with the tape. From these observations, we determined that an electrochemical reaction was causing the Au to delaminate.

In order to mitigate the delamination of Au from Kapton, we pursued four avenues. We studied the effects on the adhesion of Au to Kapton at different Au deposition rate. We also tried annealing Au on Kapton above the glass transition temperature of Kapton and determined its effect on Au adhesion to Kapton.   In addition, we examined the effect of depositing a layer of Cr between the Kapton and Au layers. Finally, we used other types of Kapton film besides Kapton HN.

3.2.1   Plasma-Treated Kapton

Motivation:

Lamendola et al. etched Kapton with oxygen and helium plasmas and reported a great improvement in adhesion between Al and Kapton [39]. The reason to use these plasmas is to remove chemical residues and to introduce "chemical functionalities" on the Kapton surface [40]. We investigated if plasma-treated Kapton would exhibit a good adhesion between Au and Kapton during electrochemical cycling.

Experiment:

A sheet of 50 μm thick Kapton HN was first cleaned with acetone, methanol, and isopropanol. A March Jupiter III reactive ion etching (RIE) system was used to etch the Kapton. Using different powers, pressures, and etch times (Table 1), Kapton was etched in both oxygen and helium plasmas.

Au was thermally evaporated onto these surfaces at 5 Å/sec below 5×10^{-6} Torr. The Au layer did not come off in the tape test. Potential steps from 0 V to –1 V at 5 sec/step in the NaDBS solution were applied to all the samples in Table 1. Current vs. step time showed that the current peak died out in less than 2 sec; this means that the electrochemical reactions were fully completed in less than 2 sec.

Table 3-1. Different powers, pressures, gases, and etch times used to treat Kapton.

Gas	Power (W)	Pressure (mTorr)	Etch time (sec)
Helium	100	150	90
Oxygen	50	150	90
	200	150	90
	200	300	90
	200	300	180
	200	300	2400

Results:

In less than 1 min (approximately 10 steps), all the samples delaminated. During the potential stepping, Au delamination was observed under an optical microscope at

100X magnification (Figure 3-3). When the surface of the Au was touched with tweezers, the whole Au layer peeled off. Thus, these surface treatments were not effective.
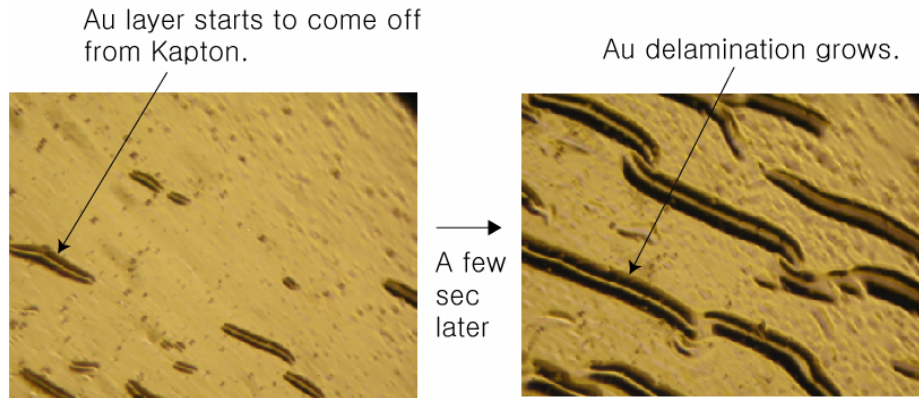
Figure 3-3. Au delamination from Kapton when voltage was applied.

3.2.2   Thermal Treatment of Kapton/Au Interface

Motivation:

This experiment was inspired by work conducted by Zaporojtchenko et al. on the adhesion of Cu to polycarbonate, which showed that annealing a polymer-metal interface above the glass transition temperature of the polymer improved the adhesion between the polymer and metal [41]. In our experiment, we determined if heat treatment of 2000 Å of thermally evaporated Au on Kapton HN would result in a stronger bond between the Au and Kapton.

Experiment:

From a sample of Kapton HN that was coated with 2000 Å of Au, twelve pieces were cut measuring approximately 1 cm x 3 cm. All the pieces were simultaneously warmed from room temperature to 380 °C (the glass transition temperature of Kapton

44

HN: 360 ~ 410°C [42]) in a Pyrex dish on a hot plate as shown in Figure 3-4. The temperature was slowly raised. The temperature as a function of position on the hot plate varied ±5 °C from the set-point (380 °C).
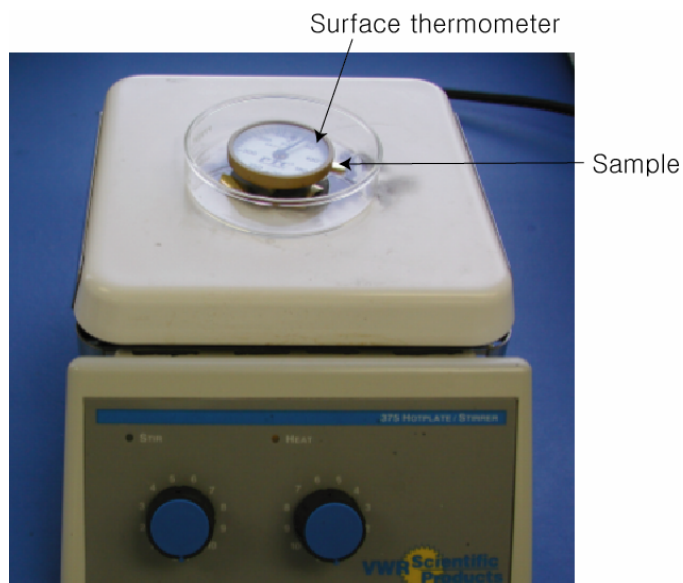
Figure 3-4. Hot plate on which Kapton-HN/Au samples were heat-treated.

After the samples reached the temperature of 380 °C, three samples were removed after 5 minutes. Other samples were removed after 15 min, 30 min, and 1 hr from the time the set-point was reached.

Each sample was tape-tested before cycling, and no samples showed signs of delamination. The samples were cleaned with acetone, methanol, and isopropanol, and DI water. Then, they were submerged in 0.1 M aqueous NaDBS and cycled from 0 V to −1 V vs. Ag/AgCl at 0.5 V/sec using a potentiostat.

Results:

Table 2 shows the results from the tape test of heat-treated samples. Each row on Table 2 shows the duration of the treatment and the number of cycles to failure for each

sample. The results in Table 2 were plotted in Figure 3-5, which shows the average

number of cycles to failure as a function of heating time. Error bars are included for each

average (except for the 5-minute treatment, since all samples failed after the same

number of cycles). All the samples treated for five minutes failed the first time they were

tested, which was after 100 cycles. Had they been tested more frequently, the number of

cycles to failure for the samples treated for 5 minutes may have varied. For the rest of

the samples, they were tape-tested every 50 cycles.

Table 3-2. Data from tape test of heat-treated samples.

Treatment time at 380 °C (min)	Number of cycles before failure for each sample		
	Sample 1	Sample 2	Sample 3
5	100	100	100
15	100	115	150
30	150	200	250
60	100	50	200

**Average Number of Cycles to Failure as a Function of
Heat Treatment Time at 380 deg C**

Figure 3-5. Graph showing average number of cycles to failure as a function of heat
treatment time at 380 °C.

The small increase in the number of cycles to failure suggested that heat treatment
slightly improved the adhesion between Au and Kapton. Heat-treatment for longer time
periods did not yield stronger bonds. In light of these observations, we decided that heat-
treatment was an ineffective method to improve adhesion between Kapton and Au.

3.2.3 Effect of Deposition Rate of Au on Kapton

Motivation:

The evaporation rate of the metal was suspected to affect the adhesion strength at
the polymer-metal interface. We thus explored changing the evaporation rate as a means
to improve the adhesion of Au to Kapton.

Experiment:

We used a new type of commercial Kapton: Kapton-Corona, which is given a
treatment that improves its adhesion to other surfaces. We included Kapton HN in the
experiment so we could compare performances of Kapton Corona to Kapton HN.

We prepared three samples measuring approximately 1 cm x 2 cm of the following materials:

- Kapton-Corona coated with 2000 Å of Au evaporated at

    a. 2 Å/sec.

    b. 5 Å/sec.

    c. 20 Å/sec.

- Kapton-HN coated with 2000 Å of Au evaporated at

    d. 5 Å/s

    e. 20 Å/sec.

Each sample was tape-tested before cycling, and all passed. The samples were cleaned with acetone, methanol, isopropanol, and DI water. Then, they were submerged in 0.1 M aqueous Na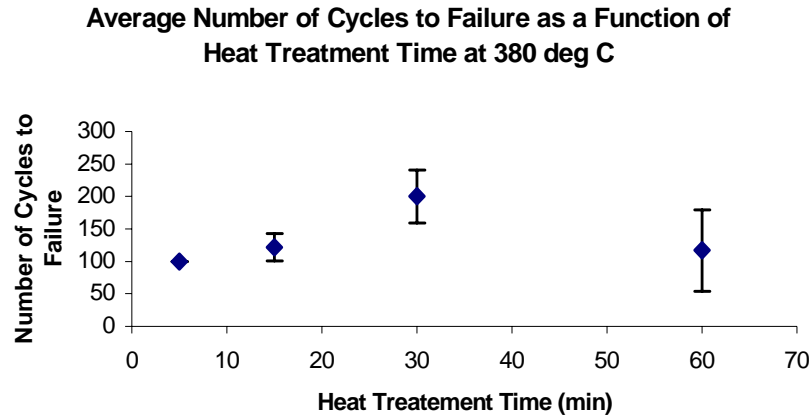DBS and cycled from 0 V to –1 V vs. Ag/AgCl at 0.5 V/sec. Every 50 cycles, the samples were removed from the NaDBS solution and washed with DI water and dried with N_2 gas. After drying, the samples were tape-tested.

Results:

Varying the deposition rate of Au on Kapton did not improve adhesion since all the samples failed after the first 50 cycles. Figure 3-6 show the cyclic voltammograms (CVs) for gold-coated Kapton HN and Corona. The CVs for material produced at other deposition rates were similar. There are no clear oxidation or reduction peaks in these figures, so it is unclear what electrochemical process is causing the delamination.
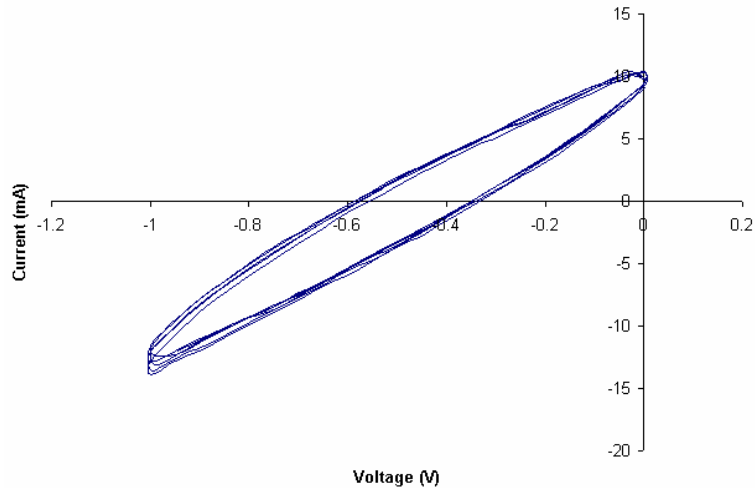
Figure 3-6. CV for Kapton HN on which 2000 Å of Au was deposited at 5 Å/sec.

3.2.4   *Effect of Cr on Adhesion between Au and Kapton*

Motivation:

On silicon wafers, it is necessary to deposit an adhesion layer of Cr (typically 30-200 Å) before depositing Au. Anecdotal reports from Risϕ National Laboratory had indicated that this would make the problem worse. Nevertheless, we were thus interested in exploring the use of Cr to improve the adhesion between Au and Kapton.

Experiment:

In this experiment both Kapton HN and Kapton E were used for a comparison. Since Kapton E absorbs less water than Kapton HN (see Figure 3-7), we hoped that it might have improved adhesion during potential cycling in NaDBS. We reasoned that a form of Kapton that could stop water from reaching the metals would hinder the movement through Kapton of species that play a role in the delamination process.
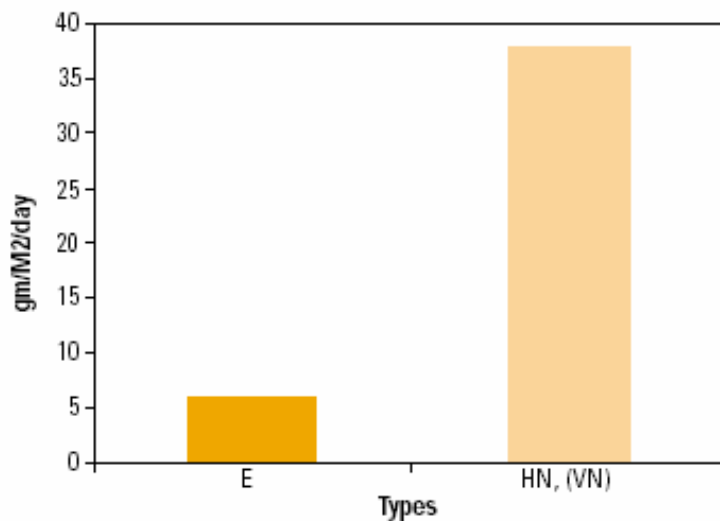
Figure 3-7. Water permeabilities of Kapton E and HN [43].

After cleaning one sheet of Kapton HN and another of Kapton E with acetone, methanol, isopropanol, and DI water, they were dried with N_2 gas. Then, 100 Å of Cr followed by 3000 Å of Au were deposited by e-beam evaporation. The Au-coated sheets were cut into small pieces (1 cm x 2 cm). Each piece was cycled in 0.1 M aqueous NaDBS using a square wave between 0 V to -1 V vs. Ag/AgCl at 3 sec/step. The period between low and high voltages was established as 3 sec since the current flattens out in less than 3 sec, as shown in Figure 3-8; the current does not go to 0 due to reduction of water (splitting water into hydrogen and oxygen gases). The samples were regularly tape-tested to evaluate the adhesion of Au to Kapton, and NaDBS solution was added as necessary to replace any evaporated over time.
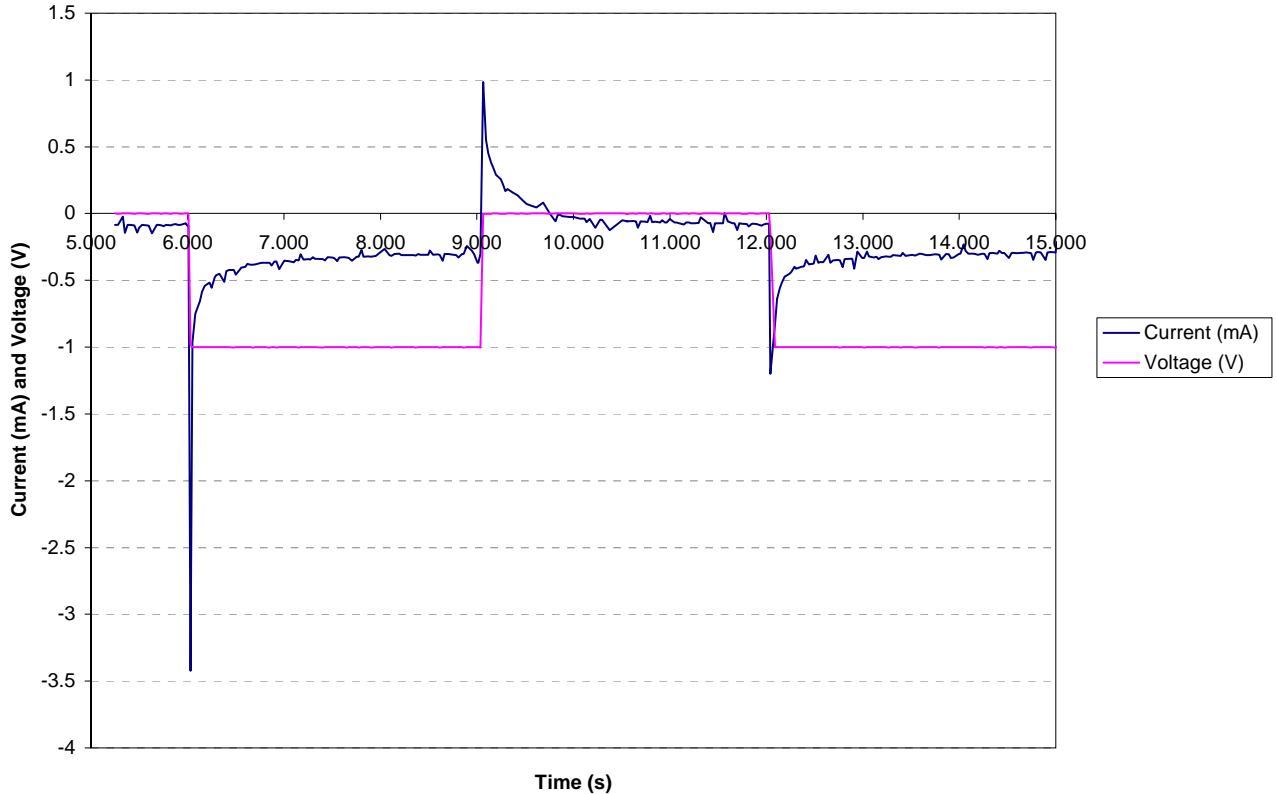
Figure 3-8. Current and voltage vs. time of Cr/Au on Kapton HN. Note that the current spike flattens out in less than 3 sec.

Results:

After 45,000 cycles, all the samples were tape-tested, and no delamination was observed. Thus, the use of Cr layer significantly increases the adhesion between Au and Kapton. From this experiment, we also learned that there was no difference in Au adhesion to Kapton E and HN during electrochemical cycling.

Later in Chapter 5.5, we learned that Kapton substrate should not be cleaned in a piranha solution ($H_2SO_4:H_2O_2 = 1:1$) prior to cleaning it in acetone, methanol, and isopropanol. We believed that cleaning the substrate in the piranha solution would remove any organic contaminants that may have accumulated on the surface of the substrate. However, the lifetime of actuators fabricated with this cleaning process was

51

much shorter than those fabricated without cleaning in the piranha solution. Thus,

Kapton should be only cleaned with acetone, methanol, and isopropanol and rinsed with

DI water.

3.3   2ND INTERFACE, AU/PPY LAYER

When PPy is electrochemically deposited, the PPy chains precipitate onto a

smooth Au surface. Because the PPy does not form any chemical bond with the Au,

there is poor adhesion between them only upon cycling. To create a mechanical bond,

we roughened the thermally evaporated Au by electroplating Au on top of it. We

investigated how this method improved the adhesion between Au and PPy.

3.3.1   *Electroplating Au on Thermally Evaporated Au*

Motivation:

Pyo et al. reported that electroplating Au on thermally evaporated Au helped PPy

adhesion in macroscopic actuators [44]. The surface of electroplated Au is rough because

of the formation of crystals of micron size. It is believed that the PPy grows around these

crystals and mechanically interlocks to the Au surface. Because of this improved

adhesion, the actuation strain also increased, an added benefit [44]

Experiment:
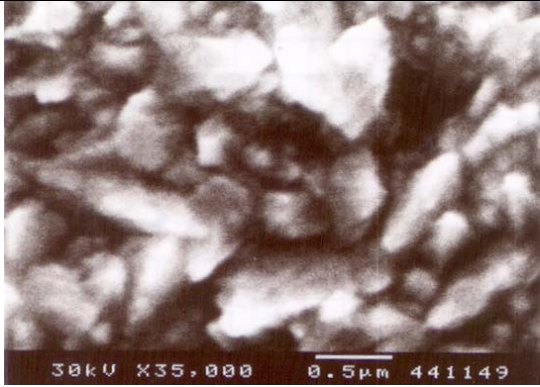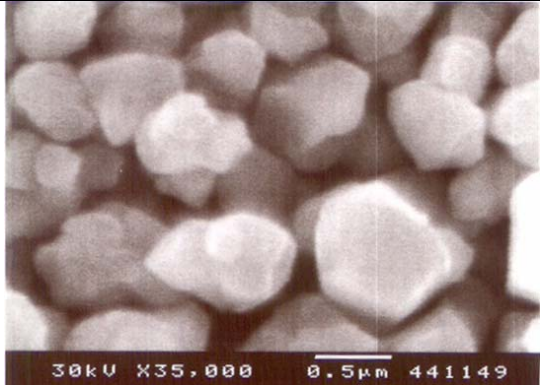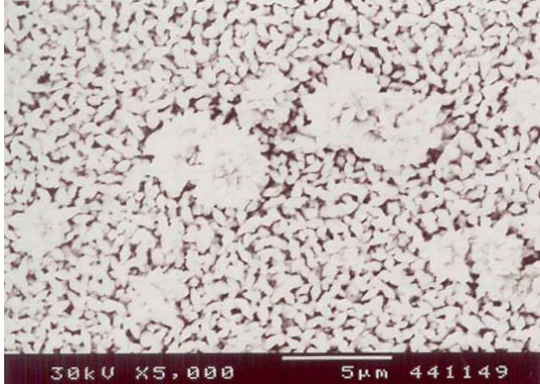
Pyo et al. reported that they obtained the best adhesion by electroplating in a

diluted Au solution (1.7M Na_2SO_3: $Na_3Au(SO_3)_2$ (Oromerse SO Part B) = 3:1) by

applying -0.9 V vs. Ag/AgCl [44]. Their work was repeated in our lab, but we could not

obtain Pyo's crystal shapes, shown in Figure 3-9. Besides, the thickness of Pyo's
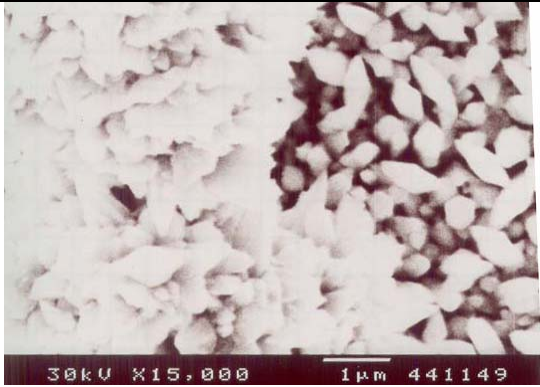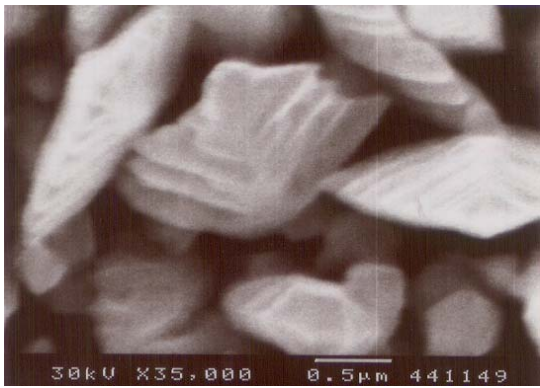
electroplated Au was greater than 5 μm, which was too thick to be used in our micro-

fabricated PPy actuators with a PPy thickness of only 3 μm. Thus, different

electroplating times, voltages, and dilution ratios were used to obtain different crystal

shapes and thinner layers. Before electroplating, 200 Å of Cr and 3000 Å of Au were

thermally evaporated at 5 Å /sec below 5×10^{-6} Torr onto a silicon wafer that was cleaned

with piranha solution (H_2SO_4:H_2O_2:H_2O = 1:1:5). The whole silicon wafer was cut into

many small pieces (about 1 cm x 2 cm) with a diamond pen, and a different piece was

used for each different experiment in Table 3-3. SEM pictures of the electroplated Au

surface are also included in Table 3-3.
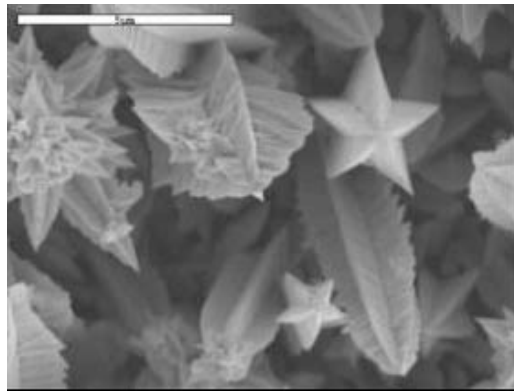
Figure 3-9. SEM picture of electroplated Au. Scale bar is 5 μm long. Figure taken from Pyo et al. [44].

Table 3-3. Electroplating Au with different dilution ratios, electroplating times, and voltages, and the corresponding SEM pictures. Note that magnifications vary.

Sample	Dilution Ratio	Voltage /Time	Surface morphology seen with SEM picture(s)
1	1:3	-0.9V /30min	
2	1:3	-1.2V /10min	
3	1:5	-0.9V /20min	

4	1:10	-0.9V /40 min	

PPy (1 μm thick) was grown on all the samples in Table 3-3 at the same time. Then, potential cycles between 0 and -1 V vs. Ag/AgCl at 0.5 V/sec were applied to all the samples at the same time. The PPy film on Sample #2 first came off in a tape test after 100 cycles. After 400 cycles, the Cr/Au layer from the silicon wafer started to come off from rest of the samples in the tape test, which must have resulted from an inadequate

cleaning process.   To solve this adhesion problem between Cr and Si, a new silicon wafer was cleaned in 49% hydrogen fluoride (HF) acid followed by cleaning in piranha solution (H_2SO_4:H_2O_2:H_2O = 1:1:5).

The day after the electroplating solutions were made, we could no longer electroplate Au uniformly. When Au was electroplated with one-day-old solution, Au electroplated only onto certain regions. Because the electroplating solution is expensive (~$1000 per 1 L), we did not want to make a new solution every time we wanted to electroplate Au. Thus, we had to investigate ways to electroplate Au uniformly in the old solutions, and the following were tried.

1. Dip Au-coated wafer pieces into concentrated Piranha solution (H_2SO_4:H_2O_2 = 1:1)

2. Dip into piranha solution and HF (49%)

3. Dip into Au etchant (Transene)

4. Dip into diluted Au etchant (Au etchant:H_2O = 1:4)

5. Sonicate wafer pieces by using Branson 1510 in methanol for 20 min

6. Piranha etch followed by sonication

7. Initial high voltage (from −1.85 V to −4.0 V) during plating for a short time (1~2 sec)

8. Heated electroplating solution (65°C)

9. New Au electroplating solutions in a new beaker, and a new reference electrode

(Note that 1 to 6 were to clean the Au surface thoroughly, 7 and 8 were to initiate the electroplating process faster, and 9 was to ensure that there were no possible contaminants during plating.)

Step 7 was successful. By using initial high voltages, Au was electroplated uniformly on the Au coated silicon wafer. When the initial high voltage was applied to the sample, a lot of bubbles (hydrogen gas) were formed on the surface. By tapping the sample, the bubbles on the surface were removed. Then, -0.9 V vs. Ag/AgCl was applied to the sample for 40 min using the potentiostat. Initial voltages from –1.7 V to –4.0 V were tried, and uniform Au was obtained below –1.85 V. When –4 V was applied to Cr/Au on the Kapton film, the Cr/Au delaminated. With a –1.85 V initial voltage, Cr/Au delamination was prevented, but there were a few holes (diameter ≈ 10 ~ 100 μm) where no Au was electroplated. It seemed that fewer holes were observed with the highest initial voltage (–4.0 V).

Step 4 was also successful. By using diluted Au etchant (Au etchant:H_2O = 1:4), 100 Å of thermally evaporated Au was etched in 10 min. Then, Au was electroplated onto the etched Au surface by applying –0.9 V vs. Ag/AgCl. With this method, 5 out of 6 samples had uniform Au. We did not investigated how this method affects the adhesion between Au and PPy.

Lastly, we could extend the period of uniformly electroplating Au solution up to one month as long as we used a beaker and a reference electrode that would be used for electroplating Au. This implies that the electroplating solution is very sensitive to other chemicals, such as the surfactant NaDBS. Perhaps a slight bit of NaDBS left on the beakers or RE contaminated the electroplating solution.

With a sample that had uniformly electroplated Au on Au/Cr/Si, 3000 Å of PPy was electrochemically deposited. Potential steps from 0 V to -1 V vs. Ag/AgCl at 5 sec/step were applied to the sample. After 6,000 steps, the tape test was performed on the

sample. Even though the PPy layer did not come off, there was some black PPy powder left on the tape. For this experiment, a Cr/Au coated silicon wafer was used as a counter electrode, and this Cr/Au delaminated after 6,000 potential steps. Also, the color of the NaDBS solution changed to reddish yellow, which might be due to contamination of the solution from the peeled-off metal layer. From this experiment, we learned that Cr/Au evaporated Si wafer should not be used in the lifetime test for the counter electrode.

With another sample that had uniform electroplated Au and 3000 Å of PPy, potential steps were applied by using a graphite counter electrode. (For this sample, a high initial voltage was not used.) After 6800 steps, the sample passed the tape test: there was nothing left on the tape. The potential stepping was stopped after this since we obtained enough life cycles for the urinary incontinence device application. An SEM picture of this plated surface was taken and is shown in Figure 3-10. Before the picture was taken, the PPy was removed in piranha solution ($H_2SO_4:H_2O_2 = 1:1$). This picture looks very similar to the picture of Sample #4 in Table 3.
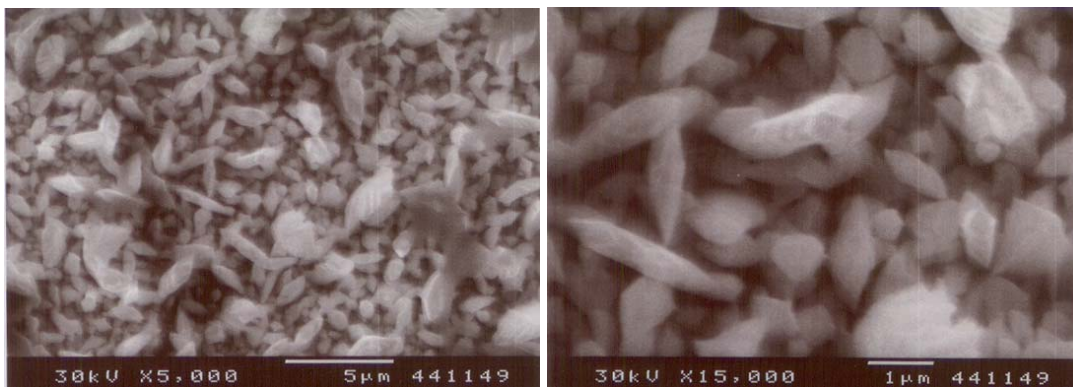
Figure 3-10. SEM pictures of the Au surface of the sample that passed 6800 potential steps.

In trying to confirm the same results as above but using a high initial voltage (-1.85 V) this time, uniform Au was electroplated onto 7 samples, and then 3000 Å of PPy was grown on the resulting rough Au surface. After 6000 potential steps, a tape test was performed, and the PPy did not come off. These results were compared to a sample that had a PPy layer on a smooth Au surface; this sample failed after 10 steps. This showed that electroplating Au dramatically improved the adhesion. An SEM picture of one of these samples after electroplating was taken and is shown in Figure 3-11. The use of the high initial voltage did not change the shape of the crystals we obtained (compare Sample #4 in Table 3 and Figure 3-10).
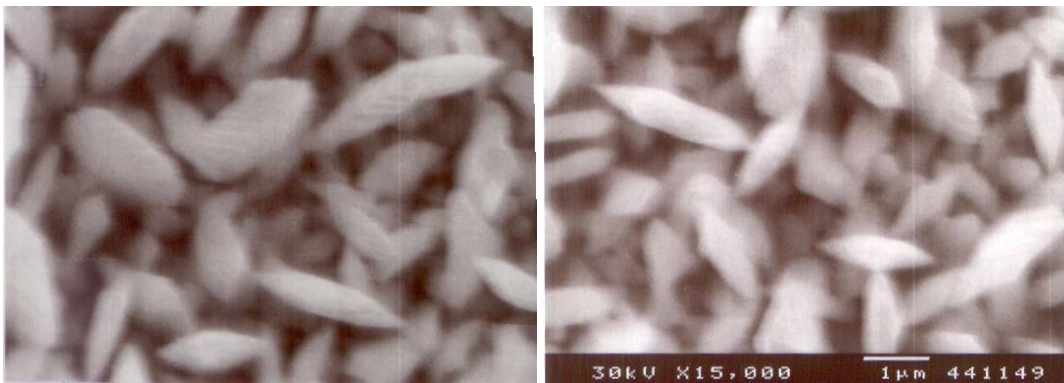
Figure 3-11. SEM pictures of the sample on which the high initial voltage was used. Two pictures above were taken at 15,000X of magnification.

The thickness of the Au film in Figure 3-11 was measured with a profilometer (Tencor Alpha-Step 500); the thickness was about 1.9 μm. Even though this sample's electroplated Au was much thinner than that of Pyo's, it was still too thick to be used in PPy micro-actuators. Thus, thinner electroplated Au was needed. First, we electroplated about 1000 Å of Au on 5 samples for 2 min in 1.7M Na_2SO_3: $Na_3Au(SO_3)_2$ = 10:1 by

59

applying –0.9 V. Figure 3-12 shows that electroplating current constantly decreases

during the 1st 100 sec, but it flattens out after 100 sec, which means that the Au

electroplating rate is not constant for first 100 sec. With 2 min of electroplating time, the

thickness of the electroplated Au on the 4 samples varied from 500 to 1500 Å. An ESEM

picture of a 500 Å thick electroplated Au surface is shown in Figure 3-13.
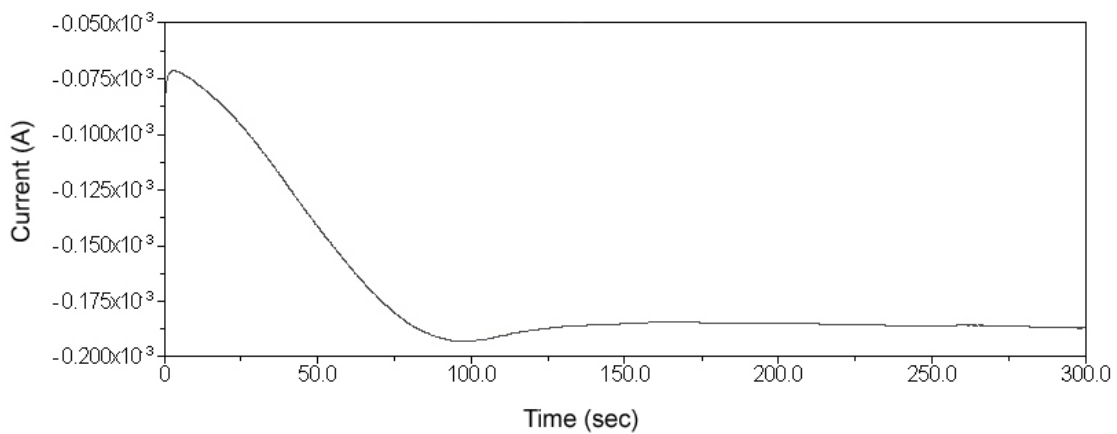
Figure 3-12. Plot of current vs. electroplating time.
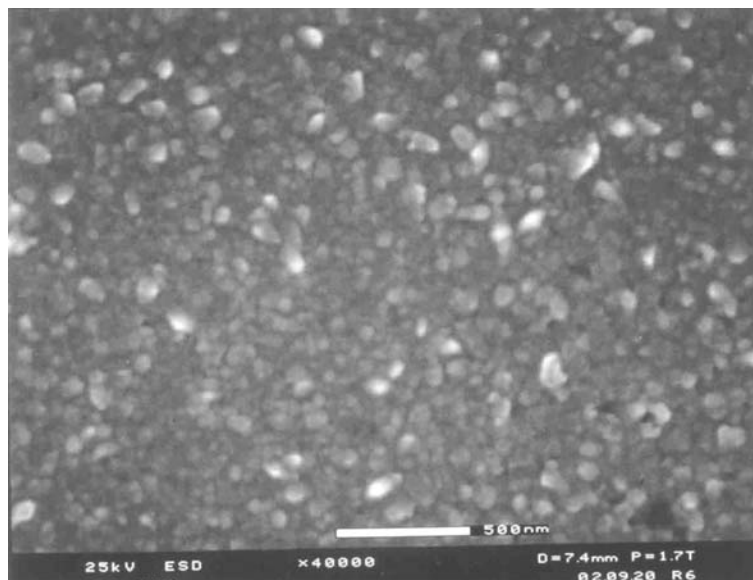
Figure 3-13. ESEM picture of 500 Å thick electroplated Au.

On the 5 samples above, 3000 Å of PPy(DBS) was deposited. Potential steps from 0 V to –1 V at 3 sec/step were applied 60,000 times, and the PPy did not come off in the tape test. However, CVs (Figure 3-14) that were collected after 10, 25,200, 34,200, and 41,400 steps indicate that the PPy becomes electrochemically inactive as the PPy was cycles; there are no oxidation and reduction peaks after 41400 cycles. PPy is known to degrade over time in aqueous solutions [45].
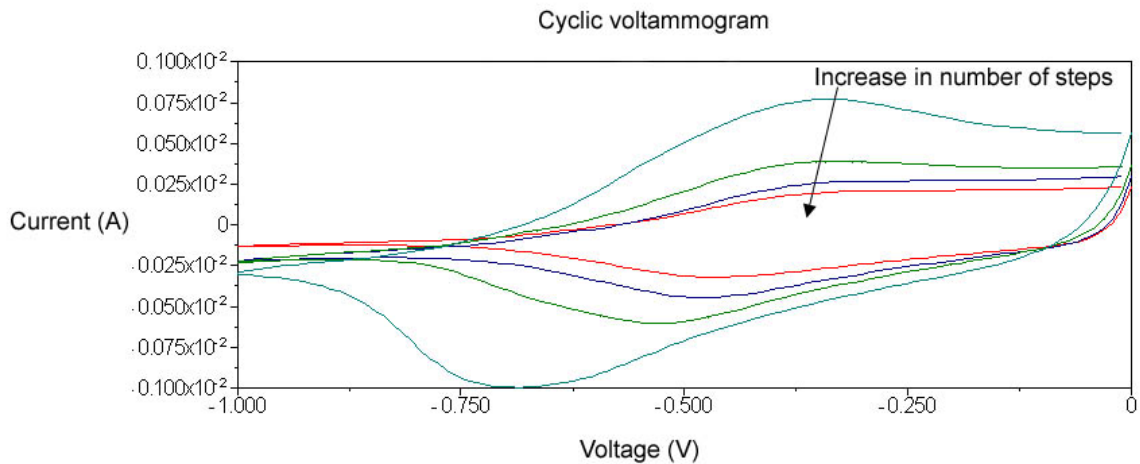
Figure 3-14. CVs after 10, 25,200, 34,200, and 41,400 steps from 0 to –1 V.

3.3.2 *Recommended Future Work*

Even though we now know that 1000 Å of electroplated Au improves the adhesion between Au and PPy, we do not know if 1000 Å of the Au is better than 1.9 μm of the Au. Thus, different thicknesses of Au (1000 Å, 3000 Å, and 5000 Å) should be electroplated and tested for which thickness gives the best adhesion. Also, the thickness that gives the best actuation strain should be determined.

3.4   3RD INTERFACE, PPY/METAL LAYER

In the fabrication of PPy/Au hinges, Al was evaporated on both Kapton and PPy to protect them during oxygen plasma RIE. For these devices, we did not encounter an adhesion problem between PPy and Al. However, in order to design more complicated devices, we planned to fabricate PPy/Au hinges on both sides of the Kapton, for which we had developed a fabrication sequence (Figure 3-15). Compared to the fabrication of one-way folding hinges, the main difference was that we thermally evaporated Al on both sides of the sample to cover the PPy. Then, we patterned the Al in Al etchant (Transene, Type A) after spinning, exposing, and developing photoresist (Shipley 1813).   When the sample was immersed into the Al etchant, we found that the Al wrinkled and came off the PPy. We investigated the reasons for the Al delamination to find a method to solve this problem.

Side View

One-way folding hinges

1. Evaporate and pattern Au on the front side of Kapton

2. Electrochemically deposit PPy on top of Au

3. Evaporate Al on the back side of Kapton

4. Pattern Al by using photo-lithography and Al etchant

5. Evaporate Al on the front side of Kapton; etch Kapton by using oxygen plasma

6. Remove Al on the both sides of Kapton

Two-way folding hinges

1. Evaporate and pattern Au on the both sides of Kapton

2. Electrochemically deposit PPy on top of Au

3. Evaporate Al on the both sides of Kapton

4. Pattern Al by using photo-lithography and Al etchant

5. Etch Kapton by using oxygen plasma

6. Remove Al on the both sides of Kapton

Figure 3-15. Process sequences to fabricate one-way and two-way folding PPy/Au hinges.

3.4.1 Al Delamination from PPy

Motivation:

In the fabrication of two-way folding hinges, Al was evaporated on top of PPy and patterned in photoresist developer (Shipley CD-30) and Al etchant, as shown in steps 4 and 5 of Figure 3-15. During patterning of Al, we speculated that PPy could absorb solutions such as the developer or etchant and swell, causing the Al to delaminate. We designed experiments to verify this speculation.

Experiment:

To test the swelling of PPy during resist developing and Al etching, PPy was deposited onto a patterned Au film on a silicon wafer. We measured the thickness of the PPy with a profilometer. After immersing samples into developer for 30 seconds and Al etchant for 5 minutes (operation times of 30 seconds and 5 minutes were the same as the times used in the fabrication process), the thickness of PPy was measured again.

Results:

Results showed that PPy did not swell in the developer (Figure 3-16), but it swelled a lot, 8%, in the Al etchant (Figure 3-17).   This is why Al came off in Al etchant.
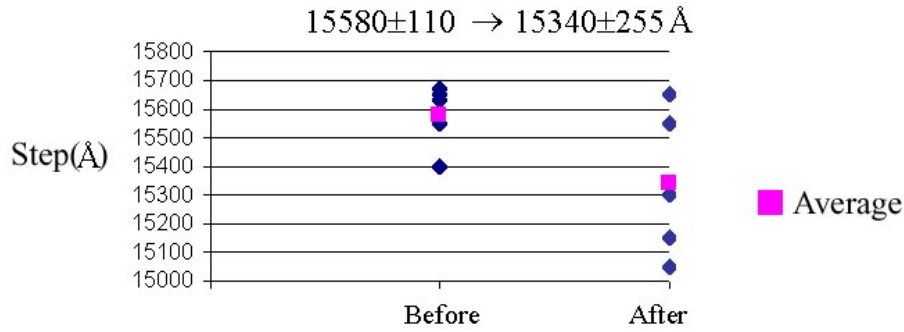
Figure 3-16. Swelling test of PPy in CD-30 for 30 sec.
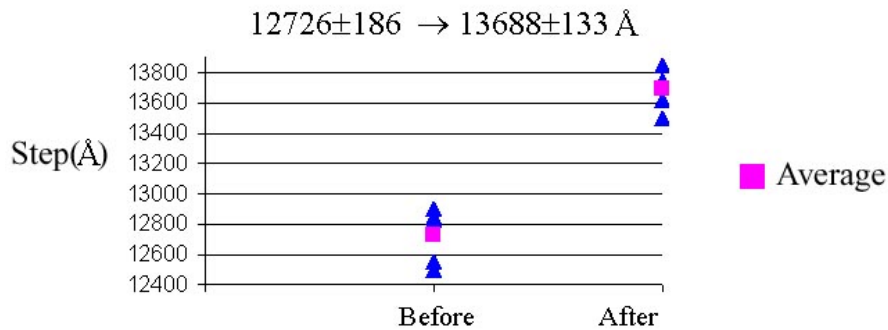
Figure 3-17. Swelling test of PPy in Al etchant for 5 min.

### 3.4.2 *Use of Au to Replace Al*

Motivation:

Since PPy swells in Al etchant, we decided to use Au if PPy did not swell in Au etchant: PPy was deposited onto a Cr/Au coated silicon piece and then immersed in Au etchant. The PPy swelled only a little, 1% (see Figure 3-18). Therefore, we concluded that we could use Au to replace Al in the process sequence. In order to verify this, Au was evaporated on PPy at a rate of 20 Å/sec and patterned by spinning, exposing, and developing photoresist. However, Au came off from the PPy during patterning. We tried to solve this adhesion problem in three ways: 1) deposit an adhesion layer, 2) deposit a transition layer, and 3) find an optimal Au evaporation rate.

Figure 3-18. Swelling test of PPy in Au etchant for 5 min.

Results:

Based on the experience that Cr improves the adhesion of Au on silicon, Cr was tested as an adhesion layer between PPy and Au. PPy(DBS) (2 μm thick) was electrochemically deposited on a piece of Cr/Au coated Kapton. Cr (100 Å thick, 10 Å/s) and Au (2000 Å thick, 20Å/s) were evaporated onto the PPy(DBS). All the samples passed the tape test. Then, Au and Cr were patterned in Au and Cr etchants after spinning, exposing, and developing photoresist. After taking the samples out of Au etchant, no color or other changes were observed by the naked eye. Thereafter, the samples were rinsed with DI water and then immersed in the Cr etchant. The color of PPy(DBS), which was previously dark green, faded. The CV shown in Figure 3-19 was run to check the electrochemical activity. In this CV, there is no oxidation peak, which means that the Cr etchant degraded the PPy, in agreement with the literature [31]. Therefore, the use of Cr was abandoned.
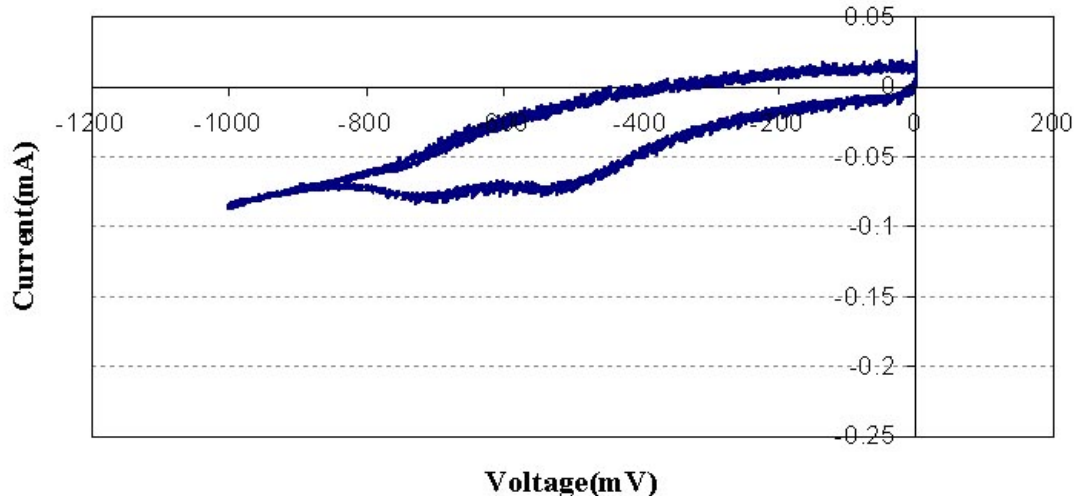
Figure 3-19. Abnormal CV obtained after Cr and Au patterning. Note that there is almost no oxidation peak, although reduction peaks are seen.

Secondly, a thin layer of PPy(Cl) was deposited on top of the PPy(DBS). DBS is a surfactant (such a material is commercially used as a detergent), and perhaps this was causing the problem. Since PPy(Cl) is not soap-like, we expected that it would help the adhesion between the PPy(DBS) and Au. PPy(Cl) was deposited in an aqueous solution of 0.1 M pyrrole and 0.1 M NaCl by applying 0.5 V of vs. Ag/AgCl for 20 sec. Au (2000 Å thick) was then evaporated onto a PPy(DBS) sample deposited with PPy(Cl) and onto a PPy(DBS) sample for a comparison; an evaporation rate of 5 Å/s was used (this was different from the evaporation rate mentioned in "Motivation".) Finally, the Au was patterned, and no delamination was observed. Since there was no obvious difference between the two samples, PPy(Cl) deposition was therefore abandoned in order to reduce number of fabrication steps.

Compared to the Au evaporated at 20 Å/sec, the Au evaporated at 5 Å/sec did not come off during patterning. We speculated that the evaporate rate played an important role in the adhesion between PPy(DBS) and Au. Thus, we repeated patterning Au that

67

had been evaporated at 5 Å/sec, and there was no delamination in any of 10 samples. In summary, we can thermally evaporate Au at 5 Å/sec on top of PPy(DBS) to replace Al and pattern it as a protective layer for the upcoming RIE etching.

3.4.3 Recommended Future Work

All the Au evaporations for this experiment were carried out in a thermal evaporator. In the future, the same experiment should be carried out using an e-beam evaporator to see if we obtain the same good adhesion.

3.5 CONCLUSIONS

For the 1st interface, experiments showed that a 100 Å layer of Cr sandwiched between Kapton and Au is the best method to prevent Au delamination among the different options investigated. For the 2nd interface, the adhesion of PPy and Au improved dramatically by electroplating Au on top of evaporated Au. Finally, for the 3rd interface, Al deposited on PPy(DBS) could not be used fabricate a two-way folding actuator because PPy(DBS) swelled in Al etchant, resulting in Al delamination. Therefore, we replaced Al with Au since PPy(DBS) swell only a little in Au etchant. It was important that Au was evaporated at 5 Å/sec in a thermal evaporator to have a good adhesion.

4   OPTIMIZATION OF FABRICATION PROCESS

Based on the delamination studies in Chapter 3, a modified fabrication sequence was developed, which is discussed in this Chapter.

4.1   FABRICATION

4.1.1   Modified Process Sequence

Figure 4-1 shows the modified fabrication sequence. The Kapton film was cut into pieces of 5×5 cm^2 and rinsed with acetone, methanol, isopropanol, and DI water and dried with N_2.
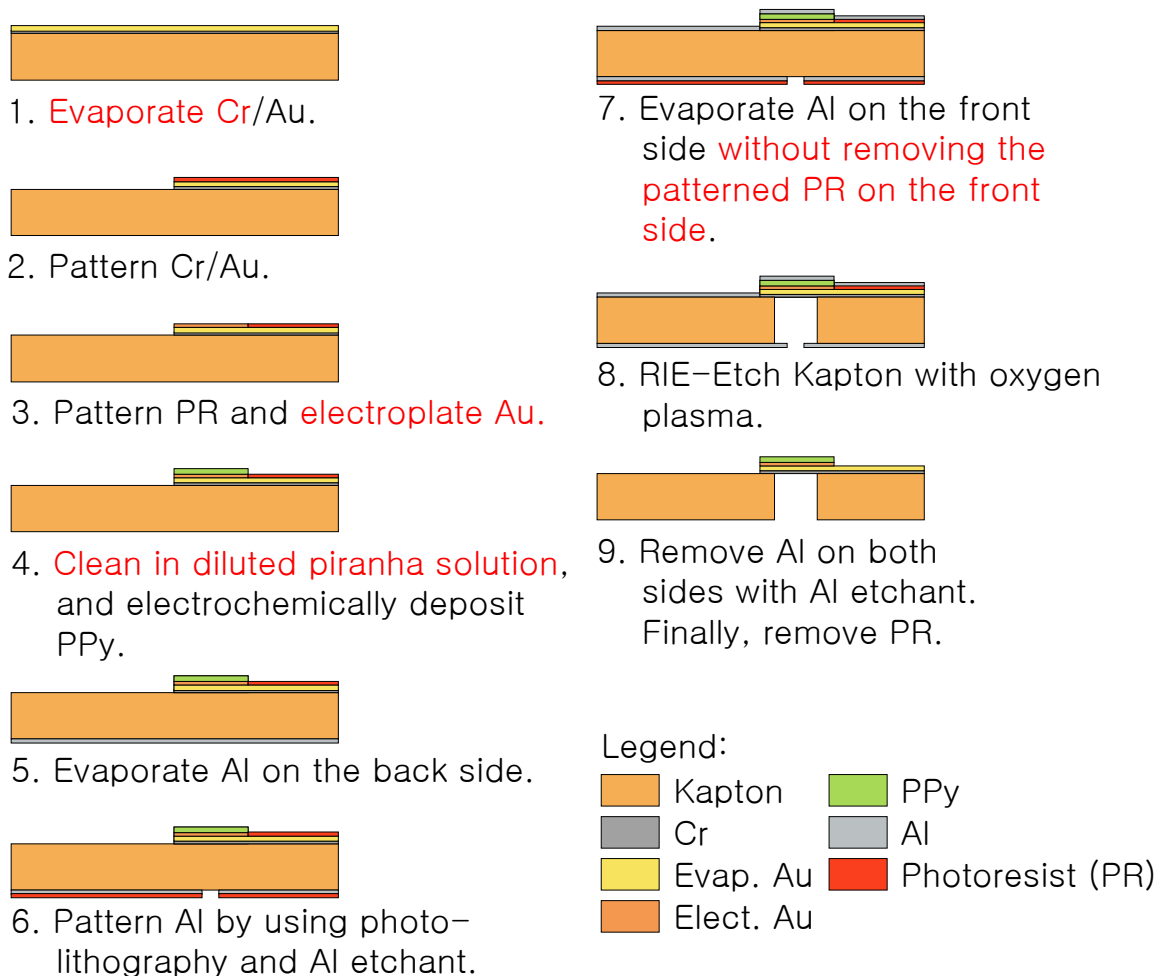
In step 1, Cr (200 Å) and Au (4000 Å) are evaporated (either thermally or by e-beam). In step 2, photoresist (Shipley 1813) is deposited on the Au, exposed, and developed by using 'Au mask' in Appendix 6.3. The Cr and Au are wet-etched (step 2). The patterned photoresist is exposed and developed again by using 'PPy mask' to deposit PPy in a selected area (step 4).

A thin layer of Au is electroplated onto the evaporated Au in a diluted Au-plating solution (1.7M Na_2SO_3: $Na_3Au(SO_3)_2$ (Oromerse SO Part B) = 10:1) by applying –0.9 V vs. Ag/AgCl for 2 min (step 3). PPy is electrochemically deposited after the sample is cleaned in a diluted piranha solution (H_2SO_4:H_2O_2 :H_2O= 1:1:10) for 5 min (step 4).

An Al layer (2000 Å) is evaporated onto the back side (step 5). photoresist is deposited and patterned on the Al layer by using 'Al mask' (step 6). The Al layer, which serves as a mask for the subsequent etching of Kapton using the RIE system (step 9), is etched in Al etchant (step 7). In order to protect the PPy on the other side of the substrate

during the next step, Al is deposited on the front side (step 8). The Kapton is etched with an oxygen plasma under 0.2 mTorr at 250 Watts in the RIE system.

After etching the Kapton, Al layers on both sides are removed (step 9). In step 9, the samples are automatically freed from the rest of the substrate, so no cutting is necessary: all processing steps are photolithographic. In Figure 4-1, step 1, 3, 4, and 7 are different from the process sequence of the 1st generation actuator, and step 4, 7, and 9 are described in detail next.

1. Evaporate Cr/Au.

2. Pattern Cr/Au.

3. Pattern PR and electroplate Au.

4. Clean in diluted piranha solution, and electrochemically deposit PPy.

5. Evaporate Al on the back side.

6. Pattern Al by using photo-lithography and Al etchant.

7. Evaporate Al on the front side without removing the patterned PR on the front side.

8. RIE-Etch Kapton with oxygen plasma.

9. Remove Al on both sides with Al etchant. Finally, remove PR.

Legend:
- Kapton
- Cr
- Evap. Au
- Elect. Au
- PPy
- Al
- Photoresist (PR)

Figure 4-1. Fabrication process sequence. Note that phrase in red means a new step added to the 1st fabrication process sequence in Figure 2-1.

70

4.1.2   New Steps and Fabrication Issues

The purposes of cleaning the sample in the diluted piranha solution in step 4 and

depositing Al on the front without removing the photoresist in step 7 will be explained in

this section. In addition, a remaining fabrication issue of the Kapton etching in the RIE

system will be discussed.

4.1.2.1   PPy deposition (step 4 of Figure 4-1)

Without cleaning the sample in the diluted piranha solution, PPy grows laterally

on Kapton as shown in Figure 4-2. This was because photoresist residue might remain on

the Kapton surface and trigger the lateral PPy deposition. After photoresist was

developed in a developer, I observed a thin layer of photoresist (rainbow color) under a

stereomicroscope at 1000X magnification. In our lab, Abraham Daium (Dr. Smela's

student) observed that PPy grew laterally when there was a thin layer of photoresist on

the Au surface.
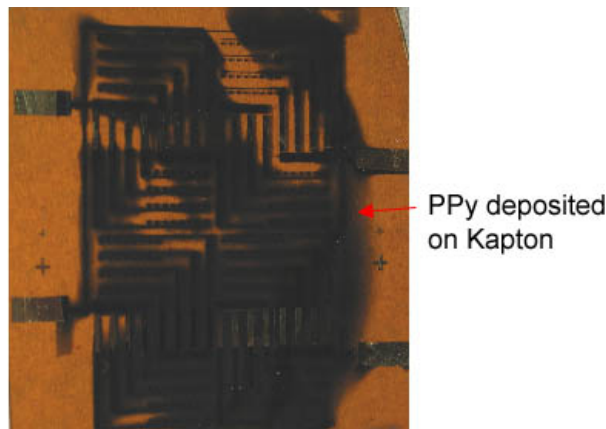
Figure 4-2. PPy grows laterally without cleaning the sample in the piranha solution.

In order to get rid of the thin film of photoresist, a diluted piranha solution

($H_2SO_4:H_2O_2:H_2O= 1:1:10$) was used (the Cr/Au layer delaminated from Kapton in

concentrated piranha solution (($H_2SO_4:H_2O_2= 1:1$)). Also, in the diluted solution, the

patterned photoresist was not stripped off, as it would be in the concentration solution. Instead of the diluted piranha solution, an oxygen plasma could also be used at low power (50 Watts) for a short period of time (30 sec) RIE etch.

4.1.2.2   Front-Side Al deposition (step 7)

In step 7, we keep the patterned photoresist between the Al and Au layers because an Al/Au alloy would be formed if Al was deposited directly on the Au (researchers in at NASA Goddard agreed the result). This alloy was oxidized and then delaminated from the Kapton substrate when voltage was applied in the NaDBS solution (see Figure 4-3).
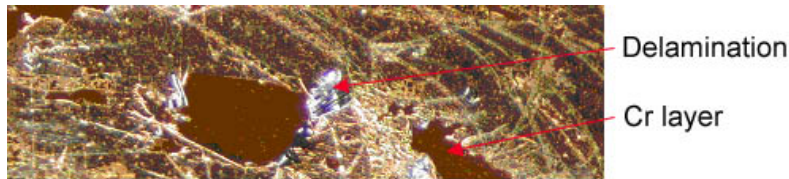
Figure 4-3. Delamination of Al/Au alloy layer when voltage was applied in the NaDBS solution. Note that Kapton color (orage) is shown though a thin layer of Cr.

4.1.2.3   Etching Kapton (step 9)

It was very important that the sample remained flat on the plate of the RIE system in order to ensure uniform etching. The Kapton had a tendency to bow, which could result in the sample's catching fire during the RIE etching. Glass slides were used to hold down the edges of the sample. However, this method was inadequate to flatten the Kapton on the plate and often resulted in non-uniform etching.

If an adhesive was used to attach the front side of the sample to another substrate, such as glass, this would keep the sample flat. Also, with this method, Al deposition on

the front side would not be necessary since the backing substrate protects PPy during the etching. After the etching, the adhesive should be dissolved in a solution.

We found that Shipley 1813 photoresist could be used as an adhesive as long as it was not baked. A Kapton film spin-coated with the photoresist glued well to a glass cover. After the Kapton RIE etching, the sample came off from the glass slide by immersing the sample in CD-30 developer after UV exposure. However, prior to the etching, a lot of air bubbles were introduced between the Kapton and glass slide when the two were pressed together. When the etching was almost finished, the oxygen plasma went into these bubbles and etched the PPy. Similarly, Micro-Chem SU-8 (thick negative resist) was tried, but it could not be used as adhesive for the same reason.

Instead of photoresist, a water soluble wax (Crystalbond 555-HMP) that has a melting point of 65 ^{o}C was tried, but it melted during the RIE etching. Also, acetone and methanol soluble wax (Crystalbond 509 and Crystalbond 590, respectively) that have melting points of 110 and 140 ^{o}C, respectively, were tried, and they did not melt during the etching. Even though this method might succeed, PPy gets dehydrated while dissolving the wax in acetone or methanol after the etching; dehydrated PPy bilayers showed poor bending angles (<10°).

4.2 CONCLUSIONS

A lot of samples (approximately 80%) came out of the RIE system that were unusable, mainly because of the non-uniform etching. This still is an ongoing problem, and plausible causes and possible solutions are listed below. Samples were tested with one of the successful fabrications with fairly uniform etching as described in Chapter 5.

4.3 RECOMMENDED FUTURE WORK

When the Kapton is etched with an oxygen plasma, the etching is faster on the outer edge of the film than at the center, which is an inherent etching property (loading effect [46]). Non-uniform etching could be improved by changing the layout of devices on the substrate. One solution may be to layout devices in a circle, as shown in Figure 4-4. Another would be to increase the area of exposed Kapton on the outer edge of the sample.
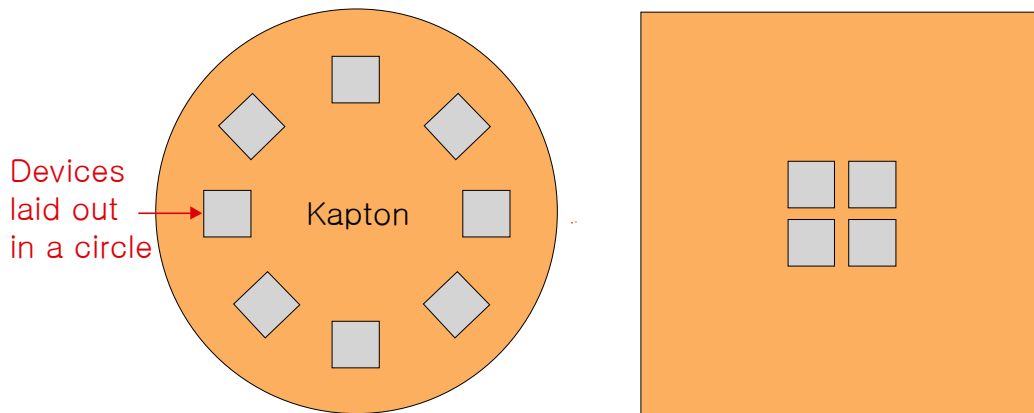
Figure 4-4. Possible device layouts for more uniform etching.

We also observed that one side of the Kapton was etched more than the other side, possibly due to imperfect gas flow in the chamber. Rotating the samples at regular intervals may help to reduce this non-uniformity during etching.

5   OPTIMIZATION OF HINGE DESIGN

5.1   OVERVIEW

During the dynamic pressure test (section 2.8.4), there were two problems with the micro-valves: (1) they opened against a flowing aqueous NaDBS under only a 1 cm depth of the solution, and (2) the flaps bent only about 30~60°. In order to solve the problem of (1), the force exerted by the PPy/Au bilayers had to be increased. The thicker the PPy is, the greater the force it can exert, but the slower the actuation speed. In order solve (2) and obtain a bending angle of 180°, an optimum hinge length is necessary; the larger the hinge length is, the larger the bending angle it produces. We wanted to determine the relationships among PPy thickness, hinge length, force, and bending angle.

5.2   NEW DESIGN OF PPY ACTUATOR AND FABRICATION

Figure 5-1 shows a new sample design that allowed us to collect both bending angle and force data. By using the process sequence in Figure 4-1 with the masks in Appendix 0.3, eight of these samples were fabricated on one sheet of Kapton. There were 4 groups of 2 samples. Each group had a different thickness of PPy (1.25, 1.85, 2.65, and 3.45 μm) deposited on it. Each sample (Figure 5-1) had 4 strips, and each strip had 8 rotating flaps. There were 2 sets of 4 different hinge lengths on every strip. Even though the hinge lengths on the photolithography mask were 20, 40, 60, and 80 μm, actual hinge lengths of 34, 56, 67, and 89 μm were obtained due to the anisotropic etch and undercutting in the RIE system.

To characterize the hinges, a fabricated sample was held vertically in the electrochemical cell, and voltages were applied to one strip at a time. Pictures of that

strip were taken from the top through a stereomicroscope through a digital camera. After the measurements were completed on all 8 flaps, that strip was cut off, and the next one was examined. This was done to remove the bent hinges from the cycled strips from blocking the view of the new one (PPy reverts to the oxidized, bent state after voltage is removed.)
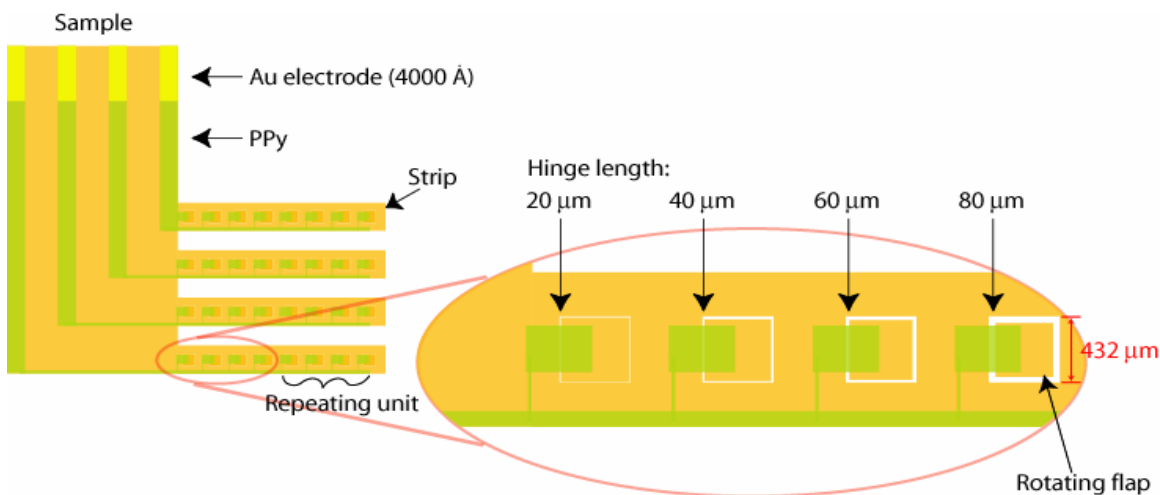
Figure 5-1. Schematic of the new PPy actuator to collect both bending angles and force.

5.3   BENDING ANGLE MEASUREMENT

Figure 5-2 and Figure 5-3 show that thinner PPy thickness layers and longer hinges resulted in larger bending angles. The bending angle data plotted in Figure 5-2 and Figure 5-3 were measured after actuating the flaps 100 times. This was because we observed that there was a "break in" period in which the bending angle increased. Comparing results after 10 cycles and after 100 cycles of actuation, there was more than a 50 % difference in bending angles (see Figure 5-4). In addition, these flaps first actuated backward, and then they gradually shifted to actuate forward after 100 cycles, as shown in Figure 5-4. The cause of the actuating backwards should be determined in the future

because there will be only small bending angles if a bottom plate with a hole is placed to

make a complete valve.
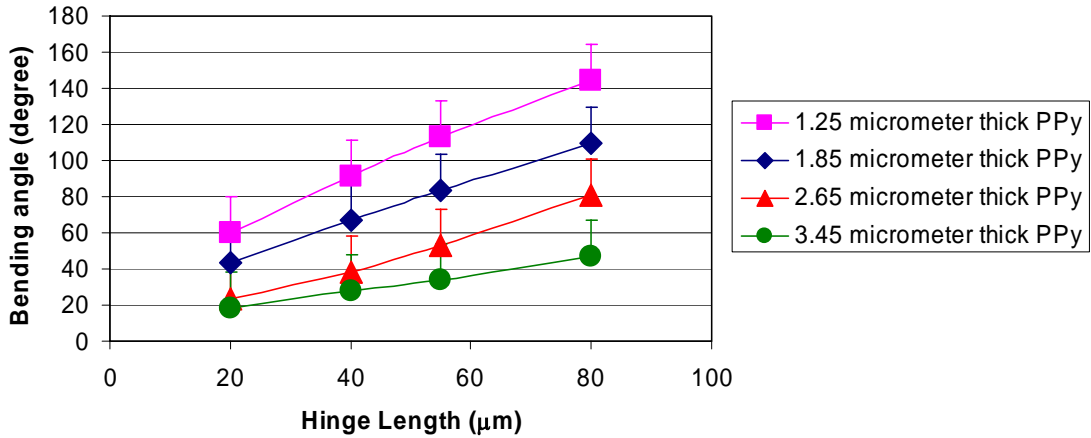
Figure 5-2. Bending angle vs. PPy thickness. The thickness of evaporated Cr and Au was 4000 Å. Note that error bars are shown on the plus side only (there is the same amount of error on the minus side, which is not shown in this graph).
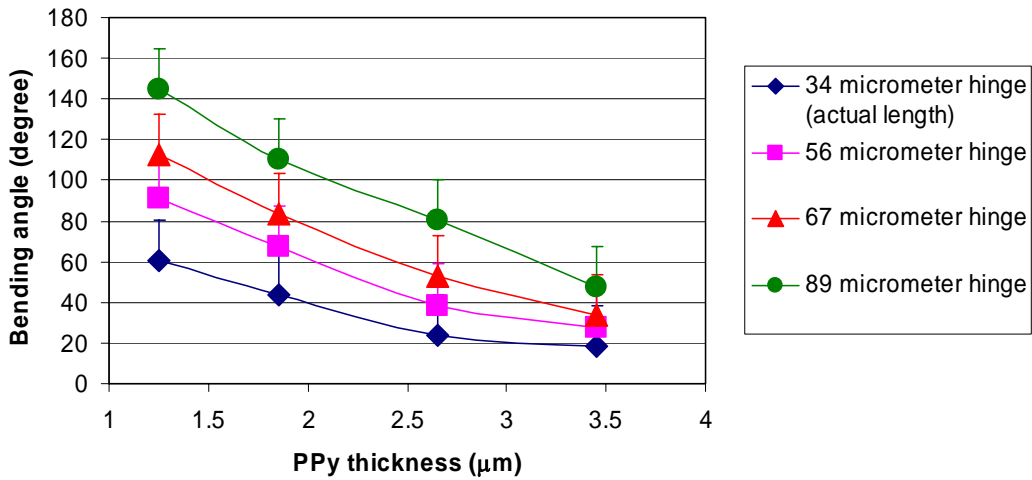
Figure 5-3. Bending angle vs. hinge length. The thickness of evaporated Cr and Au was 4000 Å. Note that error bars are shown on the plus side only (there is the same amount of error on the minus side, which is not shown in this graph).
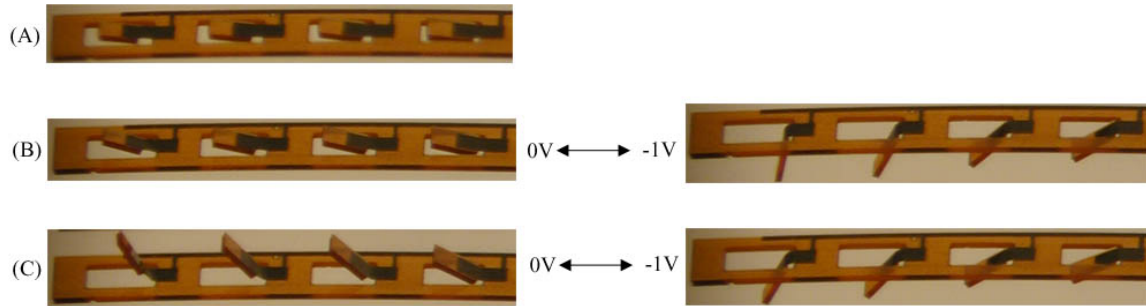
Figure 5-4. (A) is before actuation, (B) is actuation after 10 cycles, and (C) is actuation after 100 cycles. Note that the response time of all the flaps were less than 3 sec.

5.4 FORCE MEASUREMENT

In order to measure the maximum force that the PPy actuators could produce, small weights were placed on the actuators (see Figure 5-5), and the PPy bilayer was actuated. A glass cover slip (0.1 mm thick) was cut into small pieces (1 x 1 mm^2) with a diamond pen. Each piece weighed 0.52 mg. This weight was placed on a flap, and step voltages were applied. The number of weights was increased until the flap could not move the stack anymore. As predicted, the thicker PPy could lift more weights, as shown in Figure 5-6. However, accurate force measurements could not be obtained because the smallest weight I could handle was about 1 x 1 mm^2, which was larger than the size of the flap (0.432 x 0.432 mm^2). Since I could not place the weight perfectly onto the center of the flap, the weight tended to slanted during the actuation, with one of the edges resting on the supporting ground. This caused inaccurate force measurement. This experiment led me to believe that a force transducer must be used in the future to obtain accurate results. This experiment provided the specifications for the force transducer, and as a result an instrument (Aurora Scientific Inc, 406A) was purchased with a sensitivity of 0.01 μN and a maximum loading of 20 mN.

78
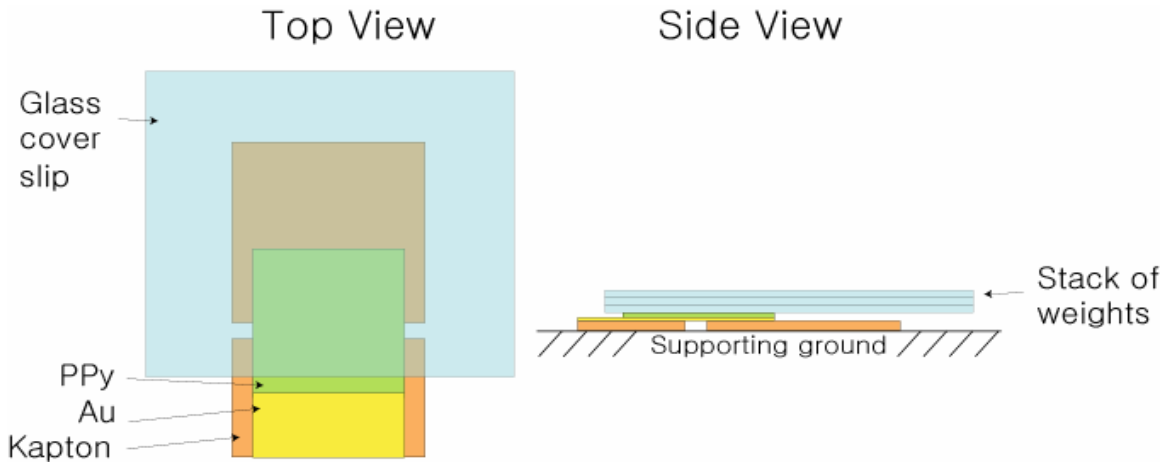
Figure 5-5. A glass cover slip used in force measurement.
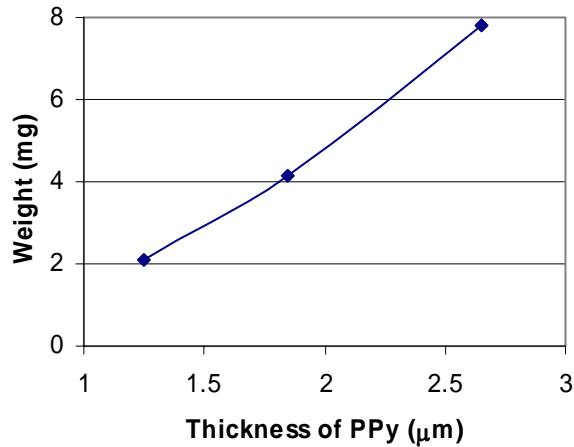
Figure 5-6. Weight (mg) vs. thickness of PPy (μm). Note that hinge length was 89 μm. Since the weight tended to slanted during the actuation, with one of the edges resting on the supporting ground, the error might be less than 50% (probably half of the weight on the flap and the other half on the supporting ground).

5.5   LIFETIME TESTING

After the techniques to prevent the delamination of Au and PPy were developed as discussed in Chapter 3, the lifetime of the PPy actuators was expected to exceed 50,000 cycles. However, samples that had Cr/Au deposited after cleaning the substrate with concentrated piranha solution (H_2SO_4:H_2O_2 = 1:1) failed to function due to Cr delamination from the Kapton substrate after only 350 cycles of step voltages from 0 V to

−1 V. Other samples that were processed after cleaning the substrate with only acetone, methanol, and isopropanol delaminated after 1050 cycles. Thus, prior to the fabrication, Kapton should be only cleaned with acetone, methanol, and isopropanol and rinsed with DI water.

A possible reason for this early delamination is the volume change of the PPy film; contractions and expansions of the PPy on the rigid Kapton might trigger the loss of the adhesion between the bilayer and Kapton.

5.6 CONCLUSIONS

A new PPy actuator was designed to collect bending angle and force. Higher bending angles were observed with longer hinges, and less bending was observed with thicker PPy. With the same actuators, force measurements were tried by stacking weights on them. The thicker the PPy was, the heavier the weight it could lift. However, the exact maximum weights they could lift could not be obtained with these experiments. This led me to believe that a force transducer with a minimum sensitivity of 0.01 μN was required to obtain an accurate maximum force that the PPy actuator could handle.

To fabricate the samples above, the techniques we had developed to prevent delamination were used. In Chapter 3, we had found that PPy/Au bilayers did not delaminate over 50,000 cycles. However, only about 1000 cycles, which is still good enough for the urinary incontinence device, were obtained when these techniques were combined and used to fabricate the actuator.

5.7   RECOMMENDED FUTURE WORK

5.7.1   Further Bending Angle and Force Measurements

Additional samples with different ratios of PPy and Au thicknesses have to be fabricated to complete bending angle measurements. After the bending angle measurements, the samples should be used with the new force transducer to measure their force. This will show the relationships among PPy thickness, hinge length, bilayer force, and bending angle.

We need a model that can predict the force and the bending angle of the bilayer with different ratios of PPy and Au thicknesses and with different hinge lengths. The modeling, however, will not be straightforward because strain and Young's modulus are functions of the applied potential (oxidation level). Furthermore, a strain gradient exists in the PPy film as a result of the electrochemical polymerization process [35].

5.7.2   Electrochemical Cell Configuration Study

In order to use the PPy micro-valves in a Foley catheter, miniaturization and packaging of the electrochemical cell setup is required. The electrochemical setup occupies a lot of space because the CE is typically at least 10 times larger than the WE, and the CE is facing the WE in parallel to ensure uniform electric field. Also, the CE and WE are separated by at least 1~2 cm. Due to the restriction in size and space in a Foley catheter, the minimum size of the CE and minimum distance between the CE and WE have to be studied. In addition, the CE may not be able to face the WE in parallel in a Foley catheter, which should be studied as well.

In order to miniaturize the cell setup, the elimination of the RE or the use of a micro-RE is required. Lewis et al. reported that there was no degradation of PPy film

with a 2-electrode system (without the RE) for 40 cycles [48]. In our lab, this should be tested over 360 cycles in order to eliminate the Ag/AgCl reference electrode. If the 2-electrode configuration is unstable, a micro-RE should be used (Jaget et al. reported that PPy actuators worked well with the micro-RE [47].)

5.8 CONTRIBUTIONS

My contributions to the research and development of a microfabricated, electroactive polymer-based urinary incontinence prevention device are the following.

- Development of PPy micro-valves fabricated on a Kapton substrate.
  - o Designed micro-valves.
  - o Developed the fabrication process.
- Testing the valves at pHs (4-9), temperatures ($30 - 42\ ^{o}C$), and pressures ($10 - 110$ cm of water) to establish the feasibility of using PPy bilayers for this application.
  - o Designed and constructed a valve-testing apparatus that reproduced the pressure in the bladder.
  - o Compared the valve's actuation in urine to that in an aqueous solution of NaDBS.
  - o Calculated the power consumption of the valve to determine if a small silver oxide battery can be used for 30 days.
  - o Tested a fail-safe mechanism (opening the valves automatically) in case there is a loss of electrical signal or batter power.

- Increasing the lifetime of the valves from 10s of cycles to 1000 cycles by adding an adhesive layers of Cr between the Kapton substrate and the evaporated Au, and of electroplated Au between the evaporated Au and the PPy.
  - Tested helium and oxygen plasma treatments to Kapton, thermal treatments to Kapton, and different Au deposition rates as possible solutions to Au/Kapton delamination.
  - Plated and characterized rough Au layers over Au.
- Initial experimental work on the relationships among PPy thickness, hinge length, force, and bending angle.
  - Designed samples and cell holder to allow bending angle measurements.
  - Determined parameters for future force measurements.
  - Obtained preliminary data for future bilayer modeling.
- Development of a process sequence for new micro-valves that required the PPy/Au hinges on front and back sides of a Kapton substrate
  - Found out that PPy swells in Al etchant, but it does not swell as much in Au etchant and CD-30 photoresist developer.
  - Tested Au as a mask during the RIE etching to replace Al.

Two journal articles are in preparation as a result of this work. One paper will focus on the design and performance of the micro-valves for urinary incontinence, and the other will be on the design and characterization of microfabricated bilayer actuators. I shall be the primary author of the first one and a contributing author on the second.

APPENDIX

6.1   **FABRICATION OF FOLDING MICROSTRUCTURES ACTUATATED**

BY PPY/AU BILAYER

FABRICATION OF FOLDING MICROSTRUCTURES ACTUATED BY POLYPYRROLE/GOLD BILAYER

Yingkai Liu[a], Lance Oh[a], Steve Fanning[a], Benjamin Shapiro[b], and Elisabeth Smela[a]
Department of Mechanical Engineering[a] and Aerospace Engineering[b]
University of Maryland, College Park, MD 20742, USA
Tel.: (301) 405-5265, Fax: (301) 314-9477, e-mail: smela@eng.umd.edu

ABSTRACT

We have developed a method to fabricate substrates that can fold themselves. The microstructures are actuated by an electroactive polymer, polypyrrole (PPy). A series of bilayers is defined on one surface of the substrate, and hinges are formed by etching the substrate from the back side to undercut the bilayers. A shape-morphing object is demonstrated that comprises multiple hinges. This object was able to bend both forward and backward. We are applying this technology to fabricate medical devices that operate in bio-fluids.

INTRODUCTION

Researchers have shown increasing interest in forming 3-dimensional structures at the micron scale since the early 1990s. Because standard microfabrication procedures produce inherently 2-dimensional structures, these must be folded to achieve 3-D objects. Various methods have been demonstrated to accomplish this. For example, Pister et al. rotated polysilicon components out of the plane of the substrate on surface micromachined pin-in-staple hinges to assembly a micro-mirror [1]. Brittain et al. patterned metal layers by microcontact printing, and then folded the layers along pre-designed hinges to make micro-origami figures, including a bird [2]. The folding step, however, has typically been realized manually at a probe station. It is time-consuming, and the tiny structures are easily broken by the operation. Thus, it is important to automate the folding.

Different approaches to automatic folding have been demonstrated based on mechanisms that include surface tension forces (using molten solder) [3], thermal expansion [4], and the residual stress of lattice mismatch [5]. These methods are "one-way" procedures: the components cannot go back to their original positions once they are actuated. Reversible folding has been achieved using electrostatic fields [6], magnetic fields [7], and shape memory alloys [8], to name just a few. Based on these techniques, microactuators have been exploited to achieve assembly of microstructures.

Another reason for developing components that can bend out of plane is for actuation. Ideally, microactuators should be robust, produce relatively large displacements, exert sufficient force, and hold fixed positions. A large number of out-of-plane bending technologies have been developed. One of these was our polypyrrole (PPy) bilayer hinge [9,10]. PPy changes volume under electrochemical stimulation when it is immersed in a salt-containing solution (electrolyte). Applied potentials change the number of electrons on the PPy backbone, and to maintain charge neutrality, ions enter and leave the film, producing an in-plane actuation strain on the order of a few percent. The second component of the bilayer is a metal film that serves not only as the electrode, but also to convert the strain in the PPy to bending. The concept is essentially the same as that of a thermal bilayer. In prior work, we have shown that such bilayers can rotate rigid plates with working electrical devices [11] out of the plane of the wafer.

In this paper, we report an extension of the PPy bilayer technology to 1. fold an entire substrate and 2. use polymer substrates such as Kapton instead of silicon. We are developing methods to make self-folding origami; reconfigurable 3D shapes would represent a new capability for MEMS. The ability to fabricate devices on polymer substrates could potentially lead to inexpensive, mass-produced MEMS made by roll-to-roll fabrication processes. In addition, this technology has a number of biomedical applications because PPy actuators operate in body fluids and require only low voltages (typically 1 V or less) [12], and the Kapton has excellent chemical resistance [13]. For example, we are collaborating with Infinite Biomedical Technologies to use this technology to develop a micro-valve to control the flow of fluids in the human body. The basic Kapton hinge concept is shown in Figure 1.
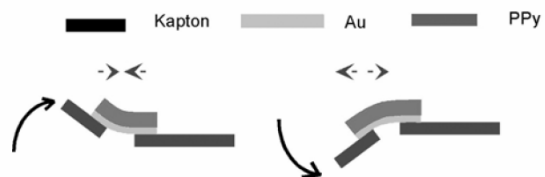
Figure 1. PPy/gold hinge to fold the Kapton substrate.

EXPERIMENTAL

In order to obtain working devices, the fabrication processes were critical. Therefore, we will describe the fabrication methods in some detail.

Process Development. The fabrication process is conceptually simple; it entailed deposition and patterning of a metal layer, deposition and patterning of the PPy, and etching through the substrate, as illustrated in Figure 3. To achieve this, however, careful attention had to be paid to each step, particularly to the interfaces.

Kapton sheets (HN200, 50 μm thick, DuPont Co.) approximately 5×5 cm^2 were carefully cleaned before use with acetone, methanol, isopropanol, and deionized (DI)

water; surface contamination prevented the deposited metals from adhering. An adhesion layer of chrome was either e-beam or thermally evaporated (10 nm, 0.3 nm/sec, $<5\times10^{-6}$ Torr) onto one side, referred to as the front side. A thick layer of chrome was used because the Kapton surface was rough (~60 nm peak to peak). The chrome layer was indispensable: without it the electrodes delaminated during actuation.

A layer of gold was evaporated next without breaking the vacuum (~200 nm, 0.5 nm/sec, $<5\times10^{-6}$ Torr). It is necessary that the electrodes be electrochemically inert; either gold or platinum can be used. The gold was patterned by photolithography and wet etching (gold etchant, Transene), and then the chrome was etched (chrome etchant, Transene) (Figure 3a). After the photoresist was stripped, surface residues left by the chrome etching step were removed in freshly mixed piranha etchant (1 part sulfuric acid, 1 part hydrogen peroxide, and 5 parts water). This was necessary to prevent PPy from electrodepositing laterally over the entire Kapton surface instead of just on the electrodes.
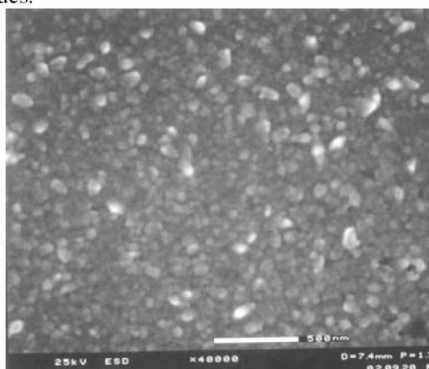
Figure 2. SEM micrograph of a 50 nm thick electroplated layer; nodules increase in size with thickness.

To prevent delamination between the PPy and gold layers during later actuation, we electroplate a rough layer of gold over the thermally evaporated metal (Figure 2). This results in mechanically interlocking the layers [14]. We electroplated at –0.9 V (vs. Ag/AgCl) using a solution of Oromerse SO part B diluted 1:10 with 1.7 M Na_2SO_3. The sample was immersed into this solution, except for the contact pads, and connected to a potentiostat (EcoChemie Autolab). A 150 nm thick layer was deposited in 2 minutes (Figure 3b). The sample was rinsed with DI water.

The pyrrole monomer (Aldrich, stored at –40 °C) was purified by passing it through aluminum oxide. An aqueous solution of 0.1 M pyrrole and 0.1 M sodium dodecylbenzene sulfonate (NaDBS, Sigma) in DI water was freshly mixed. (PPy can be grown in various electrolytes, but NaDBS results in very good actuators [15].) The PPy film was electrochemically deposited onto the gold by applying 0.5 V (vs. Ag/AgCl) until the desired thickness was deposited. (Figure 3c; see [16] for details on PPy deposition). The samples were rinsed with DI water.
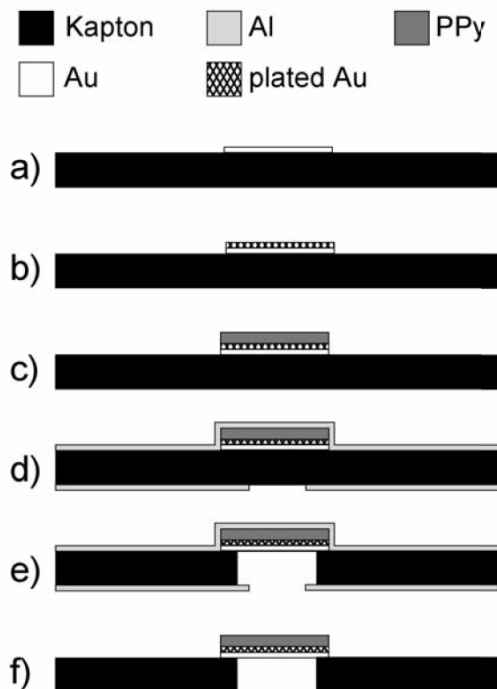
Figure 3. Process sequence for hinge formation.

Next, the aluminum for the back side etching mask was deposited. Just prior to that, the samples were rinsed in methanol and DI water to ensure Al adhesion. The Al was either e-beam or thermally evaporated (200 nm, 0.5 nm/min, $< 5\times10^{-6}$ Torr). This film was patterned photolithographically and wet etched (Al etchant, Transene). Another 200 nm Al film was deposited on the front side to protect the PPy layer during subsequent RIE etching (Figure 3d).
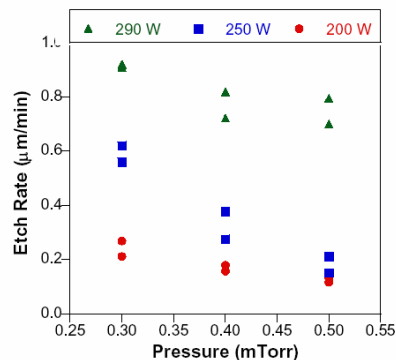
Figure 4. Kapton etch rate vs. pressure & power.

The back side of the Kapton was etched by reactive ion etching (RIE) with an oxygen plasma (March Jupiter III) to form hinges by removing the substrate beneath the bilayer (Figure 3e). The pressure and voltage during RIE were obviously important parameters. At higher O_2 pressures, the etch rate for Kapton slowed (Figure 4) and the Al was damaged; 0.2 mTorr gave good results. At 300 W and 0.2 mTorr, the Kapton etch rate was approximately 1.3 μm/min.

It was also very important that the sample remained perfectly flat on the plate in order to ensure uniform etching. The Kapton had a tendency to bow, which could result in samples catching fire during the RIE etching. The use of weights to hold down the edges of the sample was inadequate. It is best if an adhesive is used to attach the front side of the sample to another substrate, such as glass; we are working to perfect this method.

The last step was to remove the aluminum (Al etch, Transene) from both sides, completing the devices (Figure 3f).

Actuation. The devices were immersed in an aqueous electrolyte (0.1 M NaDBS) and connected to a potentiostat. A voltage cycle (from 0 V to –1 V vs. Ag/AgCl, ramp rate 0.02 V/s) was applied to the device. Upon reduction, the PPy expanded, causing the hinges to bend backwards, and upon oxidation the PPy contracted, bending the hinges forward. Fixed potentials between 0 and –1 V can be used to hold the device in particular positions (Figure 5).
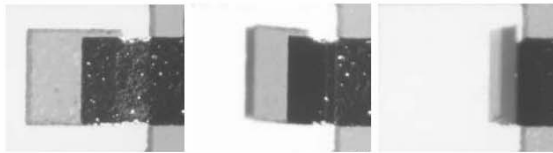
Figure 5. Kapton plate 430×430 μm^2 at 0°, 45°, and 90°.

RESULTS AND DISCUSSION

The PPy is electrodeposited in the oxidized state. When it is electrochemically reduced (-1 V), cations (Na$^+$) enter the film, resulting in volume expansion, and when it is oxidized (0 V), the cations leave, resulting in a contraction.

Figure 6 shows a demonstration device that folds into a sphere. Each segment, 400 μm wide at the center, is actuated by 27 bilayer hinges, each 50 μm wide. Figure 6a shows the device before voltage cycling. When the PPy is oxidized, the segments bend forward (Figure 6b-d). During reduction, they bend backwards into another sphere (not shown).

In order for the PPy to be adopted by the MEMS community, the material needs to be characterized and its behavior modeled. This is not straightforward because strain, stress, and Young's modulus are functions of the applied potential (oxidation level). Furthermore, a strain gradient exists in the PPy film as a result of the electropolymerization process. We have developed simple bilayer bending and force models, and their predictions are shown in Figure 7. The two bending angle curves result from using the Young's modulus of the oxidized, 0.45 GPa, and reduced, 0.2 GPa, states of PPy(DBS) [17] and a gold film modulus of 50 GPa [18]. We are verifying these curves experimentally with angle and force measurements for samples with different PPy and gold thickness ratios. These data will allow us to refine the models.
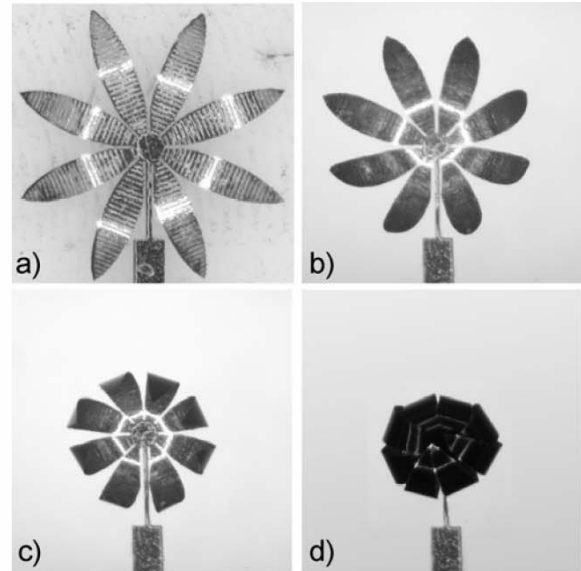
Figure 6. Multi-hinged surface folding into a sphere. The diameter of the unfolded structure is 3.5 mm.
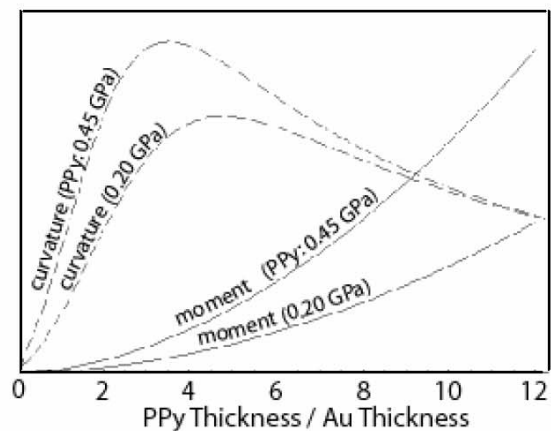
Figure 7. Predicted bending angle and moment as a function of PPy:gold thickness ratio (normalized).

The next step in this project will be to fabricate devices with hinges on both the front and back sides of the substrate. One of the challenges we have overcome was delamination of the protective aluminum on the front side over the PPy during Al etching. This was due to swelling of the PPy in the aluminum etchant, which produced cracks, holes, and peeling of the aluminum layer. Using a gold layer to replace the aluminum solved this problem. The remaining fabrication challenge is the RIE etching. Because both front and back sides of the substrate need to be etched, we must devise a method to protect the delicate, free structures during the second RIE step.

SUMMARY AND CONCLUSIONS

We have developed a microfabrication technique to create PPy/gold bilayers on polymer substrates. By

controlling the applied electrochemical potential, the substrate can be folded automatically and reversibly by the bilayers. In particular, rotating plates and a 360° curved surface have been implemented. This technique provides an approach to fold two-dimensional components to form three-dimensional, complex structures at the micron scale. The devices have potential biomedical applications due to their biocompatibility, low operational voltage, and operation in bio-fluids. Currently, we are applying the techniques reported here in the development of a microfluidic valve for use in the body. More complicated folding devices with bilayers on the both sides of the substrate are also in progress. Characterization of the bilayers and the PPy material is being performed to build models that predict device performance.

ACKNOWLEDGMENTS

REFERENCES

1. K. S. J. Pister, M. W. Judy, S. R. Burgett, and R. S. Fearing, "Microfabricated hinges", *Sens. Act. A* 33, 249-256 (1992).

2. S. T. Brittain, O. J. A. Schueller, H. Wu, S. Whitesides, and G. M. Whitesides, "Microorigami: Fabrication of small, three-dimensional, metallic structures", *J. Phys. Chem.* 105, 347-350 (2001).

3. R. R. A. Syms, "Equilibrium of hinged and hingeless structures rotated using surface tension forces", *J. Microelectromech. Syst.* 4(4), 177 -184 (1995).

4. T. Ebefors, E. Kälvesten, and G. Stemme, "New small radius joints based on thermal shrinkage of polyimide in V-grooves for robust self-assembly 3D microstructures", *J. Micromech. Microeng.* 8, 188-194 (1998).

5. P. O. Vaccaro, K. Kubota, and T. Aida, "Strain-driven self-positioning of micromachined structures", *Appl. Phys. Lett.* 78(19), 2852-2854 (2001).

6. M. J. Daneman, N. C. Tien, O. Solgaard, A. P. Pisano, K. Y. Lau, and R. S. Muller, "Linear microvibromotor for positioning optical components", *J. Microelectromech. Syst.* 5(3), 159-165 (1996).

7. I. Son and A. Lal, "A remotely actuated magnetic actuator for microsurgery with piezoresistive feedback", 2nd Annual International IEEE-EMBS Special Topic Conference on Microtechnologies in Medicine & Biology, Madison, Wisconsin, USA, 2002 p. 332-336.

8. P. Krulevitch, A. P. Lee, P. B. Ramsey, J. C. Trevino, J. Hamilton, and M. A. Northrup, "Thin film shape memory alloy microactuators", *J. Microelectromech. Syst.* 5(4), 270-282 (1996).

9. E. Smela, O. Inganäs, and I. Lundström, "Controlled folding of micrometer-size structures", *Science* 268(23 June), 1735-1738 (1995).

10. E. W. H. Jager, "Microsystems Based on Polypyrrole Microactuators: Microrobots and Cell Clinics", PhD Thesis, Department of Physics and Measurement Technology, Linköpings universitet (2001).

11. E. Smela, "A microfabricated movable electrochromic "pixel" based on polypyrrole", *Adv. Mat.* 11(16), 1343-1345 (1999).

12. E. Smela, "Conjugated polymer actuators for biomedical applications", *Adv. Mat.* 15(6), (2003).

13. D. P. Birnie, "Rational solvent selection strategies to combat striation formation during spin coating of thin films", *J. Mater. Res.* 16(4), 1145-1154 (2001).

14. C. C. Bohn, M. Pyo, S. Sadki, E. Smela, J. R. Reynolds, and A. B. Brennan, "In-situ measurement of conducting polymers on evaporated and electrochemically deposited Au surfaces", *Chem. Mater.* (accepted), (2003).

15. Q. Pei and O. Inganäs, "Electrochemical applications of the bending beam method; a novel way to study ion transport in electroactive polymers", *Sol. State Ion.* 60, 161-166 (1993).

16. E. Smela, "Microfabrication of PPy microactuators and other conjugated polymer devices", *J. Micromech. Microeng.* 9, 1-18 (1999).

17. L. Bay, S. Skaarup, K. West, T. Mazur, O. Joergensen, and H. D. Rasmussen, "Properties of polypyrrole doped with alkylbenzene sulfonates", Proc. SPIE's 8th Int. Symp. Smart Struc. Mater., Electroactive Polymer Actuators and Devices (EAPAD), Newport Beach, CA, 5-8 March 2001 Vol. 4329, p. 101-105.

18. H. D. Espinosa and B. C. Prorok, "Size Effects on the Mechanical Behavior of Thin Gold Films", Symposium on Mechanical Properties of MEMS Structures, the ASME 2001 International Mechanical Engineering Congress and Exposition, New York, 2001.

6.2   HUMAN URINE CONTROL [45]

Analytes / Instruments	Units	Level 1 Lot No. 43261		Level 2 Lot No. 43262		SI Units[1]	Level 1 Lot No. 43261		Level 2 Lot No. 43262	
		Mean	Expected Range	Mean	Expected Range		Mean	Expected Range	Mean	Expected Range
Amylase										
Abbott Aeroset	U/L	94	75 - 112	174	139 - 209	U/L	94	75 - 112	174	139 - 209
Beckman Synchron	U/L	41	33 - 49	78	63 - 94	U/L	41	33 - 49	78	63 - 94
Dade Dimension	U/L	95	76 - 114	184	147 - 221	U/L	95	76 - 114	184	147 - 221
Olympus AU 400/600	U/L	83	66 - 99	153	122 - 183	U/L	83	66 - 99	153	122 - 183
Ortho Vitros	U/L	51	41 - 61	88	70 - 105	U/L	51	41 - 61	88	70 - 105
Roche Hitachi	U/L	79	63 - 95	149	119 - 179	U/L	79	63 - 95	149	119 - 179
Roche Integra	U/L	82	66 - 99	153	123 - 184	U/L	82	66 - 99	153	123 - 184
Calcium										
Abbott Aeroset	mg/dL	6.6	5.3 - 7.9	10.9	8.7 - 13.1	mmol/L	1.65	1.32 - 1.97	2.72	2.17 - 3.27
Beckman Synchron	mg/dL	6.2	5.0 - 7.4	10.7	8.5 - 12.8	mmol/L	1.55	1.25 - 1.85	2.67	2.12 - 3.19
Dade Dimension	mg/dL	6.7	5.3 - 8.0	11.9	9.5 - 14.2	mmol/L	1.67	1.32 - 2.00	2.97	2.37 - 3.54
Olympus AU 400/600	mg/dL	5.8	4.6 - 7.0	11.0	8.8 - 13.0	mmol/L	1.45	1.15 - 1.75	2.74	2.20 - 3.24
Ortho Vitros	mg/dL	7.4	5.9 - 8.8	11.9	9.5 - 14.3	mmol/L	1.85	1.47 - 2.20	2.97	2.37 - 3.57
Roche Hitachi	mg/dL	5.9	4.8 - 7.1	10.9	8.7 - 13.1	mmol/L	1.47	1.20 - 1.77	2.72	2.17 - 3.27
Roche Integra	mg/dL	6.5	5.2 - 7.8	12.2	9.8 - 14.7	mmol/L	1.62	1.30 - 1.95	3.04	2.45 - 3.67
Chloride										
Abbott Aeroset	mmol/L	98	78 - 118	153	122 - 183	mmol/L	98	78 - 118	153	122 - 183
Beckman Synchron	mmol/L	97	78 - 117	152	122 -182	mmol/L	97	78 - 117	152	122 -182
Dade Dimension	mmol/L	102	82 - 123	172	137 - 206	mmol/L	102	82 - 123	172	137 - 206
Olympus AU 400/600	mmol/L	101	81 - 121	159	127 - 190	mmol/L	101	81 - 121	159	127 - 190
Ortho Vitros	mmol/L	99	79 - 119	155	124 - 187	mmol/L	99	79 - 119	155	124 - 187
Roche Hitachi	mmol/L	95	76 - 114	152	122 - 183	mmol/L	95	76 - 114	152	122 - 183
Roche Integra	mmol/L	98	78 - 118	161	129 - 194	mmol/L	98	78 - 118	161	129 - 194
Creatinine										
Abbott Aeroset	mg/dL	77	61 - 92	153	122 - 184	mmol/L	6.81	5.39 - 8.13	13.53	10.78 - 16.27
Beckman Synchron	mg/dL	75	60 - 90	154	123 - 184	mmol/L	6.63	5.30 - 7.96	13.61	10.87 - 16.27
Dade Dimension	mg/dL	71	57 - 85	150	120 - 180	mmol/L	6.28	5.04 - 7.51	13.26	10.61 - 15.91
Olympus AU 400/600	mg/dL	76	61 - 92	155	124 - 186	mmol/L	6.72	5.39 - 8.13	13.70	10.96 - 16.44
Ortho Vitros 2	mg/dL	62	50 - 75	139	112 - 167	mmol/L	5.48	4.42 - 6.63	12.29	9.90 - 14.76
Roche Hitachi	mg/dL	68	54 - 81	140	112 - 168	mmol/L	6.01	4.77 - 7.16	12.38	9.90 - 14.85
Roche Integra	mg/dL	75	60 - 90	156	125 - 187	mmol/L	6.63	5.30 - 7.96	13.79	11.05 - 16.53
Glucose										
Beckman Synchron	mg/dL	43	34 - 51	295	236 - 354	mmol/L	2.39	1.89 - 2.83	16.38	13.10 - 19.65
Dade Dimension	mg/dL	44	35 - 53	297	237 - 356	mmol/L	2.44	1.94 - 2.94	16.49	13.16 - 19.76
Olympus AU 400/600	mg/dL	47	37 - 56	304	243 - 365	mmol/L	2.61	2.05 - 3.11	16.88	13.49 - 20.26
Ortho Vitros	mg/dL	47	37 - 56	326	261 - 392	mmol/L	2.61	2.05 - 3.11	18.10	14.49 - 21.76
Roche Hitachi	mg/dL	44	35 - 53	293	234 - 351	mmol/L	2.44	1.94 - 2.94	16.26	12.99 - 19.48
Roche Integra	mg/dL	43	35 - 52	297	237 - 356	mmol/L	2.39	1.94 - 2.89	16.49	13.16 - 19.76
Magnesium										
Beckman Synchron	mg/dL	7.4	5.9 - 8.9	14.8	11.8 - 17.7	mmol/L	3.04	2.43 - 3.66	6.09	4.85 - 7.28
Dade Dimension	mg/dL	7.4	5.9 - 8.8	14.8	11.9 - 17.8	mmol/L	3.04	2.43 - 3.62	6.09	4.90 - 7.32
Olympus AU 400/600	mg/dL	7.0	5.6 - 8.4	13.5	10.8 - 16.2	mmol/L	2.88	2.30 - 3.46	5.55	4.44 - 6.66
Ortho Vitros	mg/dL	6.4	5.1 - 7.7	12.7	10.7 - 15.2	mmol/L	2.63	2.10 - 3.17	5.20	4.44 - 6.25
Roche Hitachi	mg/dL	6.1	4.9 - 7.3	12.2	9.7 - 14.6	mmol/L	2.51	2.02 - 3.00	5.02	3.99 - 6.01
Roche Integra	mg/dL	7.8	6.2 - 9.3	15.9	12.7 - 19.1	mmol/L	3.21	2.55 - 3.83	6.54	5.22 - 7.86
Osmolality										
Advanced Instruments (Freezing Point)	mOsm/Kg	389	311 - 466	745	596 - 894	mmol/Kg	389	311 - 466	745.0	596 - 894
Phosphorus										
Abbott Aeroset	mg/dL	22	18 - 26	47	37 - 56	mmol/L	7.11	5.81 - 8.40	15.18	11.95 - 18.09
Beckman Synchron	mg/dL	20	16 - 24	47	38 - 56	mmol/L	6.46	5.17 - 7.75	15.18	12.27 - 18.09
Dade Dimension	mg/dL	22	18 - 27	51	41 - 61	mmol/L	7.11	5.81 - 8.72	16.47	13.24 - 19.70
Olympus AU 400/600	mg/dL	20	16 - 23	46	37 - 55	mmol/L	6.46	5.17 - 7.43	14.86	11.95 - 17.77
Ortho Vitros	mg/dL	21	17 - 25	50	40 - 60	mmol/L	6.78	5.49 - 8.08	16.15	12.92 - 19.38
Roche Hitachi	mg/dL	19	16 - 23	45	36 - 55	mmol/L	6.14	5.17 - 7.43	14.54	11.63 - 17.77
Roche Integra	mg/dL	22	17 - 26	51	40 - 61	mmol/L	7.11	5.49 - 8.40	16.47	12.92 - 19.70
Potassium										
Abbott Aeroset	mmol/L	33	26 - 40	70	56 - 85	mmol/L	33	26 - 40	70	56 - 85
Beckman Synchron	mmol/L	32	26 - 39	70	56 - 84	mmol/L	32	26 - 39	70	56 - 84
Dade Dimension	mmol/L	32	26 - 38	68	54 - 82	mmol/L	32	26 - 38	68	54 - 82
Olympus AU 400/600	mmol/L	34	27 - 41	73	59 - 88	mmol/L	34	27 - 41	73	59 - 88
Ortho Vitros	mmol/L	33	26 - 39	73	59 - 88	mmol/L	33	26 - 39	73	59 - 88
Roche Hitachi	mmol/L	33	26 - 40	70	56 - 84	mmol/L	33	26 - 40	70	56 - 84
Roche Integra	mmol/L	34	27 - 41	72	58 - 87	mmol/L	34	27 - 41	72	58 - 87
Sodium										
Abbott Aeroset	mmol/L	84	68 - 101	162	129 - 194	mmol/L	84	68 - 101	162	129 - 194
Beckman Synchron	mmol/L	85	68 - 103	161	129 - 193	mmol/L	85	68 - 103	161	129 - 193
Dade Dimension	mmol/L	84	67 - 101	154	124 - 185	mmol/L	84	67 - 101	154	124 - 185
Olympus AU 400/600	mmol/L	86	68 - 103	165	132 - 198	mmol/L	86	68 - 103	165	132 - 198
Ortho Vitros	mmol/L	84	67 - 101	163	130 - 196	mmol/L	84	67 - 101	163	130 - 196
Roche Hitachi	mmol/L	85	68 - 102	164	131 - 197	mmol/L	85	68 - 102	164	131 - 197
Roche Integra	mmol/L	88	70 - 105	165	132 - 198	mmol/L	88	70 - 105	165	132 - 198
Total Protein										
Abbott Aeroset (Benzethonium Chloride)	mg/dL	15	12 - 17	46	37 - 56	g/L	0.15	0.12 - 0.17	0.46	0.37 - 0.56
Beckman Synchron (M-TP) (Pyrogallol Red)	mg/dL	17	12 - 21	64	45 - 84	g/L	0.17	0.12 - 0.21	0.64	0.45 - 0.84
Dade Dimension (Pyrogallol Red)	mg/dL	19	13 - 25	63	50 - 76	g/L	0.19	0.13 - 0.25	0.63	0.50 - 0.76
Quantimetrix QuanTest Red (Pyrogallol Red)	mg/dL	14	9 - 18	47	38 - 57	g/L	0.14	0.09 - 0.18	0.47	0.38 - 0.57
Olympus AU 400/600 (Pyrogallol Red)	mg/dL	14	11 - 17	48	38 - 57	g/L	0.14	0.11 - 0.17	0.48	0.38 - 0.57
Ortho Vitros (Pyrocatechol Violet-Molyb.)	mg/dL	29	20 - 38	75	52 - 97	g/L	0.29	0.20 - 0.38	0.75	0.52 - 0.97
Roche Hitachi (Benzethonium Chloride)	mg/dL	15	12 - 18	48	38 - 57	g/L	0.15	0.12 - 0.18	0.48	0.38 - 0.57
Roche Integra (Pyrogallol Red)	mg/dL	14	12 - 17	52	42 - 63	g/L	0.14	0.12 - 0.17	0.52	0.42 - 0.63
Urea Nitrogen										
Abbott Aeroset	mg/dL	389	311 - 467	644	515 - 773	mmol/L	139	111 - 167	230	184 - 276
Beckman Synchron	mg/dL	402	321 - 482	677	542 - 813	mmol/L	144	115 - 172	242	193 - 290
Dade Dimension	mg/dL	423	338 - 508	712	570 - 855	mmol/L	151	121 - 181	254	203 - 305
Olympus AU 400/600	mg/dL	384	307 - 460	637	510 - 764	mmol/L	137	110 - 164	227	182 - 273
Ortho Vitros	mg/dL	382	306 - 459	642	514 - 771	mmol/L	136	109 - 164	229	183 - 275
Roche Hitachi	mg/dL	366	293 - 439	618	495 - 742	mmol/L	131	105 - 157	221	177 - 265
Roche Integra	mg/dL	404	323 - 485	681	545 - 817	mmol/L	144	115 - 173	243	195 - 292
Uric Acid										
Abbott Aeroset	mg/dL	3.0	2.4 - 3.5	8.8	7.0 - 10.6	mmol/L	0.18	0.14 - 0.21	0.52	0.42 - 0.63
Beckman Synchron	mg/dL	6.2	5.0 - 7.5	15.0	12.0 - 18.0	mmol/L	0.37	0.30 - 0.45	0.89	0.71 - 1.07
Dade Dimension	mg/dL	5.9	4.7 - 7.1	15.1	12.1 - 18.1	mmol/L	0.35	0.28 - 0.42	0.90	0.72 - 1.08
Olympus AU 400/600	mg/dL	5.0	4.0 - 6.0	14.4	11.5 - 17.3	mmol/L	0.30	0.24 - 0.36	0.86	0.68 - 1.03
Ortho Vitros	mg/dL	5.1	4.0 - 6.1	13.5	10.8 - 16.1	mmol/L	0.30	0.24 - 0.36	0.80	0.64 - 0.96
Roche Hitachi	mg/dL	2.8	2.0 - 3.6	9.7	6.8 - 12.6	mmol/L	0.17	0.12 - 0.21	0.58	0.40 - 0.75
Roche Integra	mg/dL	4.5	3.6 - 5.4	13.8	11.1 - 16.6	mmol/L	0.27	0.21 - 0.32	0.82	0.66 - 0.99

(1) SI International System of Units
(2) Dilute 1:42 (See Limitations Section)

Abbott Diagnostics, Aeroset™
Advanced Instruments, Inc.,
Beckman Coulter, Inc., Synchron®
Olympus America Inc., AU 400/600™

Ortho Clinical Diagnostics, Vitros™
Osmometer Quantimetrix Corp., QuanTest Red
Roche Diagnostics Corporation, Hitachi, Cobas Integra®

6.3   MASK DESIGN

Au Mask

1. Au pad
2. Thin Au wiring
3. Thick Au wiring

PPy Mask

Al Mask

Masks combined

Legend:
Au mask
Al mask
PPy mask
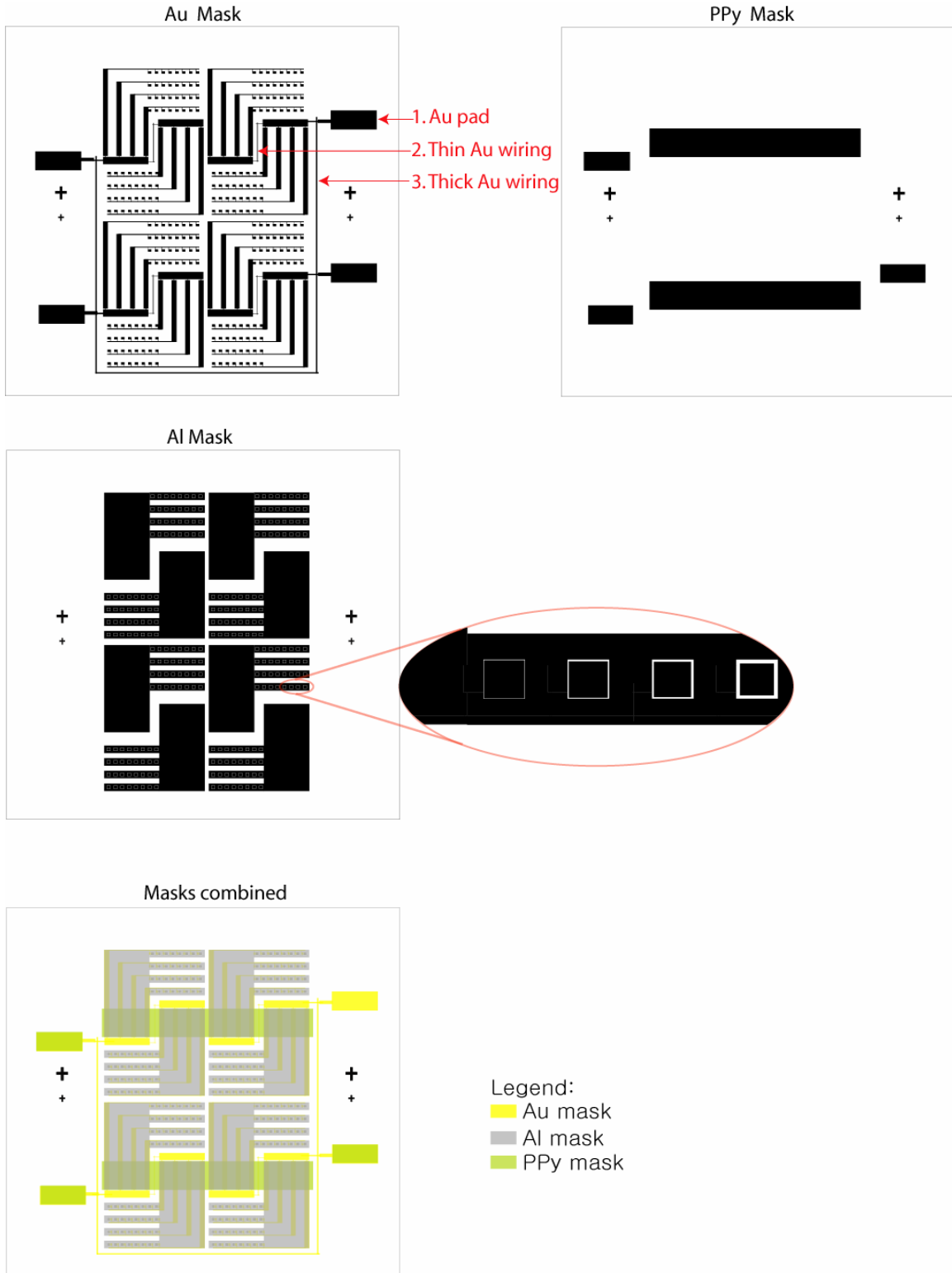
A copper micro-clip holds a sample at the Au pad in the 'Au mask' so that voltage can be applied to deposit PPy. The thick Au wiring in the Au mask connects 4 pairs of samples. The thin Au wiring connects each of the pair. There are 4 Au pads to allow deposition of 4 different thicknesses of PPy. After the deposition of the first thickness of PPy(the thinnest of the 4), the thick Au wiring that leads to the next 3 Au pads is cut to isolate the pair. Then, the next Au pad is clamped with the clip, and voltage is applied to deposit additional PPy. This is repeated until the last Au pad is used.

REFERENCES

[1]   J. A. Fantl, D. K. Newman, J. Colling, and e. al., "Urinary incontinence in adults: acute and chronic management," US Department of Health and Human Services, Agency for Health Care Policy and Research, Rockville, MD Clinical Practice Guideline No. 2, 1996 Update, AHCPR Publication No. 96-0682, March 1996.

[2]   T. H. Wagner and T. W. Hu, "Economic costs of urinary incontinence in 1995," *Urology*, vol. 51, pp. 355-361, 1998.

[3]   D. R. Knowles. (2001). Urinary catheters. http://health.yahoo.com/health/encyclopedia/003981/0.html (Aug. 2003).

[4]   P. B. Chu and K. S. J. Pister, "Analysis of Closed -Loop Control of Parallel-Plate Electrostatic Microgrippers," *Proceedings 1994 IEEE International Conference on Robotics and Automation*, vol. 1, pp. 820-25, 1994.

[5]   C. J. Kim, A. P. Pisano, R. S. Muller, and M. G. Lim, "Polysilcon Microgripper," *Tech. Digest IEEE Solid State Sensor and Actuator Workshop*, pp. 48-51, 1990.

[6]   C. J. Kim, Pisano, A.P., Muller, R.S., "Polysilicon Microgripper," *Tech. Digest IEEE Solid State Sensor and Actuator Workshop*, pp. 48-51, 1990.

[7]   C. J. Kim and A. P. Pisano, "Silicon-Processed Overhanging Microgripper," *Journal of Microelectromechanical System*, vol. 1, pp. 31-36, 1992.

[8]   J. D. Grade, K. Y. Yasumura, and H. Jerman, " Manipulation Biological and Mechanical Micro-Objects Using LIGA-Microfabricated End-Effectors," *Transducers, Solid-State Sensors, Actuators and Microsystems, 12th International Conference*, vol. 1, pp. 568-71, 2003.

[9]   M. C. Carrozza, P. Dario, A. Menciassi, and A. Fenu, "Manipulation Biological and Mechanical Micro-Objects Using LIGA-Microfabricated End-Effectors," *Proceedings. 1998 IEEE/RSJ International Conference on Intelligent Robots and Systems*, vol. 2, pp. 1811-6, 1998.

[10]   Y. Haddab, N. Chaillet, and A. Bourjault, "A Microgripper Using Smart Piezoelectric Actuators," *Proceedings. 2000 IEEE/RSJ International Conference on Intelligent Robots and Systems*, vol. 1, pp. 659-62, 2000.

[11]   G. Greitmann and R. A. Buser, "Tactile Microgripper for Automated Handling of Microparts," *Sensors and Actuators A*, vol. A53, pp. 410-5, 1996.

[12]   Q. Huang and N. Lee, "Analysis and design of polysilicon thermal flexure actuator," *J. Micromech. Microeng.*, vol. 9, pp. 64-70, 1999.

[13]   J. M. Maloney, D. L. DeVoe, and D. S. Schreiber, "Analysis and Design of Electrothermal actuators Fabricated from Single Crystal Silicon," *Micro-Electro-Mechanical Systems (MEMS). 2000 ASME International Mechanical Engineering Congress and Exposition*, pp. 233-40, 2000.

[14]   J. W. Suh, C. W. Storment, and G. T. A. Kovacs, "Characterization of Multi-Segment Organic Thermal Acutators," *8th Int'l. Conf. on Solid-State Sensors and Actuators/Eurosensors IX*, vol. 2, pp. 316, 1995.

[15]   A. P. Lee, D. R. Ciarlo, P. A. Krulevitch, S. Lehew, J. Trevino, and M. A. Northrup, "A Practical Microgripper by Fine Alignment, Eutectic Bonding and SMA Acutation," *8th International Conference on Solid-State Sensors and Actuators and Eurosensors IX. Digest of Technical Papers*, vol. 2, pp. 368-71, 1995.

[16]   E. Fullin, J. Gobet, H. A. C. Tilmans, and J. Bergqvist, "A New Basic Technology for magnetic Micro-Actuators," presented at 11th Annual International Workshop on Micro Electro Mechanical Systems, Heidelberg, Germany, 1998.

[17]   J. A. Wright, Y. Tai, and S. Chang, "A Large-Force, Fully-Integrated MEMS Magnetic Actuator," *Technical Digest: 1997 International Conference on Solid-State Sensors and Actuators: Transducers '97*, vol. 2, pp. 793-796, 1997.

[18]   D. J. Beebe, J. Moore, J. M. Bauer, Q. Yu, R. H. Liu, C. Devadoss, and B. Jo, "Functional Hydrogel Structures for Autonomous Flow Control Inside Microfluidic Channels," *Nature*, vol. 404, pp. 588-90, 2000.

[19]   S. Hattori, T. Fukuda, R. Kishi, H. Ichijo, Y. Katsurayama, H. Katayama, H. Matsuura, T. Watarai, S. Nagamori, and T. Hiramatsu, "Structrure and machanism of two types of micro-pump using polymer gel," *micro Electro mechanical Systems '92*, pp. 110-115, 1992.

[20]   B. Johnson, D. J. Niedermaier, W. C. Crone, J. Moorthy, and D. J. Beebe, "Mechanical Properties of a pH Sensitive Hydrogel," presented at Session on Biologyically Inspire Synthesis and Properties, Proceedings of the SEM Annual Conference on Experimental MechanicsProceedings, Milwaukee, WI, 2002.

[21]   E. W. H. Jager, E. Smela, and O. Inganäs, "Microfabricating conjugated polymer actuators," *Science*, vol. 290, pp. 1540-1545, 2000.

[22]   R. C. D. Peres, M.-A. De Paoli, and R. M. Torresi, "The role of ion exchange in the redox processes of polypyrrole/dodecyl sulfate films as studied by electrogravimetry using a quartz crystal microbalance," *Synth. Met.*, vol. 48, pp. 259, 1992.

95

[23] M. K. Song, M. S. Gong, and H. W. Rhee, "Anion movement in polypyrrole films prepared in lithium dodecylsulfate aqueous solutions," *Molecular Crystals and Liquid Crystals Science and Technology Section A - Molecular Crystals and Liquid Crystals*, vol. 280, pp. 145-150, 1996.

[24] E. Smela, "Conjugated polymer actuators for biomedical applications," *Adv. Mat.*, vol. 15, pp. 481-94, 2003.

[25] L. Bay, T. Jacobsen, S. Skaarup, and K. West, "Mechanism of actuation in conducting polymers: osmotic expansion," *J. Phys. Chem. B*, vol. 105, pp. 8492-8497, 2001.

[26] S. Shimoda and E. Smela, "The effect of pH on polymerization and volume change in PPy(DBS)," *Electrochim. Acta*, vol. 44, pp. 219-238, 1998.

[27] Q. Pei and O. Inganäs, "Electrochemical applications of the bending beam method. 1. Mass transport and volume changes in polypyrrole during redox," *J. Phys. Chem.*, vol. 96, pp. 10507-10514, 1992.

[28] M. R. Gandhi, P. Murray, G. M. Spinks, and G. G. Wallace, "Mechanism of electromechanical actuation in polypyrrole," *Synth. Met.*, vol. 73, pp. 247-256, 1995.

[29] K. Naoi, M. Lien, and W. H. Smyrl, "Quartz crystal microbalance study: ionic motion across conducting polymers," *J. Electrochem. Soc.*, vol. 138, pp. 440-445, 1991.

[30] M. Hepel, "Composite polypyrrole films switchable between the anion- and cation-exchanger states," *Electrochim. Acta*, vol. 41, pp. 63-76, 1996.

[31]   E. Smela, "Microfabrication of PPy microactuators and other conjugated polymer devices," *Journal of Micromechanics and Microengineering*, vol. 9, pp. 1-18, 1999.

[32]   E. Smela, O. Inganäs, and I. Lundström, "Micro-robot controlled by conducting polymer muscles: multi-hinged, folding actuators," presented at International Symposium on Microsystems, Intelligent Materials, and Robots, Sendai, Japan, pp. 79-83, 1995.

[33]   E. W. H. Jager, O. Inganas, and I. Lundstrom, "Microrobots for micrometer-size objects in aqueous media: potential tools for single-cell manipulation," *Science*, vol. 288, pp. 2335-2338, 2000.

[34]   E. W. H. Jager, "Microsystems Based on Polypyrrole Microactuators: Microrobots and Cell Clinics," in *Department of Physics and Measurement Technology*. Linköping, Sweden: Linköpings universitet, 2001.

[35]   E. Smela, M. Kallenbach, and J. Holdenried, "Electrochemically driven polypyrrole bilayers for moving and positioning bulk micromachined silicon plates," *J. Microelectromech. Syst.*, vol. 8, pp. 373-383, 1999.

[36]   E. Smela, L. Oh, and P. Seth, "Urinary Incontinence Micro-valves," University of Maryland, MIPS Technical Proposal, Phase 2, pp. 8a-n, 2002.

[37]   General Specification KAPTON Polyimide Film. http://www.dupont.com/kapton/general/H-38479-4.html (Aug. 2003).

[38]   Q. Pei and O. Inganäs, "Electrochemical applications of the bending beam method; a novel way to study ion transport in electroactive polymers," *Sol. State Ion.*, vol. 60, pp. 161-166, 1993.

[39]   R. Lamendola, E. Matarrese, M. Creatore, P. Favia, and R. d'Agostino, "Plasma Treatment of Polymers for Improving Al Adhesions," *Materials Research Society Symposium Proceedings*, vol. 544, pp. 269-75, 1998.

[40]   E. M. R. Lamendola, M. Creatore, P. Favia, and R. d'Agostino, "Plasma Treatment of Polymers for Improving Al Adhesions," *Materials Research Society Symposium Proceedings*, vol. 544, pp. 269-275, 1998.

[41]   T. S. V. Zaporojchenko, K. Behnke, C. v. Bechtolsheim, A. Thran, and F. Faupel, "Formation of Metal-polymer Interfaces by Metal Evaporation: Influence of Deposition Parameters and Defects," *Microelectronic Engineering*, vol. 50, pp. 465-471, 2000.

[42]   Physical and Thermal Properties of Kapton. http://www.dupont.com/kapton/general/spphythe.html (Nov. 2003).

[43]   Technical Information KAPTON E Polyimide Film. http://www.dupont.com/kapton/products/H-78305.pdf (Nov. 2003).

[44]   M. Pyo, C. C. Bohn, E. Smela, J. R. Reynolds, and A. B. Brennan, "Direct strain measurement of polypyrrole actuators controlled by the polymer/gold interface," *Chem. Mater.*, vol. 15, pp. 916-22, 2003.

[45]   F. Beck and U. Barsch, "Corrosion of conducting polymers in aqueous electrolytes," *Synth. Met.*, vol. 55-57, pp. 1299, 1993.

[46]   Y. Kuo, K. Okajima, and M. Takeichi, "Plasma processing in the fabrication of amorphous silicon thin-film-transistor arrays," *IBM Journal of Research and Development*, vol. 43, pp. 73-88, 1999.

[47]   E. W. H. Jager, E. Smela, and O. Inganäs, "On-chip microelectrodes for

electrochemistry with moveable PPy bilayer actuators as working electrodes,"

Sens. Act. B, vol. 56, pp. 73-78, 1999.